Copy 5
RM L9G15

NACA RM L9G15

NACA

RESEARCH MEMORANDUM

INVESTIGATION AT LARGE SCALE OF THE PRESSURE DISTRIBUTION AND FLOW PHENOMENA OVER A WING WITH THE LEADING EDGE SWEPT BACK 47.5° HAVING CIRCULAR-ARC AIRFOIL SECTIONS AND EQUIPPED WITH DROOPED-NOSE AND PLAIN FLAPS

By Roy H. Lange, Edward F. Whittle, Jr., and Marvin P. Fink

Langley Aeronautical Laboratory
Langley Air Force Base, Va.

NATIONAL ADVISORY COMMITTEE FOR AERONAUTICS

WASHINGTON
September 8, 1949

NACA RM L9G15

NATIONAL ADVISORY COMMITTEE FOR AERONAUTICS

RESEARCH MEMORANDUM

INVESTIGATION AT LARGE SCALE OF THE PRESSURE DISTRIBUTION AND FLOW PHENOMENA OVER A WING WITH THE LEADING EDGE SWEPT BACK 47.5° HAVING CIRCULAR-ARC AIRFOIL SECTIONS AND EQUIPPED WITH DROOPED-NOSE AND PLAIN FLAPS

By Roy H. Lange, Edward F. Whittle, Jr., and Marvin P. Fink

SUMMARY

An investigation of the pressure distribution over a wing with the leading-edge swept back 47.5° and having symmetrical circular-arc airfoil sections has been conducted in the Langley full-scale tunnel at a Reynolds number of 4.3×10^6 and a Mach number of 0.07. The investigation included measurements of the surface static pressures along the chord for six spanwise stations, for a large angle-of-attack range, and for several angles of yaw. The configurations tested included the basic wing, the wing with a full-span drooped-nose flap, an inboard semispan plain flap, and a combination of these two flap configurations.

The results show that a separation vortex was formed along the leading edge of the basic wing at a low angle of attack as a result of flow separation from the sharp leading edge. With increasing angle of attack, the diameter of the separation vortex increased over the outboard spanwise stations. At an angle of attack of about 11°, the vortex core turned back along the chord and a trailing vortex was shed off the wing at about 70 percent of the semispan. The values of maximum section lift coefficient for the basic wing were considerably higher than the two-dimensional values for all spanwise stations inboard of the station where the vortex core left the wing. The span load distribution of the basic wing did not agree with that predicted by the method based on potential flow. The effect of yaw on the basic wing was to increase the tip stalling of the advancing wing and also to increase the lift of the inboard sections of the advancing wing. The effect of the separation vortex was evident over a considerably larger spanwise extent of the retreating wing than for the advancing wing. The effect of the separation vortex on the span load distribution of

the wing with the inboard semispan plain flap deflected is essentially the same as that for the basic wing except that the span load coefficients are higher for the inboard stations and lower for the outboard stations. The angle of attack at which the separation vortex forms increases with increasing drooped-nose flap deflection, and the maximum section lift coefficients of the outboard stations also increase. With the drooped-nose flap deflected 40°, the span load distribution approaches the additional load distribution predicted by the method based on potential flow. The span load distribution of the combined deflections of the flaps shows a similarity to the combination of the separate effects of each flap.

INTRODUCTION

Low-speed investigations at both small and large scale of highly sweptback wings designed for high-speed flight have revealed complex flow phenomena because of the relatively large regions of separated flow. The boundary-layer action and the stall progressions of some of these wings have been reported in references 1 to 4; however, there are relatively few experimental pressure distributions over highly sweptback wings (other than that of reference 5 for triangular wings). Data of this type are necessary for an understanding of the problems associated with flow separation and for correlation with available theory. Since there is increasing interest in highly sweptback wings with thin airfoil sections, an investigation has been conducted in the Langley full-scale tunnel to determine the pressure distribution over a wing with the leading edge swept back 47.5° and having 10-percent-thick symmetrical circular-arc airfoil sections. The longitudinal and lateral characteristics of the wing, as determined from force tests, are given in references 1 and 2.

The investigation included measurements at a Reynolds number of 4.3×10^6 and a Mach number of 0.07 of the surface static pressures along the chord for stations located at 5, 10, 20, 40, 60, and 80 percent of the wing semispan for a large angle-of-attack range and for several angles of yaw. The configurations tested include the basic wing, the wing with a full-span drooped-nose flap, an inboard semispan plain flap, and a combination of these two flap configurations. In addition to the pressure measurements, the stalling characteristics of the wing were determined by means of tuft observations.

COEFFICIENTS AND SYMBOLS

C_L	lift coefficient $\left(\frac{\text{Lift}}{qS} \text{ or } \int_0^1 c_l \frac{c}{c_{av}} d\left(\frac{2y}{b}\right)\right)$
c_l	section lift coefficient $\left(\cos \alpha \int_0^1 P_R d\left(\frac{x}{c}\right)\right)$
P	pressure coefficient $\left(\frac{p - p_o}{q}\right)$
P_R	resultant pressure coefficient
$\frac{c_l c}{C_L c_{av}}$	span loading coefficient
q	free-stream dynamic pressure
p	local static pressure
p_o	free-stream static pressure
c	local chord
c_{av}	average chord $\left(\frac{S}{b}\right)$
b	wing span
y	spanwise coordinate perpendicular to plane of symmetry
x	chordwise coordinate parallel to plane of symmetry
S	wing area
α	angle of attack, degrees
ψ	angle of yaw, degrees

c' chord, perpendicular to line of maximum thickness

δ_n drooped-nose-flap deflection perpendicular to hinge line, degrees

MODEL

The geometric characteristics of the wing are given in figure 1. The wing has an angle of sweepback of 45° at the quarter-chord line or 47.5° sweep at the leading edge, an aspect ratio of 3.5, a taper ratio of 0.5, and has no geometric dihedral or twist. The wing has 10-percent-thick, symmetrical circular-arc airfoil sections perpendicular to the line of maximum thickness. A more detailed description of the wing is given in references 1 and 2.

The wing was equipped with flush, surface static-pressure orifices arranged in chordwise rows located at 5, 10, 20, 40, 60, and 80 percent of the right-wing semispan as shown in figure 2. The chordwise locations of the orifices, which are the same for all spanwise stations, are also given in figure 2.

The wing is equipped with a full-span drooped-nose flap and an inboard semispan plain flap which are 20 percent of the chord measured perpendicular to the line of maximum thickness. These flaps are pivoted on piano hinges mounted flush with the lower wing surface and, when deflected, produce a gap on the upper wing surface which is covered and faired with a sheetmetal seal.

METHODS AND TESTS

The surface static pressures were measured on a multiple-tube manometer and photographically recorded. Each configuration was tested through a large angle-of-attack range at a yaw angle of 0°, and the basic wing was also tested at yaw angles of ±6.0° and ±9.8°. The configurations tested include the basic wing, the wing with semispan inboard plain flaps deflected 40°, with full-span drooped-nose flaps deflected 10°, 20°, 30°, and 40°, and with semispan inboard plain flaps and full-span drooped-nose flaps deflected 40°. All tests were made at a Reynolds number of about 4.3×10^6 and a Mach number of about 0.07 inasmuch as the results of reference 1 showed no appreciable scale effect on the aerodynamic characteristics.

In addition to the pressure-distribution measurements, tuft studies were made of each of the above configurations, and force tests were also made of the basic wing configuration at 0° yaw. The force measurements and tuft studies of the basic wing were identical with the results of reference 1 indicating that no appreciable change in wing contour resulted from the installation of the static-pressure orifices.

REDUCTION OF DATA

The measured static pressures were reduced to coefficient form and plotted against their respective chordwise locations. Calculations showed that the effects of forces parallel to the chord produced negligible changes in the values of section and wing lift coefficients and, therefore, these effects are not included. From these chordwise pressure distributions, the values of section and wing lift coefficients and span loading coefficients were determined by a considerable amount of mechanical integration and by the usual calculation procedures.

RESULTS AND DISCUSSION

Presentation of Results

The presentation of the test results and the analysis of the data have been grouped into two main sections. The first section deals with the chordwise and spanwise aerodynamic load characteristics of the basic wing both for the zero yaw conditions (figs. 3 to 8) and for angles of yaw of ±6.0° and ±9.8° (figs. 9 to 18). The second section presents results of tests of the wing with the inboard semispan plain flaps deflected (figs. 19 to 23), the full-span drooped-nose flaps deflected (figs. 24 to 29 and tables I to III), and with a combination of these two flapped configurations (figs. 30 to 34). Tuft studies are presented wherever possible to aid in the analysis of the flow over the wing.

The results have been corrected for the stream alinement, the blocking effects, the tares caused by the wing supports, and the jet-boundary effects which were calculated on the basis of an unswept wing.

Basic-Wing Characteristics

Chordwise pressure distributions and air-flow studies.- The chordwise pressure distributions of the six spanwise stations of the basic-wing configuration (fig. 3) show that at the lowest angle of attack ($\alpha = 1.1^\circ$) the pressure distribution is similar to that measured at an angle of attack of 0.5° for a symmetrical circular-arc airfoil section in two-dimensional flow (reference 6) for all spanwise stations except $0.60\frac{b}{2}$. With a small increase in angle of attack, flow separation occurs as a result of the effects of the sharp leading edge. This leading-edge separation was noted in the two-dimensional tests (reference 6) and was described as a bubble of separation localized at the leading edge followed by smooth flow over the remaining airfoil chord. The data of figure 3 indicate that this local separation first occurs at the 80-percent spanwise station at $\alpha = 2.9^\circ$ as shown by the broadening of the pressure peak at the leading edge. The stall diagrams of figure 7 show a spanwise flow of the boundary-layer air at the leading edge toward the tip at an angle of attack of 2.9° and rough flow in the outer 50 percent of the semispan at an angle of attack of 4.8°. For angles of attack greater than about 4° (fig. 3), the leading-edge peak negative pressures are well developed over the inboard semispan, and progressively lower and broader negative pressure peaks are developed with increasing spanwise distance from the plane of symmetry. These distributions show a much larger chordwise extent of the region of increased negative pressures near the leading edge in the outboard semispan as compared with the inboard semispan. The leading-edge peak negative pressure of the 5-percent station increases rapidly with further increase in angle of attack up to an angle of attack of 18° and is considerably higher than the two-dimensional values of peak negative pressure obtained in reference 6. As shown by the flat pressure distributions on the upper surface, the flow is completely separated from the wing for angles of attack greater than about 10.2° and 16°, respectively, for the 80- and 60-percent spanwise stations (fig. 3). An inspection of the stall diagrams of figure 7 merely shows a gradual increase in the stalled area from tip to root with increasing angle of attack and, therefore, gives no further information regarding the nature of the flow over the wing beyond that indicated by the pressure distributions.

In order to study in more detail the character of the flow that produced such an unusual pressure distribution over the forward part of the wing, an air-flow investigation was made in the $\frac{1}{15}$-scale model of the Langley full-scale tunnel on a scale model of the wing with flat-plate airfoil sections and sharp leading edges. Although such a study involved rather low Reynolds numbers, the results of this method of flow observation on a model of the DM-1 glider with sharp leading-edge

extensions proved very useful in the analysis of the flow over the full-scale DM-1 glider (reference 7). In addition to these tests, there is excellent agreement between small-scale-model tests of triangular wings with biconvex airfoil sections in the Langley full-scale tunnel (unpublished) and large-scale tests on a triangular wing with modified double-wedge airfoil sections (reference 5). The force measurements of reference 1 show no scale effects; and, therefore, it is felt that the flow observations of the small-scale model truly represent the type of flow that exists over the large wing.

The flow above and on the model sweptback-wing surface was investigated by means of a tuft attached to a search probe. The air-flow studies showed flow separation from the leading edge at a low angle of attack, as expected from the pressure distributions. The reattachment of the flow occurred immediately behind the leading edge, forming a local region of separation which, because of the reversed flow in the separated region, formed a separation vortex along the leading edge with the flow at the upper extremity in a rearward direction and with the flow near the wing surface in a forward direction. Within this separated region at the leading edge an outward spanwise flow of the boundary-layer air was observed which agrees with the reasoning of reference 8. With a small increase in angle of attack, the separation vortex along the leading edge was approximately cone shaped and the tip of the cone appeared to be at the wing apex. The vortex region increased in size from root to tip, and over the outboard sections the search tuft clearly showed the larger chordwise extent of the influence of the vortex and its disturbed flow as compared with the inboard sections. This effect increased with increasing angle of attack such that at an angle of attack of about 11° the vortex core turned back along the chord and was shed off the wing at about 70 percent of the wing semispan. Outboard of this point, the flow was completely separated from the wing upper surface. The triangular-wing tests (reference 5) show chordwise pressure distributions which are similar in shape and in spanwise variation to those shown in figure 3, and in both the small- and large-scale tests the air-flow studies clearly revealed the existence of a separation vortex over the upper wing surface. These flow studies at both small and large scale also show a displacement of the vortex core toward the plane of symmetry with increasing angle of attack.

Section lift coefficients.- The variations of section lift coefficient with angle of attack given in figure 4 show values of maximum section lift coefficients considerably higher than the two-dimensional value of about 0.7 (reference 9) for all stations except the 80-percent spanwise station. For the angle-of-attack range investigated, the highest value of $c_{l_{max}}$ of 1.08 was obtained at the 40-percent spanwise station, and, as would be expected, the result of complete flow

separation was to produce the lowest value of $c_{l_{max}}$ of about 0.51 at the 80-percent spanwise station. The effect of the vortex on the section loading of the outboard stations is evident from a comparison of the chordwise pressure distributions of figure 3 and the section lift curves of figure 4. It is seen that flow separation at the leading edge does not result in a loss in section lift at the low and moderate angles of attack, for any loss in lift at the leading edge is more than compensated for by an increase in lift due to the low-pressure bumps in the chordwise pressure distributions. These low-pressure bumps are induced by the increased negative pressure field of the vortex, and the same effect is noted in reference 5. This effect is more pronounced for the 40- and 60-percent spanwise stations (fig. 3). The section lift curves for the 5-, 10-, and 20-percent spanwise stations are linear up to an angle of attack of 16° and have an average slope of about 0.054 per degree, whereas for the 40- and 60-percent stations, the section lift coefficient increases rapidly with angle of attack between angles of attack of 6° and 10° with slopes of 0.072 and 0.095 per degree, respectively, being measured at an angle of attack of 8°. The high values of maximum section lift coefficient and lift-curve slope for the 40- and 60-percent stations are attributed to the increased pressure field due to the action of the vortex as it turns back along the chord before being shed off the wing.

The spanwise variations of section lift coefficient given in figure 5 show more clearly the higher values of section lift coefficients measured for the 60- and 40-percent stations for the moderate and high angle-of-attack ranges, respectively.

Span load distribution.- The span load distributions given in figure 6 show no definite trends up to an angle of attack of 10.2°. As the 80- and 60-percent spanwise stations stall at 12.1° and 14.0°, respectively, the loading peak is located at about 40 percent of the span and remains in that region up to an angle of attack of 18.0°. At the highest angle of attack the loading is concentrated at about 20 percent of the span.

The theoretical span load distribution obtained from reference 10 is also presented in figure 6 for comparison with the experimental values. Because of the unusual flow over the wing resulting from the action of the separation vortex previously described in detail, it can be seen that the measured span load distribution is in poor agreement with the loading predicted by the theoretical method based on potential flow.

Comparison of wing lift coefficients.- The wing lift coefficients plotted against angle of attack as determined from pressure-distribution measurements are compared in figure 8 with those obtained from force

measurements. The data are in relatively good agreement with the larger differences occurring in the moderate angle-of-attack range.

Pressure-distribution measurements in yaw.- The chordwise pressure distributions of the wing in yaw (figs. 9 to 12) show a difference in the action of the separation vortex in the outboard span on the advancing (negative yaw) wing panel as compared with the retreating (positive yaw) panel. The data for the 80-percent spanwise station indicates the influence of the separation vortex on the retreating wing up to an angle of attack of 10.0° for $\psi = 6.0°$ and for all angles of attack investigated for $\psi = 9.8°$. In contrast, the influence of the vortex is not clearly defined on the advancing wing for angles of attack greater than 6.7° for either yaw angle. For the 60-percent spanwise station the influence of the vortex is indicated for all angles of attack at positive yaw angles but is not shown for angles of attack greater than about 10° for negative yaw angles. Since the influence of the vortex is to delay the angle of attack for complete separation, the flow phenomena as indicated by these pressure distributions show clearly why the tip sections of a sweptback wing with circular-arc airfoil sections stall more severely when the sweep is decreased. For a similar sweptback wing having conventional airfoil sections, however, the tip stalling is relieved when the sweep is decreased. The pronounced increase in the outboard section loadings of the retreating wing panel appears to be the result of a more intense separation vortex as the leading-edge sweep increases from 47.5° to 57.3°. The pressures on this panel of higher sweep are very similar to those obtained on the large-scale triangular wing of 60° sweepback with modified double-wedge airfoil sections given in reference 5. Tuft studies of the wing in yaw (reference 1) show the same results in that the advancing wing begins to stall at a lower angle of attack than does the retreating wing panel, and from the force-test data this type of flow breakdown ultimately results in a negative dihedral effect.

The section lift coefficients presented in figures 13 and 14 show that, although decreasing the sweepback on the advancing wing panel aggravates the tip stalling and results in lower values of maximum section lift coefficients in the region of the tip, the inboard sections show higher values of section lift coefficients for the advancing wing than for the retreating wing. The variations of section lift coefficient across the wing span show a gradual inboard shift of the location of the peak section lift coefficient at the higher angles of attack to about $0.40\frac{b}{2}$ for the retreating wing panel. (See figs. 15 and 16.) For the advancing wing panel there is a rapid inboard shift of the location of the peak section lift coefficient with angle of attack to about $0.20\frac{b}{2}$ at $\psi = 6.0°$ and to about $0.15\frac{b}{2}$ at $\psi = 9.8°$ for the highest angles of attack.

The span load distributions given in figures 17 and 18 for the retreating wing panel are similar in trend and in magnitude to those obtained for the wing at 0° yaw. For the advancing wing panel, however, the loading peaks are shifted more inboard and the peak values of load coefficient are considerably higher than those obtained at 0° yaw. The loading is somewhat increased as the yaw angle is increased from 6.0° to 9.8°.

Effect of Plain-Flap Deflection

The chordwise pressure distributions for the wing with the semispan plain flap deflected 40° are shown in figure 19. These pressure distributions show that the effects of the separation vortex are similar to the effects shown for the basic wing except that these effects appear at an angle of attack of about 2° lower than they do on the basic wing. It is of interest to note the favorable pressure gradient for the 5-, 10-, and 20-percent-semispan sections immediately behind the leading-edge pressure peaks and extending aft to the plain flap at all angles of attack.

The section lift curves for the 40- and 60-percent-semispan sections have greater slopes in the lower angle-of-attack range than those for the 5-, 10-, 20-, and 80-percent-semispan sections (fig. 20). Similar effects are also shown for the corresponding basic-wing sections (fig. 4). The slope of the lift curve for the 80-percent-semispan section progressively decreases forming a well-rounded peak up to stall of the section. This inefficiency of the tip section may be explained by the earlier complete flow separation of the outboard spanwise sections and by the piling up of the boundary-layer air at the tip.

At a given angle of attack, the 5-, 10-, 20-, and 40-percent-semispan sections attain higher section lift coefficients (figs. 20 and 21) than the corresponding basic-wing sections (fig. 4). For example, at an angle of attack of 12°, the average increment in section lift coefficient, due to the plain flap, is about 0.37. The 5-percent-semispan section appears to be approaching stall, but the 10- and 20-percent-semispan sections seem to be capable of attaining higher section lift coefficients than were attained at the largest angle of attack tested. The 60- and 80-percent-semispan sections attain slightly lower values of maximum section lift coefficients than the corresponding basic-wing sections. The 40- and 60-percent-semispan sections stall at an angle of attack of about 4° lower than the corresponding basic-wing sections. The effect of the separation vortex on the span load distribution is essentially the same as that for the basic wing. (See fig. 22.)

Effect of Drooped-Nose-Flap Deflection

Deflecting the drooped-nose flap 10°, 20°, 30°, and 40° progressively decreases the peak negative pressures at the leading edge of the wing and, consequently, delays the formation of the separation vortex. Therefore, it is considered advisable to discuss the data with the drooped-nose flap deflected 40° in order to illustrate the greatest effects on the pressure distribution and flow characteristics. The data for the wing with the drooped-nose flap deflected 10°, 20°, and 30° are presented in tables I, II, and III.

The chordwise pressure distributions for the wing with the drooped-nose flap deflected 40° (fig. 24) show that the negative pressure peaks at the leading edge, which were prevalent for the basic wing, have been eliminated for angles of attack up to 14.4°. The elimination of the negative pressure peaks at the lower angles of attack results primarily from the effective camber at the leading edge introduced by the deflected flap, and the leading-edge separation is delayed to a much higher angle of attack because of the decrease in the adverse pressure gradients. The pressure distributions of figure 24 show that the flow separation is evident at the leading edge for the 80-percent-semispan section at an angle of attack of 18.2°. In this high range of angles of attack, the tuft studies of figure 28 show a spanwise flow of the boundary layer. With further increases in angle of attack, the leading-edge separation progresses inboard to the 60-percent-semispan section at an angle of attack of 22.0° and to the 20-percent-semispan section at an angle of attack of 25.8°. A further change in the pressure distribution occurs in this high angle-of-attack range at the outboard sections where the double-peak pressure distributions at the leading edge merge into one peak, which extends over the flap chord. The pressure distributions of figure 24 show considerably higher loading on the outboard sections for this drooped-nose flap configuration as compared with the outboard sections of the basic wing.

Before leading-edge separation appears, the slopes of the section lift curves (fig. 25) for the wing with the drooped-nose flap deflected 40° are generally less than the slopes of the section lift curves for the basic wing at the corresponding angles of attack. The combined effects of the delay of the formation of the separation vortex and the disturbed flow over the lower surface of the wing caused by the large drooped-nose-flap deflection contributes to the reduced lift effectiveness of the sections. After the appearance of the separation vortex (fig. 24, $\alpha = 18.2°$) the slope of the section lift curve for the 80-percent-semispan section increases, and for angles of attack greater than 22°, the section lift curves for the 40- and 60-percent-semispan sections also increase considerably. It appears that these increases in the slopes of the section lift curves occur at the angles of attack where the double-peak pressure distributions over the drooped-nose flap

merge into one large peak. However, only the section lift curves for the 60- and 80-percent-semispan sections attain slopes as great as the maximum slopes for the corresponding basic-wing sections.

At large angles of attack, the section lift coefficients for the inboard sections (figs. 25 and 26) are not so large as for the corresponding basic-wing sections (figs. 4 and 5). The maximum values of section lift coefficients for the 60- and 80-percent-semispan sections (1.12 and 0.95, respectively) are considerably larger than for the corresponding basic-wing sections (0.85 and 0.50, respectively) and are obtained at much higher angles of attack.

The alleviation of the large peak negative pressures at the inboard sections and the increase in the section lift of the outboard sections result in a more uniform span load distribution (fig. 27) for the wing with the drooped-nose flap deflected 40°. For most of the angles of attack, this distribution approaches the calculated theoretical additional span load distribution based on the potential-flow method of reference 10. A summary of the tabulated data of tables I, II, and III showing the effects of drooped-nose-flap deflection on the span load distribution at angles of attack of approximately 14.2° and 23.8° is presented in figure 29. The span load distribution shows that, as the drooped-nose-flap deflection increases to 40°, the loading on the inboard sections decreases, whereas the loading on the outboard sections increases.

Effect of Combined Deflections of Drooped-Nose and Plain Flaps

The effect of combined deflections of the drooped-nose and plain flaps on the chordwise pressure distribution of the wing is shown in figure 30 to consist of a delay in the appearance of negative pressure peaks at the leading edge of the wing as well as to produce an increase in the loading at the aft end of the 5-, 10-, 20-, and 40-percent-semispan sections. The influence of the separation vortex first appears on the outboard portion of the wing at an angle of attack of 15.9°, which is about a 2° lower angle of attack than for the wing with the drooped-nose flap deflected alone and moved inboard as the angle of attack increased. However, the region of separation did not extend beyond the 20-percent-semispan section for the highest angle of attack tested. The spanwise flow of the boundary layer along the leading edge of the wing moved progressively inboard with increasing angle of attack (fig. 34).

In general, the slopes of the section lift curves up to an angle of attack of about 14° (fig. 31) are lower than the slopes of the section lift curves for the corresponding basic-wing sections, through the same angle-of-attack range, because of the lifting inefficiency

of the drooped-nose flap at the lower angles of attack due to the delay of the formation of the separation vortex. For angles of attack greater than 16°, the drooped-nose flap is effective, so that at an angle of attack of 21°, the slopes of all the section lift curves are higher than the slopes of the corresponding section lift curves for any configuration tested. The slopes at this angle of attack increase from about 0.09 per degree for the 5- and 80-percent-semispan sections to about 0.14 per degree for the 10-, 20-, 40-, and 60-percent-semispan sections. These results indicate the predominant effect on the wing lift characteristics of the drooped-nose flap over the plain flap. The increases in lift-curve slope above those for other configurations are greater for the 5-, 10-, and 20-percent-semispan sections than for the 40-, 60-, and 80-percent-semispan sections.

Although peak values of section lift coefficients were not obtained for the range of angles of attack investigated (figs. 31 and 32), the highest section lift coefficients that were attained ($c_l \approx 1.46$ at the 10-, 20-, and 40-percent spanwise stations) indicate that the flap combination produced a considerable increase in section lift coefficients at the high angles of attack as compared with any previous configuration, particularly for the 60- and 80-percent-semispan sections.

The span load distributions for the combined flap configuration (fig. 33) show a similarity to a combination of the separate effects of the drooped-nose flap deflected 40° and the plain flap deflected 40°. The inboard sections carry more load than the drooped-nose-flap configuration but less load than the plain-flap configuration. The outboard sections carry less load than the drooped-nose-flap configuration and more load than the plain-flap configurations.

SUMMARY OF RESULTS

The results of an investigation of the effect of drooped-nose-flap and plain-flap deflection on the pressure distribution over a wing with the leading edge swept back 47.5° and having symmetrical circular-arc airfoil sections showed the following:

1. A separation vortex was formed along the leading edge of the basic wing at a low angle of attack as a result of flow separation from the sharp leading edge. With increasing angle of attack the diameter of the separation vortex increased over the outboard spanwise stations until, at an angle of attack of about 11°, the core turned back along the chord and a trailing vortex was shed off the wing at about 70 percent of the semispan. This type of flow was most pronounced on the basic wing and appreciably influenced the pressure distributions.

2. In general, the chordwise pressure distributions of the basic wing showed high, narrow, peak-negative-pressure coefficients at the nose for the most inboard station (5-percent-semispan) and in the spanwise direction these peaks progressively became lower and broader. The 80-percent-semispan section was stalled for angles of attack greater than 10.2°, whereas the 60-percent section was stalled for angles of attack greater than 16°.

3. The maximum values of section lift coefficient attained for the basic wing were considerably higher than the two-dimensional values for all spanwise stations inboard of the station where the vortex core left the wing. The highest value of maximum section lift coefficient of 1.08 was measured at the 40-percent spanwise station, whereas the lowest value of 0.51 was measured at the 80-percent station.

4. The span load distribution of the basic wing did not agree with that predicted by the methods based on potential flow.

5. The effect of yaw on the basic wing was to increase the tip stalling of the advancing wing and also to increase the lift of the inboard sections of the advancing wing. These trends increased with increasing yaw, and for the highest yaw angle of 9.8° the effects of the separation vortex were evident on the retreating wing out to 80 percent of the semispan for the entire angle-of-attack range.

6. The effect of deflecting an inboard semispan plain flap 40° is to cause the formation of the separation vortex at a 2° earlier angle of attack than for the basic wing and to increase the loading over the inboard sections. The effect of the separation vortex on the span load distribution is essentially the same as that for the basic wing.

7. Deflecting the drooped-nose flap 10°, 20°, 30°, and 40° progressively increases the angle of attack at which the separation vortex forms and also increases the maximum section lift coefficients for the outboard stations. With the drooped-nose flap deflected 40°, the span load distribution approaches the additional load distribution predicted by the method based on potential flow.

8. The combined deflections of the drooped-nose and plain flaps give the highest values of section lift-curve slope (0.141 per degree) and section lift coefficients (1.46 between 10 and 20 percent of the

semispan) attained in the tests at high angles of attack. The resulting span load distribution shows a similarity to the combination of the separate effects of each flap.

Langley Aeronautical Laboratory
National Advisory Committee for Aeronautics
Langley Air Force Base, Va.

REFERENCES

1. Proterra, Anthony J.: Aerodynamic Characteristics of a 45° Swept-Back Wing with Aspect Ratio of 3.5 and NACA 2S-50(05)-50(05) Airfoil Sections. NACA RM L7C11, 1947.

2. Guryansky, Eugene R., and Lipson, Stanley: Effect of High-Lift Devices on the Longitudinal and Lateral Characteristics of a 45° Sweptback Wing with Symmetrical Circular-Arc Sections. NACA RM L8D06, 1948.

3. Neely, Robert H., and Conner, D. William: Aerodynamic Characteristics of a 42° Swept-Back Wing with Aspect Ratio 4 and NACA 64_1-112 Airfoil Sections at Reynolds Numbers from 1,700,000 to 9,500,000. NACA RM L7D14, 1947.

4. Fitzpatrick, James E., and Foster, Gerald V.: Static Longitudinal Aerodynamic Characteristics of a 52° Sweptback Wing of Aspect Ratio 2.88 at Reynolds Numbers from 2,000,000 to 11,000,000. NACA RM L8H25, 1948.

5. Anderson, Adrien E.: Chordwise and Spanwise Loadings Measured at Low Speed on Large Triangular Wings. NACA RM A9B17, 1949.

6. Underwood, William J., and Nuber, Robert J.: Aerodynamic Load Measurements over Leading-Edge and Trailing-Edge Plain Flaps on a 6-Percent-Thick Symmetrical Circular-Arc Airfoil Section. NACA RM L7H04, 1947.

7. Wilson, Herbert A., Jr., and Lovell, J. Calvin: Full-Scale Investigation of the Maximum Lift and Flow Characteristics of an Airplane Having Approximately Triangular Plan Form. NACA RM L6K20, 1947.

8. Jones, Robert T.: Effects of Sweepback on Boundary Layer and Separation. NACA Rep. 884, 1947.

9. Underwood, William J., and Nuber, Robert J.: Two-Dimensional Wind-Tunnel Investigation at High Reynolds Numbers of Two Symmetrical Circular-Arc Airfoil Sections with High-Lift Devices. NACA RM L6K22, 1947.

10. DeYoung, John: Theoretical Additional Span Loading Characteristics of Wings with Arbitrary Sweep, Aspect Ratio, and Taper Ratio. NACA TN 1491, 1947.

TABLE I.- PRESSURE COEFFICIENTS FOR THE WING WITH DROOPED-NOSE FLAPS DEFLECTED

(a) $\delta_n = 10^\circ$

		$\alpha = 4.9^\circ$						$\alpha = 8.6^\circ$					
	x/c	$\frac{2y}{b} = 0.05$	0.10	0.20	0.40	0.60	0.80	$\frac{2y}{b} = 0.05$	0.10	0.20	0.40	0.60	0.80
Upper surface	2.5	0.16	0.06	-0.06	-0.33	-0.51	-0.20	0.03	-0.90	-0.90	-1.00	-1.00	-0.90
	7.5	-.31	0	-.06	-.40	-.14	-.11	-.30	-.06	-----	-.39	-.55	-.90
	15.0	-.08	-.15	-.18	-.21	-.20	-.20	-.23	-.26	-.29	-.39	-.62	-.51
	18.0	-.25	-.34	-.35	-.34	-.34	-.35	-.41	-.47	-.50	-.40	-.42	-.40
	22.5	-.25	-.29	-.30	-.35	-.21	-----	-.39	-.39	-.44	-.45	-.44	-----
	32.5	-.21	-.25	-.28	-.29	-.30	-.33	-.34	-.36	-.40	-.38	-.39	-.39
	42.5	-.22	-.25	-.25	-.25	-.28	-----	-.32	-.34	-.35	-.34	-.35	-----
	52.5	-.24	-.25	-.24	-.26	-.28	-.25	-.32	-.30	-.31	-.34	-.34	-.26
	62.5	-.21	-.24	-.23	-.20	-.20	-.19	-.28	-.25	-.28	-.26	-.24	-.19
	75.0	-.18	-.19	-.15	-.14	-.15	-.11	-.21	-.20	-.20	-.15	-.15	-.09
	85.0	-.10	-.10	-.06	-.06	-.05	-.05	-.11	-.09	-.08	-.06	-.06	-.03
	92.5	0	.04	.05	.01	.01	.05	.01	.05	.04	0	0	.04
	97.5	.15	.15	.14	.10	.10	.12	.15	.15	.10	.09	.08	.09
Lower surface	95.0	.08	.08	.05	0	.10	.08	.10	.10	.06	.04	.06	.05
	85.0	----	-.05	-.05	-.16	0	-----	----	0	-.01	-.10	-.02	-----
	75.0	-.05	-.05	.05	-.22	-.02	-.04	0	.01	0	-.15	-.02	-.01
	52.5	-.03	-.04	-.03	.05	-.10	-.04	.10	.08	.05	.10	-.06	.04
	42.5	.04	0	.05	.13	-.08	-.01	.15	.14	.12	.16	-.03	.08
	30.0	.19	.15	-----	.15	.03	.06	.30	.25	-----	.21	.08	.15
	15.0	.20	.19	.19	.17	.15	.10	.34	.32	.30	.30	.24	.21
	5.0	.22	.21	.22	.25	.26	.16	.40	.40	.37	.40	.35	.31

TABLE I.- PRESSURE COEFFICIENTS FOR THE WING WITH DROOPED-NOSE FLAPS DEFLECTED - Continued

(a) $\delta_n = 10^\circ$ - Continued

		$\alpha = 12.3^\circ$						$\alpha = 14.2^\circ$					
	x/c	$\frac{2y}{b} = 0.05$	0.10	0.20	0.40	0.60	0.80	$\frac{2y}{b} = 0.05$	0.10	0.20	0.40	0.60	0.80
Upper surface	2.5	-1.29	-1.88	-1.26	-1.30	-1.11	-0.77	-2.22	-2.31	-1.60	-1.41	-1.10	-0.73
	7.5	-----	-.49	-1.57	-----	-----	-.73	-----	-.93	-2.06	-----	-----	-.71
	15.0	-.37	-.31	-.85	-1.39	-1.15	-.70	-.44	-.31	-1.33	-1.50	-1.06	-.67
	18.0	-.54	-.58	-.39	-.99	-1.11	-.68	-.59	-.60	-.36	-1.39	-1.07	-.65
	22.5	-.49	-.50	-.45	-.60	-.47	-----	-.55	-.54	-.40	-1.21	-.89	-----
	32.5	-.42	-.45	-.45	-.50	-.96	-.62	-.48	-.48	-.43	-1.08	-1.11	-.60
	42.5	-.40	-.40	-.40	-.35	-.70	-----	-.44	-.45	-.40	-.70	-1.06	-----
	52.5	-.37	-.36	-.35	-.31	-.50	-.50	-.41	-.40	-.36	-.38	-.97	-.55
	62.5	-.31	-.30	-.30	-.26	-.30	-.44	-.35	-.34	-.31	-.22	-.75	-.55
	75.0	-.24	-.23	-.21	-.15	-.19	-.38	-.25	-.23	-.22	-.11	-.47	-.48
	85.0	-.14	-.10	-.05	-.05	-.08	-.31	-.14	-.10	-.07	-.04	-.25	-.45
	92.5	0	.05	.05	.04	-.01	-.25	.02	.06	.06	.03	-.12	-.14
	97.5	.15	.15	.13	.09	.05	-.21	.16	.14	.14	.14	-.04	-.38
Lower surface	95.0	.10	.11	.08	.07	.05	-.10	.12	.12	.10	.10	.05	-.20
	85.0	-----	.05	.04	-.05	-.01	-----	-----	.08	.05	-.02	.01	-----
	75.0	.08	.08	.05	-.07	.01	-.02	.11	.12	.08	-.05	.05	-.05
	52.5	.17	.16	.14	.20	.01	.07	.22	.21	.18	.24	.06	.08
	42.5	.23	.24	.20	.25	.06	.14	.29	.27	.25	.30	.12	.15
	30.0	.36	.35	-----	.34	.16	.23	.43	.40	-----	.35	.22	.24
	15.0	.45	.41	.40	.40	.31	.31	.50	.47	.43	.43	.37	.34
	5.0	.54	.51	.46	.50	.45	.40	.59	.56	.53	.52	.50	.43

TABLE I.- PRESSURE COEFFICIENTS FOR THE WING WITH DROOPED-NOSE FLAPS DEFLECTED - Continued

(a) $\delta_n = 10^\circ$ - Concluded

	$\alpha = 19.9^\circ$							$\alpha = 23.8^\circ$					
	x/c	$\frac{2y}{b} = 0.05$	0.10	0.20	0.40	0.60	0.80	$\frac{2y}{b} = 0.05$	0.10	0.20	0.40	0.60	0.80
Upper surface	2.5	-4.10	-2.94	-2.12	-1.48	-0.90	-0.59	-5.20	-3.15	-2.09	-1.20	-0.85	-0.56
	7.5	-----	-2.70	-2.37	-----	-----	-.59	------	-3.97	-2.23	-----	-----	-.55
	15.0	-.53	-.34	-2.78	-1.44	-.85	-.58	-.55	-1.13	-2.23	-1.15	-.78	-.53
	18.0	-.72	-.65	-1.42	-1.40	-.83	-.56	-.80	-.72	-1.90	-1.12	-.75	-.51
	22.5	-.69	-.60	-.56	-1.38	-1.13	-----	-.80	-.65	-1.53	-1.12	-.89	-----
	32.5	-.59	-.56	-.39	-1.35	-.80	-.54	-.71	-.65	-1.30	-1.11	-.72	-.49
	42.5	-.55	-.53	-.36	-1.20	-.79	-----	-.69	-.65	-.99	-1.05	-.70	-----
	52.5	-.51	-.48	-.36	-1.05	-.79	-.51	-.66	-.59	-.80	-1.00	-.70	-.47
	62.5	-.45	-.41	-.31	-.90	-.72	-.50	-.59	-.52	-.64	-.96	-.66	-.44
	75.0	-.34	-.30	-.24	-.59	-.68	-.46	-.46	-.40	-.46	-.79	-.64	-.42
	85.0	-.19	-.12	-.09	-.37	-.66	-.44	-.29	-.23	-.24	-.69	-.61	-.40
	92.5	-.01	.05	.06	-.24	-.70	-.41	-.05	0	-.09	-.64	-.64	-.38
	97.5	.13	.13	.15	-.18	-.80	-.39	-.07	.09	-.02	-.72	-.67	-.38
Lower surface	95.0	.13	.13	.13	0	-.35	-.24	.11	.14	.06	-.24	-.34	-.22
	85.0	-----	.14	.11	-.02	-.20	-----	-----	.15	.10	-.10	-.21	-----
	75.0	.20	.19	.17	-.02	-.04	-.07	.24	.24	.19	-.03	-.05	-.06
	52.5	.35	.34	.31	.31	.10	.10	.41	.40	.36	.32	.11	.12
	42.5	.42	.40	.38	.39	.17	.18	.50	.49	.45	.42	.20	.21
	30.0	.55	.51	-----	.46	.29	.30	.61	.60	-----	.48	.32	.31
	15.0	.64	.60	.60	.57	.45	.40	.71	.69	.65	.57	.48	.42
	5.0	.71	.66	.65	.64	.54	.48	.79	.75	.68	.62	.55	.50

TABLE I.- PRESSURE COEFFICIENTS FOR THE WING WITH DROOPED-NOSE FLAPS DEFLECTED - Continued

(b) $\delta_n = 20^\circ$

		$\alpha = 4.9^\circ$						$\alpha = 10.5^\circ$					
	x/c	$\frac{2y}{b} = 0.05$	0.10	0.20	0.40	0.60	0.80	$\frac{2y}{b} = 0.05$	0.10	0.20	0.40	0.60	0.80
Upper surface	2.5	0.44	0.32	0.26	0.21	0.17	0.20	0.08	-0.11	-0.69	-0.99	-0.97	-0.90
	7.5	----	.14	.09	----	----	.07	----	-.11	-.18	-----	-----	-.66
	15.0	0	-.06	-.10	-.11	-.14	-.10	-.22	-.29	-.37	-.40	-.40	-.39
	18.0	-.32	-.35	-.40	-.39	-.38	-.35	-.56	-.60	-.68	-.68	-.64	-.66
	22.5	-.34	-.35	-.39	-.44	-.48	----	-.54	-.55	-.60	-.67	-.72	-----
	32.5	-.25	-.29	-.33	-.34	-.36	-.36	-.44	-.45	-.50	-.53	-.56	-.57
	42.5	-.25	-.27	-.28	-.28	-.30	----	-.39	-.38	-.41	-.42	-.45	-----
	52.5	-.25	-.25	-.25	-.29	-.30	-.27	-.36	-.35	-.35	-.38	-.40	-.34
	62.5	-.23	-.22	-.23	-.24	-.24	-.20	-.31	-.30	-.30	-.30	-.27	-.23
	75.0	-.18	-.16	-.18	-.15	-.18	-.12	-.24	-.21	-.20	-.16	-.18	-.11
	85.0	-.10	-.09	-.06	-.08	-.09	-.05	-.14	-.10	-.05	-.06	-.05	-.02
	92.5	.02	.05	.05	0	0	.04	.01	.05	.05	.04	.04	.06
	97.5	.15	.15	.13	.08	.10	.12	.13	.13	.10	.09	.10	.09
Lower surface	95.0	.07	.09	.07	.01	.09	.07	.08	.10	.05	.05	.07	.04
	85.0	----	-.02	-.02	-.18	-.02	----	----	.02	0	-.09	0	-----
	75.0	-.05	-.02	-.02	-.21	-.04	-.04	.04	.06	.03	-.14	0	0
	52.5	0	.01	.01	.09	-.11	-.02	.13	.14	.01	.17	0	.06
	42.5	.08	.06	.06	.15	-.07	.01	.20	.18	.18	.25	.05	.12
	30.0	.26	.21	----	.21	.05	.12	.36	.35	-----	.32	.17	.25
	15.0	.17	.20	.18	.16	.11	.08	.33	.35	.32	.32	.28	.25
	5.0	.05	.06	.05	.12	.11	.01	.31	.35	.35	.39	.38	.31

NACA

TABLE I.- PRESSURE COEFFICIENTS FOR THE WING WITH DROOPED-NOSE FLAPS DEFLECTED - Continued

(b) $\delta_n = 20^\circ$ - Continued

	$\alpha = 14.2^\circ$							$\alpha = 16.2^\circ$					
	x/c	$\frac{2y}{b} = 0.05$	0.10	0.20	0.40	0.60	0.80	$\frac{2y}{b} = 0.05$	0.10	0.20	0.40	0.60	0.80
Upper surface	2.5	0.01	-1.27	-1.20	-1.38	-1.41	-1.25	-0.38	-1.79	-1.73	-1.63	-1.50	-1.20
	7.5	----	-.13	-1.30	-----	-----	-1.28	-----	-.37	-1.63	-----	-----	-1.21
	15.0	-.35	-.40	-.38	-1.03	-1.51	-1.28	-.42	-.42	-.69	-1.68	-1.54	-1.15
	18.0	-.70	-.78	-.75	-.60	-1.06	-.93	-.77	-.85	-.69	-.80	-1.34	-1.11
	22.5	-.64	-.67	-.70	-.70	-.78	-----	-.69	-.71	-.72	-.70	-1.04	-----
	32.5	-.51	-.54	-.60	-.59	-.67	-.65	-.56	-.58	-.64	-.60	-.91	-1.00
	42.5	-.45	-.47	-.50	-.47	-.50	-----	-.48	-.50	-.50	-.48	-.66	-----
	52.5	-.42	-.40	-.40	-.41	-.41	-.39	-.45	-.43	-.41	-.44	-.46	-.76
	62.5	-.35	-.33	-.34	-.31	-.28	-.28	-.37	-.35	-.34	-.31	-.29	-.63
	75.0	-.25	-.23	-.21	-.17	-.16	-.16	-.26	-.23	-.21	-.17	-.14	-.46
	85.0	-.14	-.09	-.06	-.06	-.05	-.09	-.15	-.09	-.08	-.05	-.04	-.34
	92.5	.02	.06	.06	.03	.02	-.04	.02	.06	.05	.03	.04	-.22
	97.5	.15	.13	.10	.07	.05	-.04	.15	.11	.10	.05	.05	-.15
Lower surface	95.0	.12	.11	.08	.05	.05	-.01	.14	.11	.09	.04	.05	-.05
	85.0	----	.06	.05	-.04	0	-----	-----	.10	.06	-.04	.04	-----
	75.0	.11	.11	.09	-.06	.05	.01	.15	.14	.12	-.05	.09	.01
	52.5	.22	.21	.19	.25	.07	.11	.27	.25	.23	.27	.11	.14
	42.5	.30	.27	.26	.32	.13	.18	.35	.32	.29	.35	.17	.21
	30.0	.45	.41	-----	.39	.24	.29	.49	.46	-----	.41	.27	.32
	15.0	.43	.43	.43	.41	.35	.33	.49	.49	.45	.45	.40	.36
	5.0	.45	.48	.48	.49	.45	.40	.53	.55	.53	.55	.50	.45

TABLE I.- PRESSURE COEFFICIENTS FOR THE WING WITH DROOPED-NOSE FLAPS DEFLECTED - Continued

(b) $\delta_n = 20^\circ$ - Concluded

		$\alpha = 19.9^\circ$						$\alpha = 23.8^\circ$					
	x/c	$\frac{2y}{b} = 0.05$	0.10	0.20	0.40	0.60	0.80	$\frac{2y}{b} = 0.05$	0.10	0.20	0.40	0.60	0.80
Upper surface	2.5	-3.85	-2.52	-2.03	-1.92	-1.26	-0.89	-6.47	-2.89	-2.25	-1.50	-1.01	-0.65
	7.5	-----	-1.28	-2.79	-----	-----	-.75	-----	-2.60	-2.64	-----	-----	-.59
	15.0	-.55	-.41	-1.59	-2.02	-1.20	-.73	-.60	-.39	-2.69	-1.44	-.95	-.57
	18.0	-.54	-.88	-.52	-1.88	-1.12	-.70	-.99	-.90	-1.40	-1.39	-.90	-.55
	22.5	-.84	-.79	-.69	-1.54	-1.08	-----	-.90	-.88	-.80	-1.30	-.89	-----
	32.5	-.66	-.66	-.63	-1.37	-1.08	-.67	-.75	-.75	-.70	-1.26	-.85	-.51
	42.5	-.58	-.56	-.55	-.94	-1.05	-----	-.65	-.68	-.59	-1.15	-.81	-----
	52.5	-.51	-.48	-.45	-.52	-.97	-.60	-.59	-.59	-.54	-1.05	-.80	-.50
	62.5	-.44	-.39	-.36	-.34	-.85	-.58	-.50	-.50	-.45	-.95	-.75	-.49
	75.0	-.31	-.25	-.24	-.19	-.68	-.55	-.38	-.35	-.31	-.70	-.70	-.45
	85.0	-.15	-.09	-.05	-.09	-.50	-.51	-.21	-.17	-.10	-.51	-.66	-.44
	92.5	.01	.05	.06	-.01	-.40	-.49	-.04	0	.05	-.40	-.71	-.40
	97.5	.12	.12	.10	.05	-.38	-.46	.09	.05	.06	-.47	-.80	-.39
Lower surface	95.0	.15	.15	.10	.09	-.10	-.25	.15	.14	.10	-.06	-.35	-.21
	85.0	-----	.15	.11	.04	-.05	-----	-----	.15	.15	-.02	-.16	-----
	75.0	.20	.20	.16	.04	.05	-.05	.25	.25	.20	.03	-.03	-.04
	52.5	.36	.35	.30	.34	.15	.15	.44	.40	.36	.35	.15	.15
	42.5	.44	.41	.38	.40	.20	.22	.51	.54	.45	.45	.24	.25
	30.0	.58	.55	-----	.46	.31	.34	.65	.60	-----	.50	.33	.40
	15.0	.60	.57	.54	.52	.43	.40	.70	.65	.61	.56	.45	.45
	5.0	.66	.63	.59	.56	.51	.49	.75	.74	.65	.61	.51	.50

TABLE I.- PRESSURE COEFFICIENTS FOR THE WING WITH DROOPED-NOSE FLAPS DEFLECTED - Continued

(c) $\delta_n = 30°$

		$\alpha = 12.5°$						$\alpha = 18.2°$					
	x/c	$\frac{2y}{b} = 0.05$	0.10	0.20	0.40	0.60	0.80	$\frac{2y}{b} = 0.05$	0.10	0.20	0.40	0.60	0.80
Upper surface	2.5	0.28	0.15	0.01	-0.41	-0.71	-0.66	0.01	-1.01	-1.25	-1.54	-1.73	-1.63
	7.5	----	0	-.10	-----	-----	-.26	----	-.16	-.10	-----	-----	-1.69
	15.0	-.16	-.28	-.38	-.45	-.49	-.45	-.41	-.51	-.50	-.77	-1.35	-1.63
	18.0	-.65	-.75	-.88	-.89	-.90	-.86	-.90	-1.01	-1.09	-.95	-.99	-1.03
	22.5	-.65	-.69	-.76	-.88	-.99	-----	-.82	-.89	-.99	-1.01	-1.07	-----
	32.5	-.50	-.55	-.60	-.66	-.72	-.70	-.65	-.70	-.76	-.80	-.85	-.78
	42.5	-.45	-.46	-.46	-.50	-.55	-----	-.55	-.56	-.59	-.60	-.64	-----
	52.5	-.40	-.40	-.40	-.44	-.45	-.36	-.49	-.49	-.46	-.50	-.49	-.45
	62.5	-.34	-.34	-.31	-.34	-.31	-.24	-.41	-.40	-.35	-.35	-.32	-.34
	75.0	-.25	-.24	-.20	-.20	-.17	-.10	-.29	-.26	-.21	-.16	-.20	-.25
	85.0	-.45	-.10	-.05	-.06	-.04	-.01	-.15	-.11	-.05	-.05	-.10	-.17
	92.5	.01	.05	.05	.01	.05	.05	0	.04	.05	.04	-.05	-.05
	97.5	.15	.11	.10	.05	.06	.07	.15	.11	.10	.04	-.02	-.14
Lower surface	95.0	.10	.10	.09	.04	.06	.05	.15	.11	.10	.05	.01	-.05
	85.0	----	.05	.04	-.06	0	-----	----	.11	.11	.01	0	-----
	75.0	.06	.07	.07	-.10	.05	.04	.18	.19	.16	.01	.09	.05
	52.5	.19	.17	.16	.20	.05	.14	.31	.30	.30	.31	.15	.16
	42.5	.25	.25	.25	.26	.11	.20	.40	.40	.35	.39	.20	.25
	30.0	.45	.40	----	.36	.24	.30	.55	.51	-----	.45	.30	.35
	15.0	.35	.36	.36	.33	.30	.29	.50	.50	.50	.45	.40	.36
	5.0	.21	.25	.34	.33	.35	.31	.45	.50	.51	.52	.50	.45

TABLE I.- PRESSURE COEFFICIENTS FOR THE WING WITH DROOPED-NOSE FLAPS DEFLECTED - Continued

(c) $\delta_n = 30^\circ$ - Continued

	$\alpha = 20.0^\circ$							$\alpha = 21.8^\circ$					
	x/c	$\frac{2y}{b} = 0.05$	0.10	0.20	0.40	0.60	0.80	$\frac{2y}{b} = 0.05$	0.10	0.20	0.40	0.60	0.80
Upper surface	2.5	0	-1.49	-1.54	-1.87	-2.06	-1.59	-0.90	-1.96	-1.78	-2.13	-2.17	-1.44
	7.5	----	-.14	-1.59	-----	-----	-1.60	-----	-.25	-2.16	-----	-----	-1.35
	15.0	-.48	-.55	-.50	-1.78	-2.07	-1.59	-.55	-.54	-.70	-2.39	-2.21	-1.31
	18.0	-.99	-1.10	-1.12	-1.00	-1.34	-1.39	-1.04	-1.11	-1.00	-1.21	-1.88	-1.20
	22.5	-.85	-.95	-1.00	-.98	-1.06	-----	-.95	-.99	-.99	-.97	-.98	-----
	32.5	-.69	-.75	-.80	-.85	-.89	-1.06	-.74	-.75	-.81	-.85	-1.25	-1.00
	42.5	-.56	-.60	-.63	-.64	-.65	-----	-.60	-.60	-.63	-.65	-.85	-----
	52.5	-.50	-.50	-.50	-.52	-.50	-.73	-.54	-.50	-.50	-.50	-.55	-.91
	62.5	-.41	-.41	-.40	-.37	-.35	-.57	-.44	-.40	-.38	-.36	-.31	-.85
	75.0	-.29	-.29	-.23	-.20	-.20	-.41	-.30	-.26	-.21	-.20	-.16	-.70
	85.0	-.16	-.11	-.05	-.10	-.10	-.31	-.16	-.10	-.04	-.08	-.08	-.59
	92.5	.01	.02	.05	-.05	-.05	-.25	0	.05	.05	-.04	-.05	-.45
	97.5	.15	.11	.09	-.05	-.03	-.18	.15	.12	.09	-.04	-.05	-.39
Lower surface	95.0	.15	.15	.10	.05	.04	-.05	.17	.16	.14	.05	.05	-.11
	85.0	----	.15	.15	.05	.03	-----	-----	.19	.15	.05	.05	-----
	75.0	.20	.20	.20	.05	.10	.06	.25	.25	.24	.05	.15	.05
	52.5	.39	.35	.35	.35	.20	.20	.44	.40	.36	.40	.25	.22
	42.5	.45	.44	.43	.41	.25	.30	.50	.45	.45	.45	.30	.30
	30.0	.60	.55	-----	.49	.36	.40	.64	.60	-----	.54	.40	.40
	15.0	.55	.55	.55	.50	.45	.43	.60	.60	.58	.55	.55	.44
	5.0	.54	.55	.57	.55	.54	.49	.60	.60	.60	.58	.55	.50

TABLE I.- PRESSURE COEFFICIENTS FOR THE WING WITH DROOPED-NOSE FLAPS DEFLECTED - Concluded

(c) $\delta_n = 30^\circ$ - Concluded

	$\alpha = 23.8^\circ$						
	x/c	$\frac{2y}{b} = 0.05$	0.10	0.20	0.40	0.60	0.80
Upper surface	2.5	-1.64	-2.43	-2.07	-2.31	-1.63	-1.00
	7.5	-----	-.80	-2.64	-----	-----	-.96
	15.0	-.57	-.51	-1.29	-2.46	-1.58	-.94
	18.0	-1.06	-1.16	-.90	-1.92	-1.49	-.86
	22.5	-.96	-.98	-1.03	-1.35	-1.31	-----
	32.5	-.75	-.80	-.87	-1.19	-1.25	-.75
	42.5	-.61	-.65	-.70	-.91	-1.12	-----
	52.5	-.55	-.53	-.55	-.65	-1.01	-.65
	62.5	-.44	-.44	-.45	-.47	-.90	-.64
	75.0	-.30	-.30	-.26	-.25	-.70	-.56
	85.0	-.15	-.10	-.06	-.13	-.50	-.55
	92.5	.04	.05	.05	-.05	-.40	-.50
	97.5	.16	.10	.06	-.05	-.35	-.47
Lower surface	95.0	.20	.18	.11	.05	-.07	-.25
	85.0	-----	.20	.15	.05	0	-----
	75.0	.30	.30	.24	.10	.10	0
	52.5	.50	.45	.40	.40	.24	.20
	42.5	.55	.54	.49	.50	.30	.30
	30.0	.66	.65	-----	.55	.40	.40
	15.0	.65	.65	.60	.58	.50	.45
	5.0	.65	.69	.63	.61	.55	.50

TABLE II.- SECTION LIFT COEFFICIENTS FOR THE WING WITH DROOPED-NOSE FLAPS DEFLECTED

$\delta_n = 10°$

α (deg)	2y/b					
	0.05	0.10	0.20	0.40	0.60	0.80
4.9	0.201	0.212	0.230	0.231	0.234	0.205
8.6	.367	.386	.390	.405	.388	.373
12.3	.534	.593	.604	.636	.668	.580
14.2	.637	.685	.706	.812	.895	.631
19.9	.830	.856	.951	1.173	.816	.577
23.8	.995	1.165	1.246	1.100	.752	.537

$\delta_n = 20°$

α (deg)	2y/b					
	0.05	0.10	0.20	0.40	0.60	0.80
4.9	0.182	0.205	0.203	0.199	0.186	0.185
10.5	.405	.420	.416	.431	.444	.439
14.2	.529	.559	.655	.636	.641	.626
16.2	.623	.651	.681	.718	.748	.621
19.9	.842	.858	.890	1.040	.981	.529
23.8	1.008	.949	1.030	1.156	.824	.578

$\delta_n = 30°$

α (deg)	2y/b					
	0.05	0.10	0.20	0.40	0.60	0.80
12.5	0.442	0.445	0.455	0.491	0.499	0.463
18.2	.629	.674	.635	.669	.737	.758
20.0	.689	.706	.778	.772	.847	.917
21.8	.766	.773	.857	.932	.955	.971
23.8	.834	.879	.956	1.089	1.097	.746

TABLE III.- LIFT COEFFICIENTS AND SPAN LOAD COEFFICIENTS FOR THE WING WITH DROOPED-NOSE FLAPS DEFLECTED

$\delta_n = 10°$

α (deg)	C_L	$\frac{c_l c}{C_L c_{av}}$					
		$\frac{2y}{b} = 0.05$	0.10	0.20	0.40	0.60	0.80
4.9	0.214	1.219	1.258	1.292	1.148	1.035	0.765
8.6	.371	1.281	1.316	1.262	1.159	.989	.802
12.3	.580	1.195	1.295	1.249	1.165	1.088	.809
14.2	.699	1.173	1.230	1.202	1.224	1.201	.715
19.9	.845	1.273	1.281	1.348	1.474	.913	.545
23.8	.900	1.432	1.637	1.659	1.297	.789	.476

$\delta_n = 20°$

α (deg)	C_L	$\frac{c_l c}{C_L c_{av}}$					
		$\frac{2y}{b} = 0.05$	0.10	0.20	0.40	0.60	0.80
4.9	0.182	1.290	1.424	1.335	1.160	0.961	0.808
10.5	.412	1.273	1.289	1.211	1.112	1.019	.850
14.2	.598	1.147	1.181	1.313	1.130	1.012	.835
16.2	.647	1.257	1.273	1.261	1.179	1.093	.766
19.9	.813	1.342	1.335	1.312	1.359	1.141	.519
23.8	.876	1.493	1.369	1.408	1.401	.889	.526

$\delta_n = 30°$

α (deg)	C_L	$\frac{c_l c}{C_L c_{av}}$					
		$\frac{2y}{b} = 0.05$	0.10	0.20	0.40	0.60	0.80
12.5	0.455	1.258	1.239	1.200	1.147	1.038	0.812
18.2	.662	1.231	1.288	1.151	1.073	1.053	.914
20.0	.790	1.131	1.132	1.181	1.160	1.013	.927
21.8	.862	1.152	1.134	1.191	1.149	1.046	.899
23.8	.903	1.197	1.232	1.269	1.281	1.148	.659

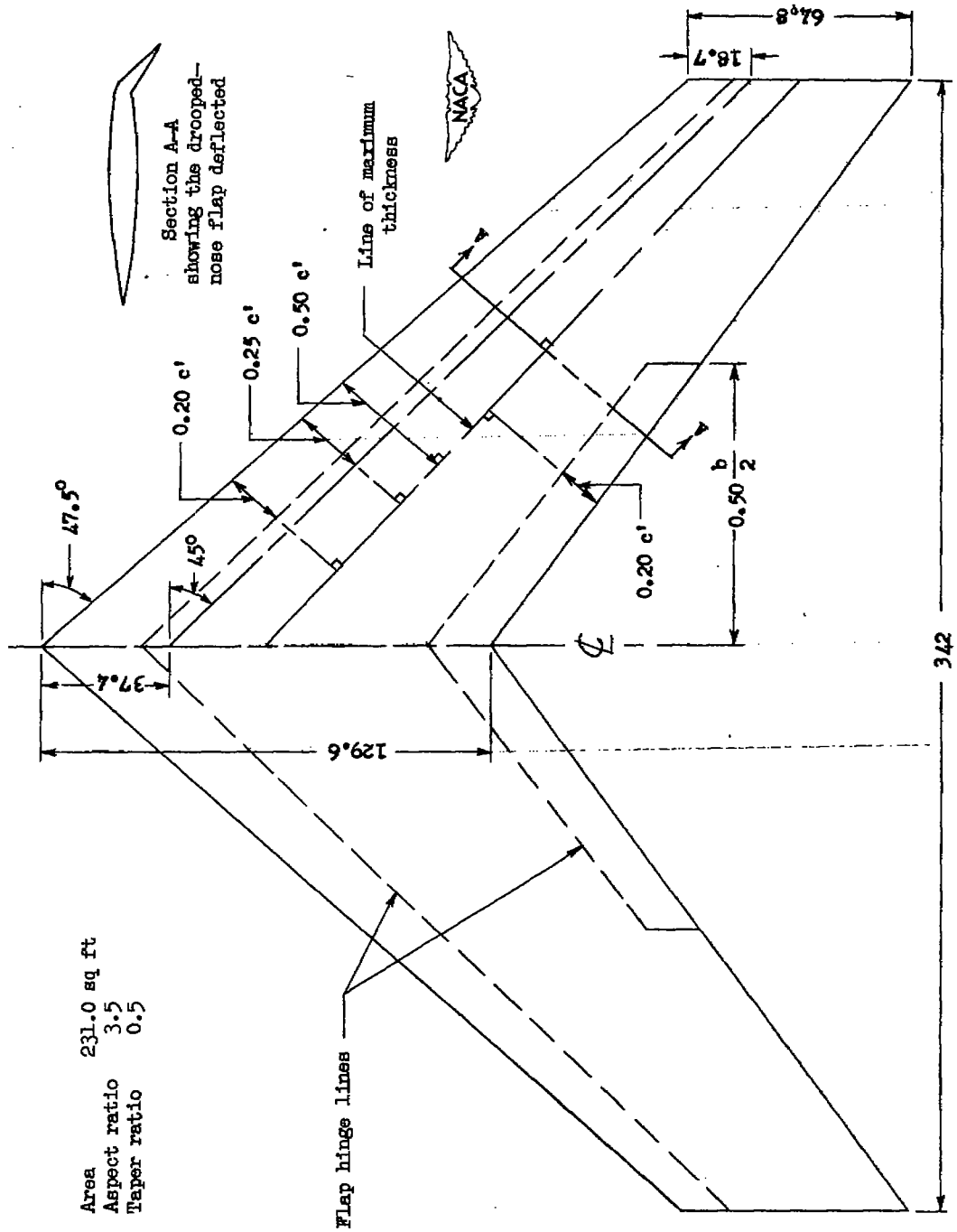

Figure 1.- Plan form of 47.5° swoptback wing. All dimensions are in inches.

Pressure orifice locations, percent chord	
Upper surface	Lower surface
2.5	5.0
7.5	15.0
15.0	30.0
18.5	42.5
22.5	52.5
32.5	75.0
42.5	85.0
52.5	95.0
62.5	
75.0	
85.0	
92.5	
97.5	

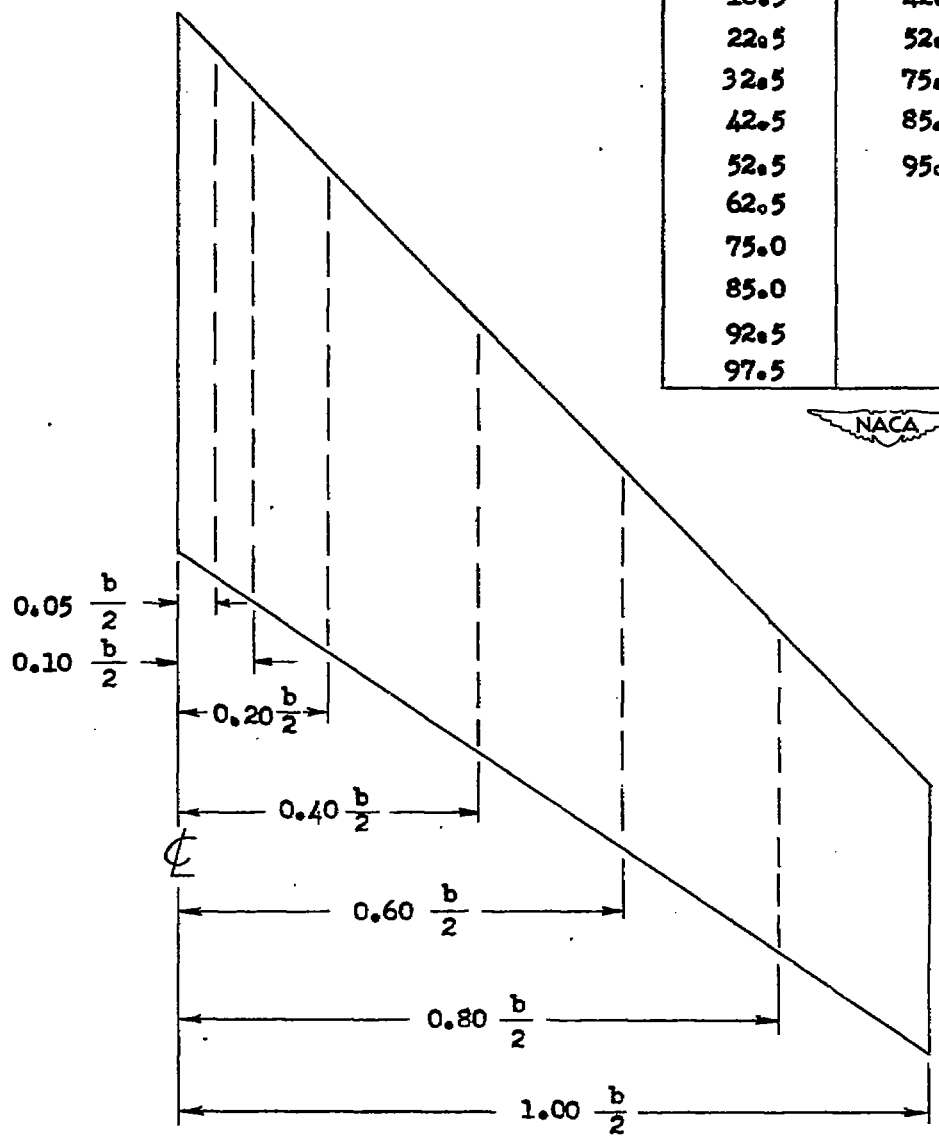

Figure 2.– Spanwise and chordwise locations of the pressure orifices.

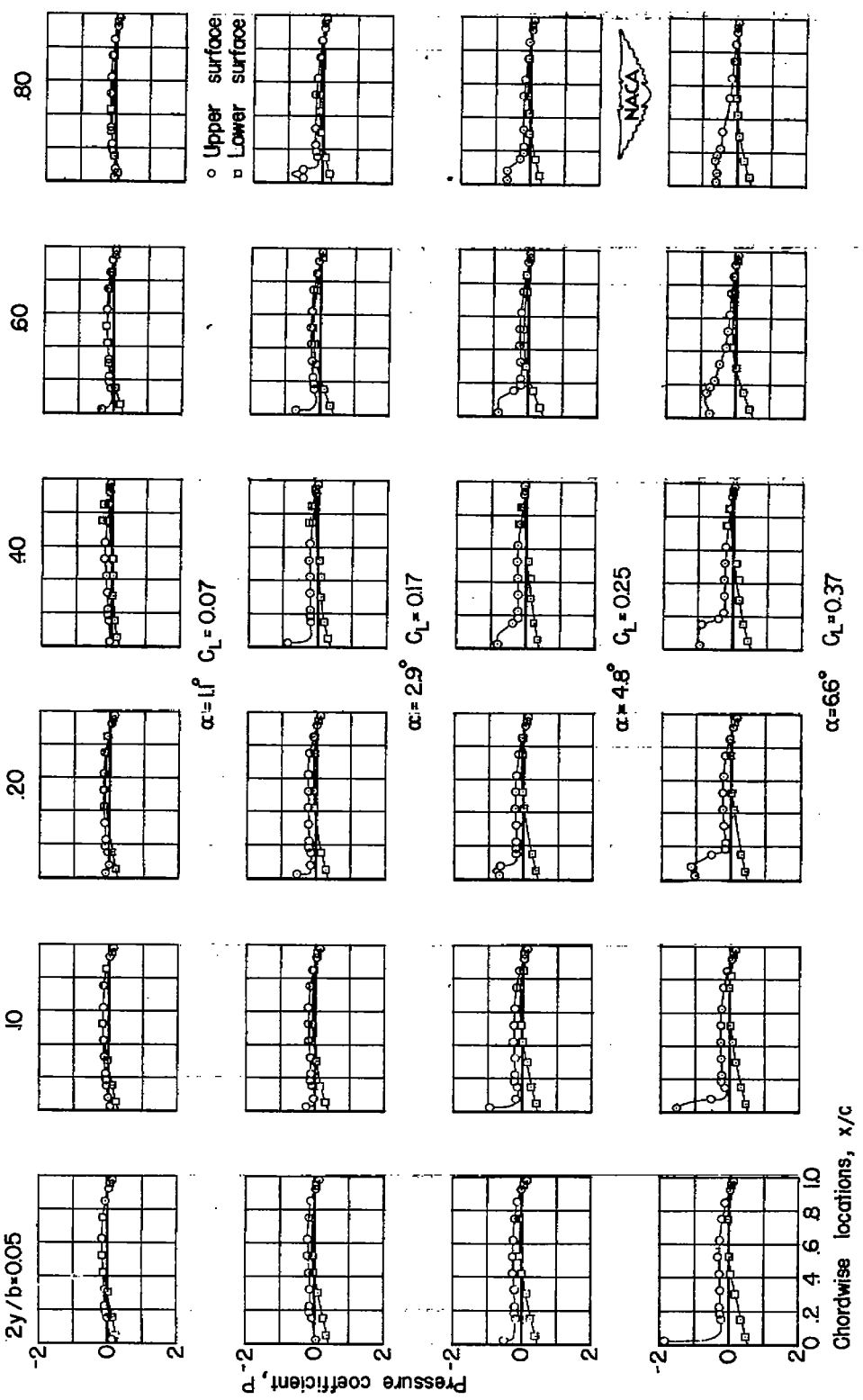

Figure 3.— Chordwise pressure distribution for six spanwise stations. Basic wing. $\psi = 0°$.

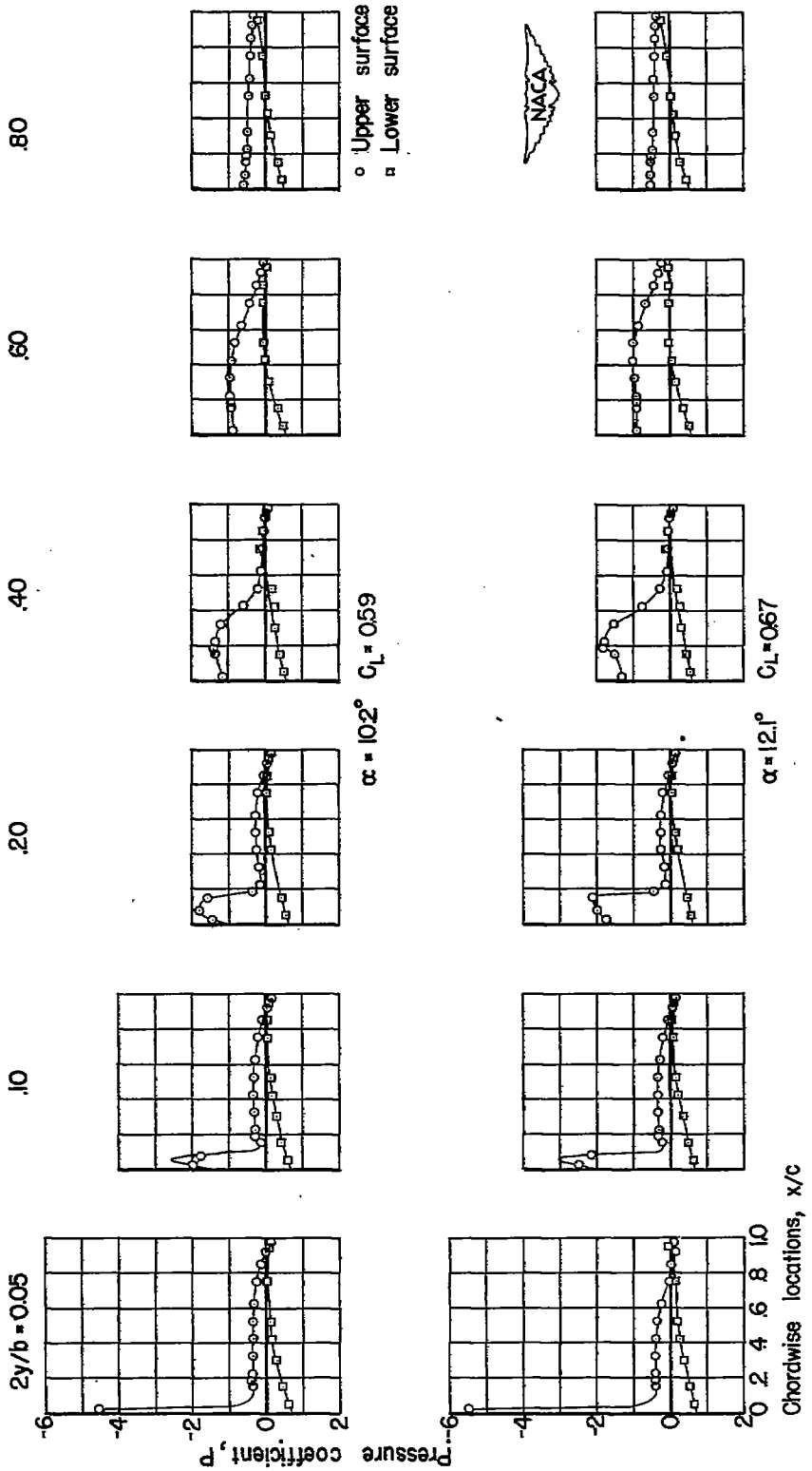

Figure 3.— Continued.

$\psi = 0°$

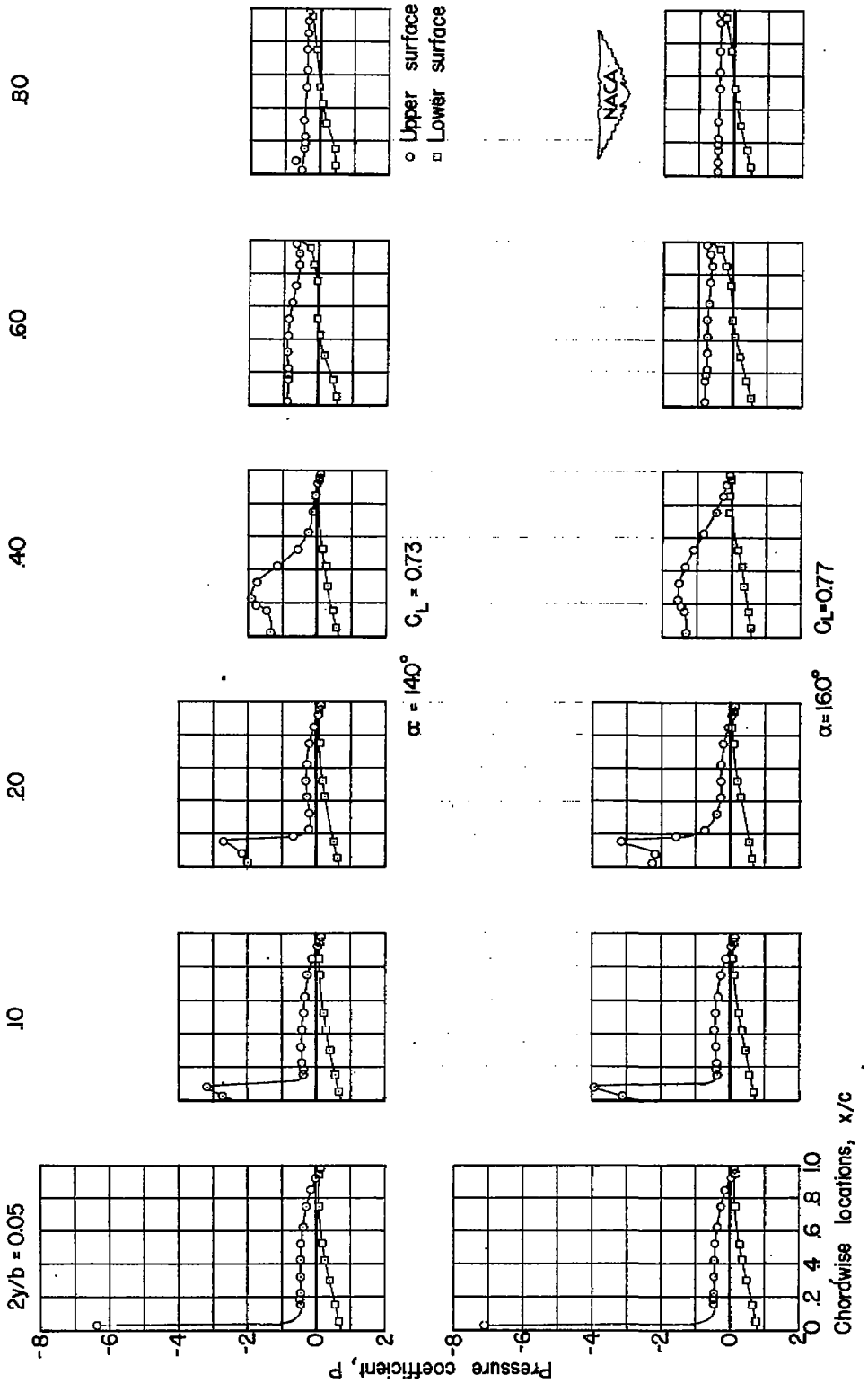

Figure 3.- Continued.

$\psi = 0°$

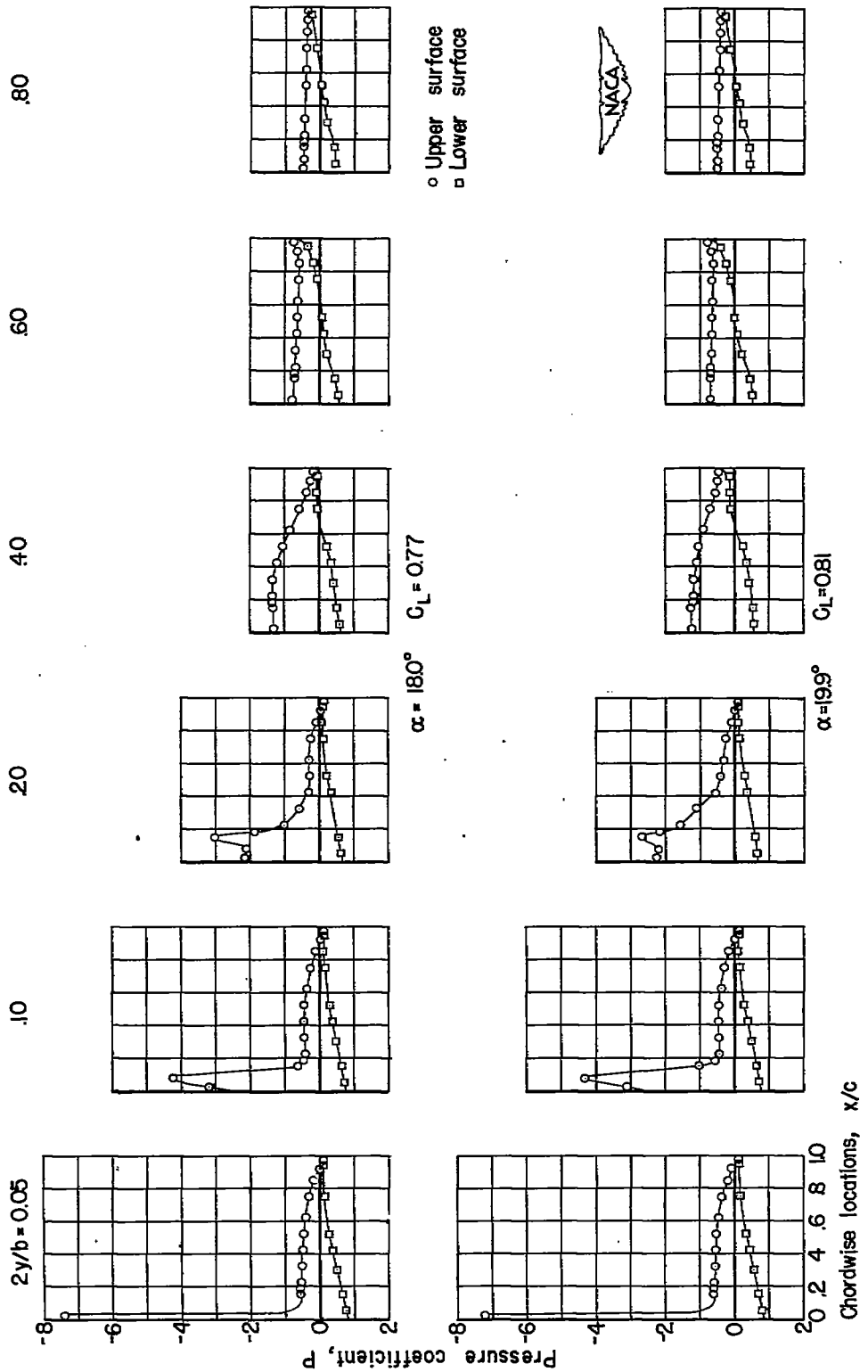

Figure 3.- Concluded. $\psi = 0^\circ$

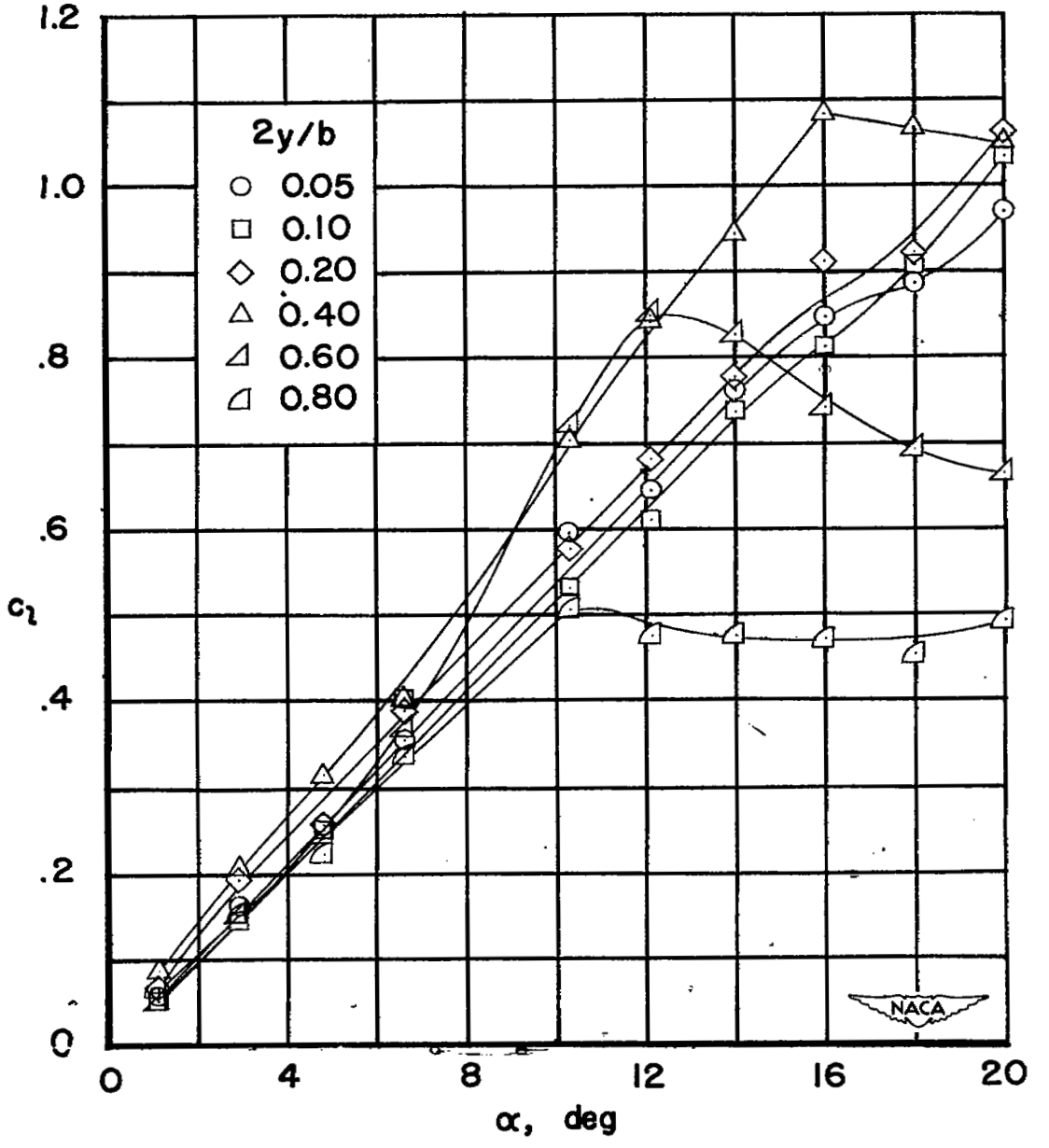

Figure 4.— Variation of section lift coefficient with angle of attack for six spanwise stations. Basic wing. $\psi = 0^{\circ}$.

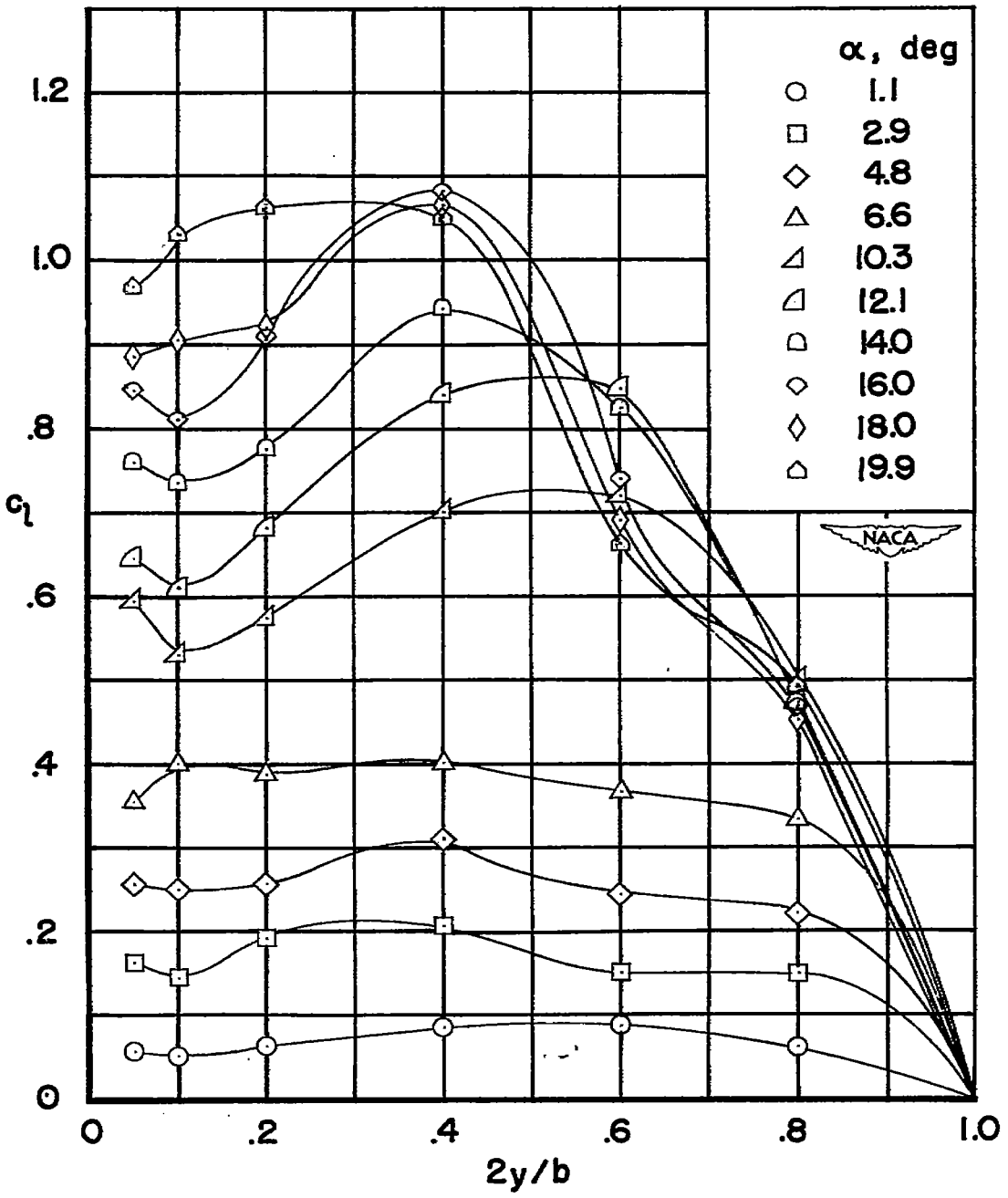

Figure 5.— Spanwise variation of section lift coefficient for several angles of attack. Basic wing. $\psi = 0^\circ$.

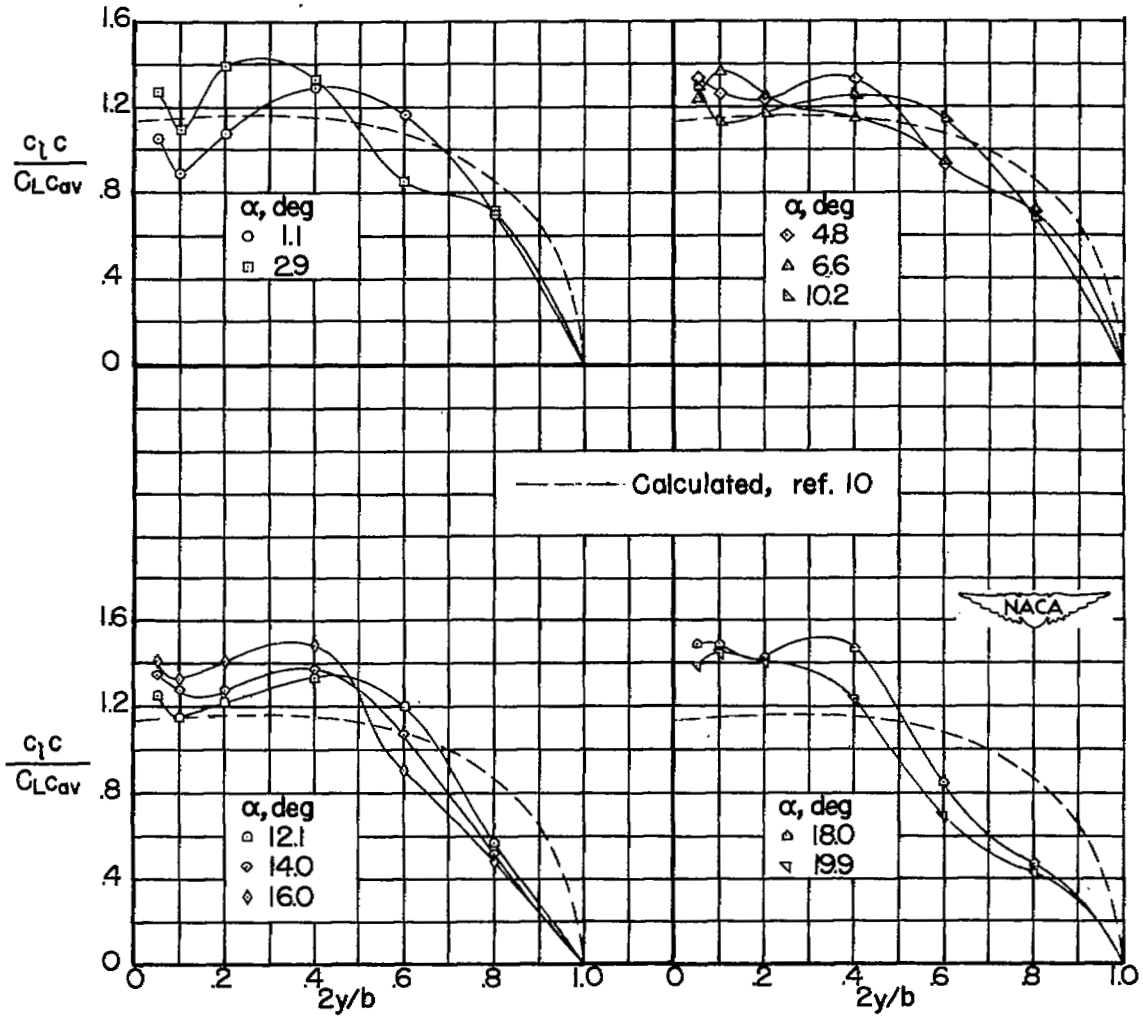

Figure 6.– Span load distribution for several angles of attack. Basic wing. $\psi = 0^{\circ}$.

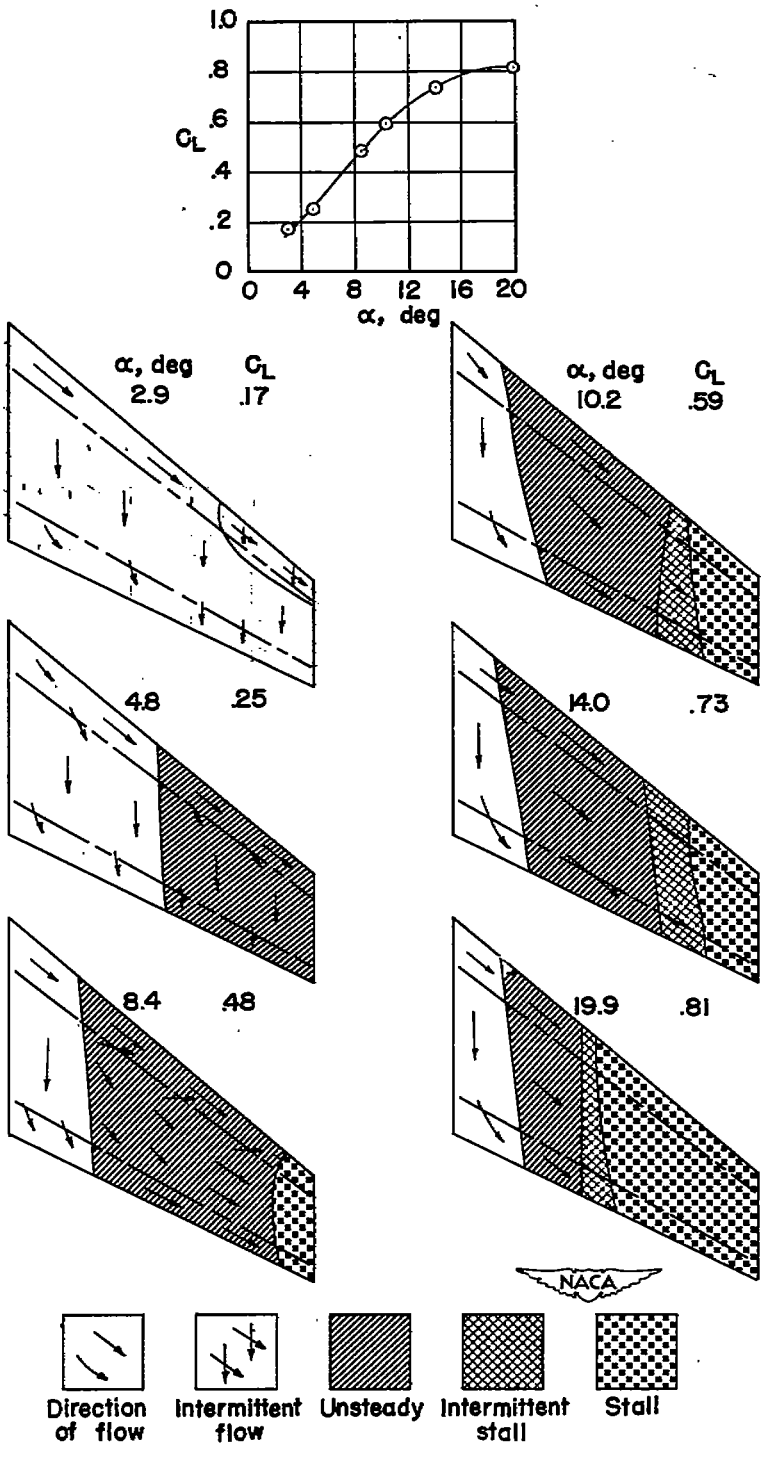

Figure 7.— Stalling characteristics of the basic wing. $\psi = 0^{\circ}$.

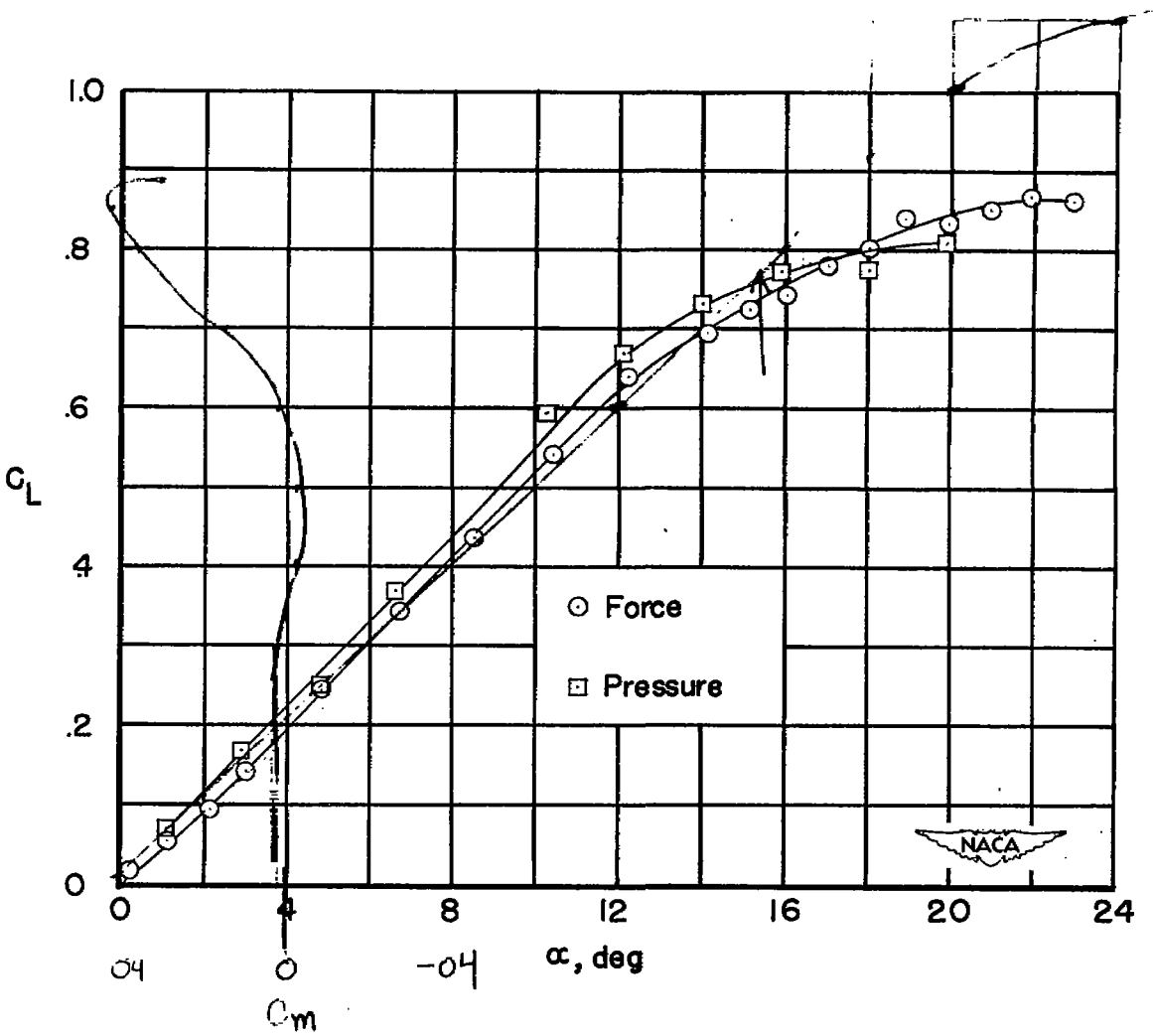

Figure 8.— Comparison of the wing lift curves as obtained from force and pressure measurements. Basic wing. $\Lambda = 0^\circ$.

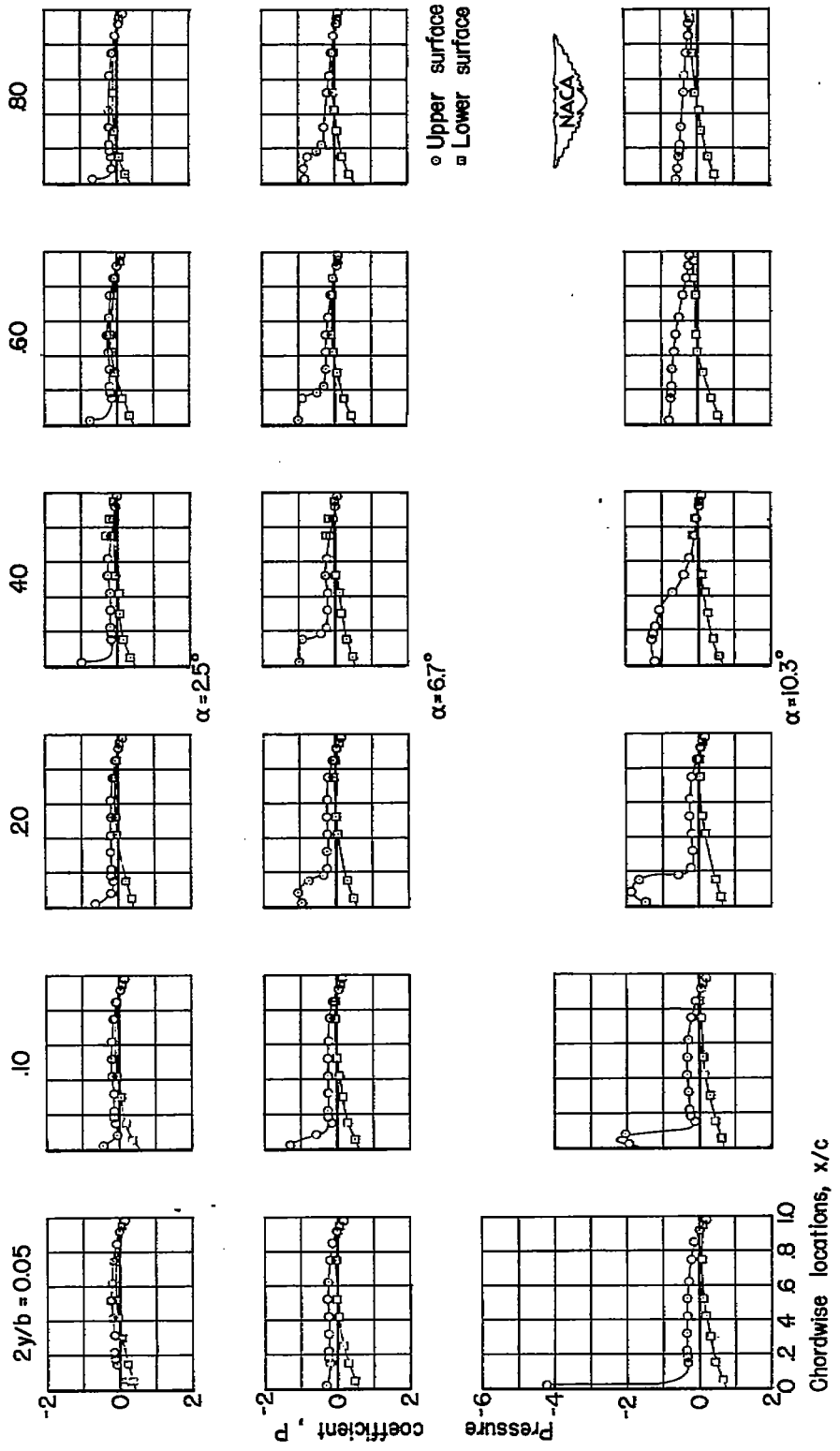

Figure 9.- Chordwise pressure distribution for six spanwise stations of the basic wing. $\psi = -6°$.

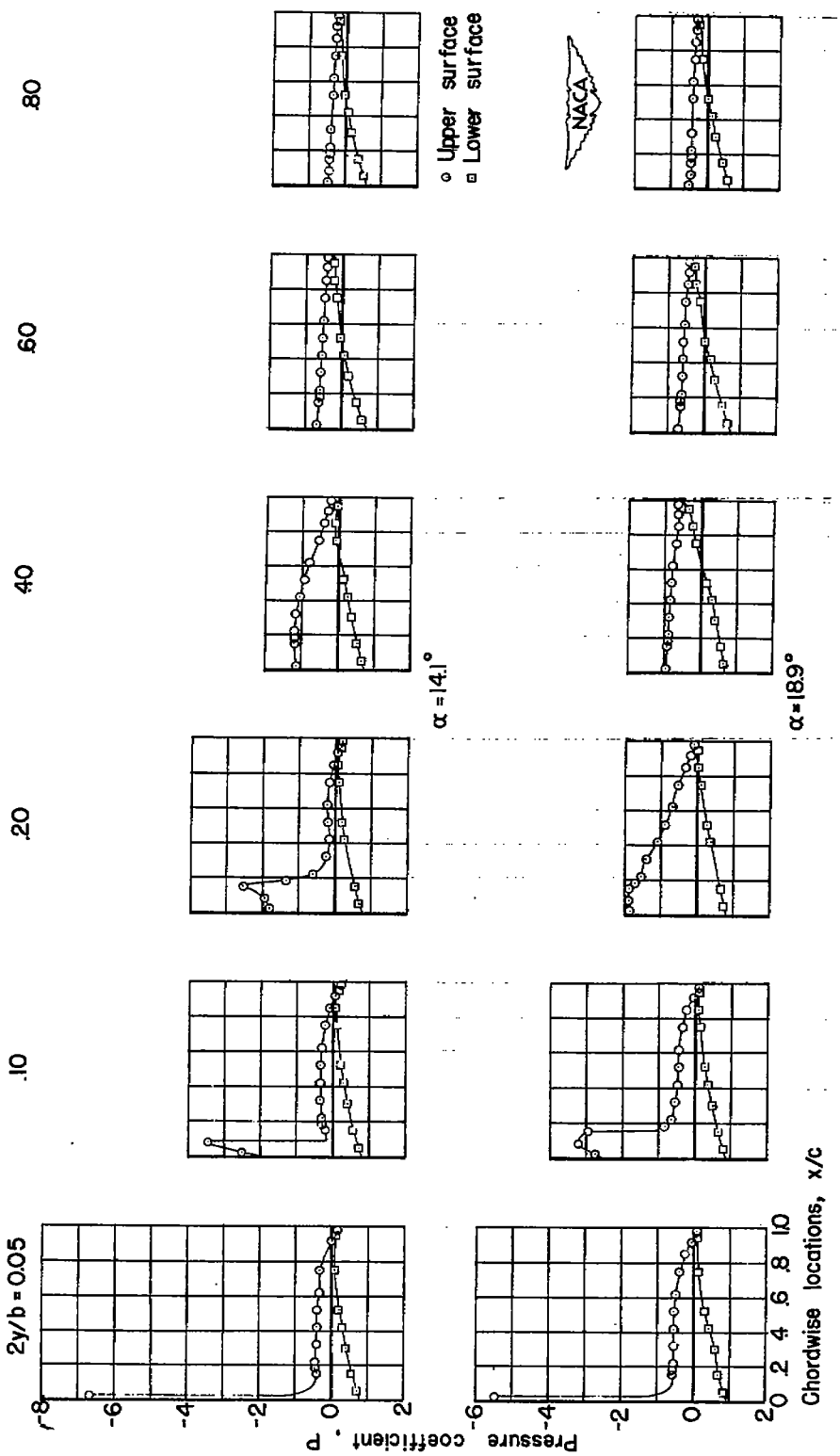

Figure 9.— Concluded.

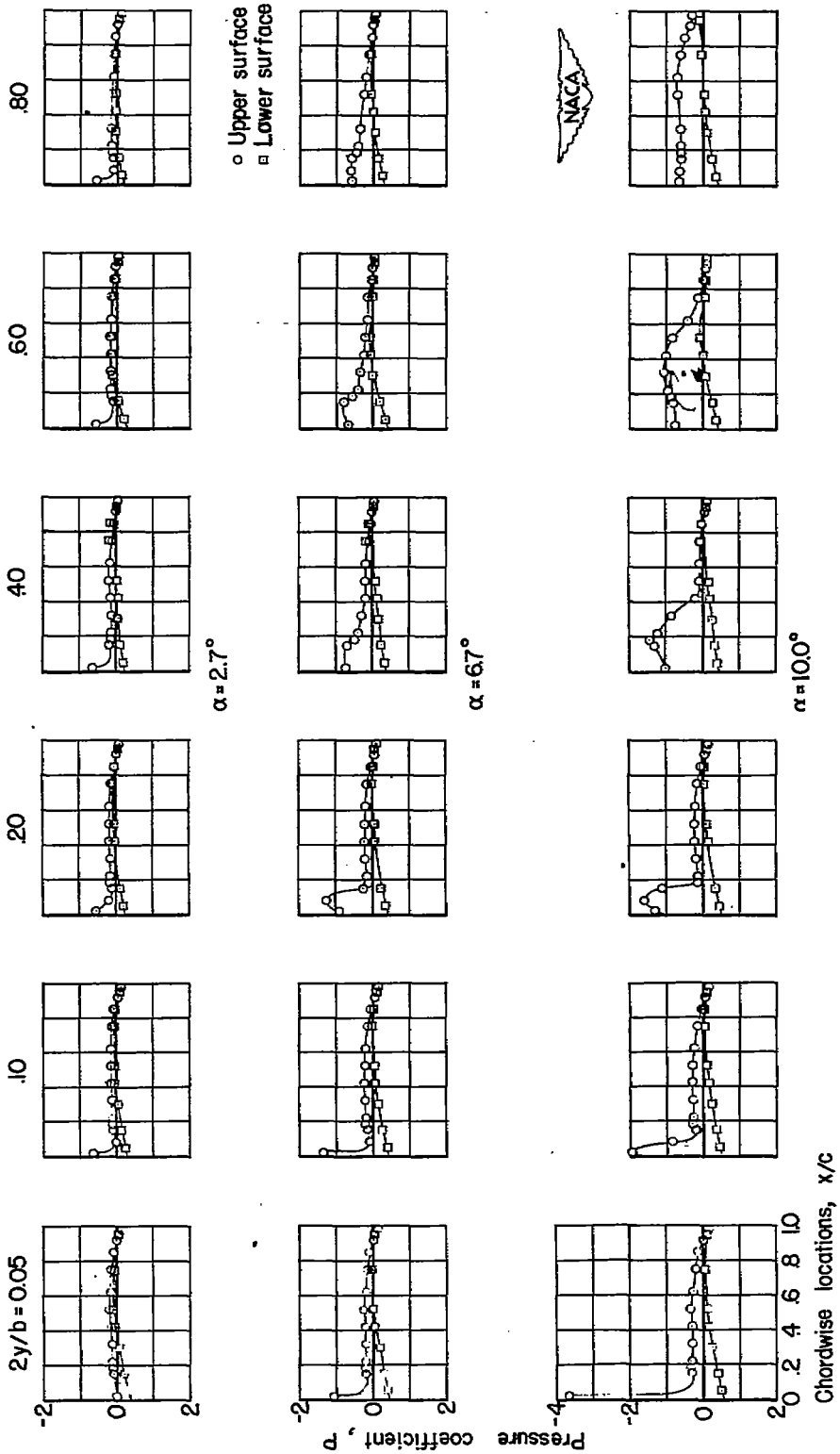

Figure 10.- Chordwise pressure distribution for six spanwise stations of the basic wing. $\psi = 6^{\circ}$.

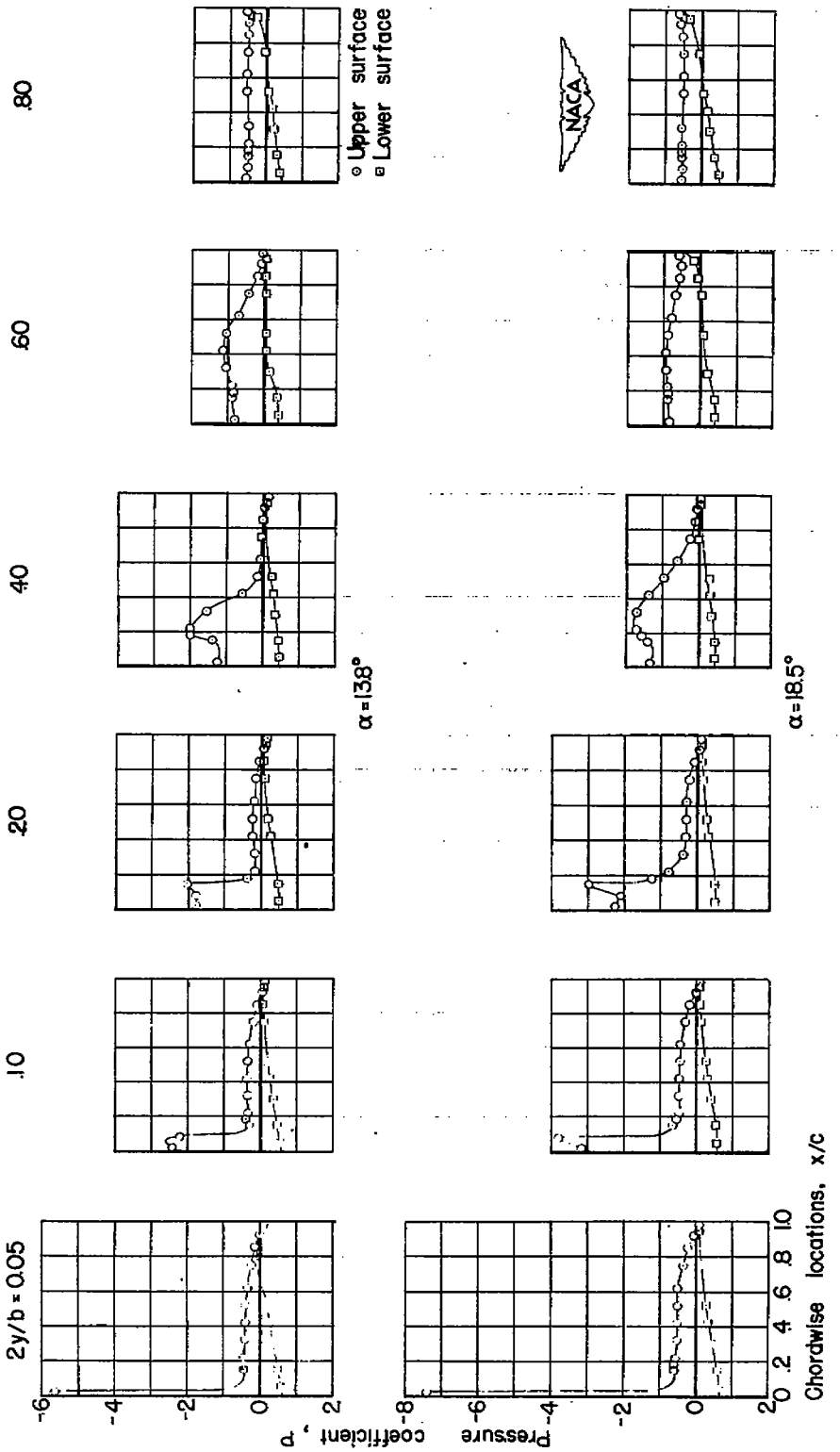

Figure 10.- Concluded.

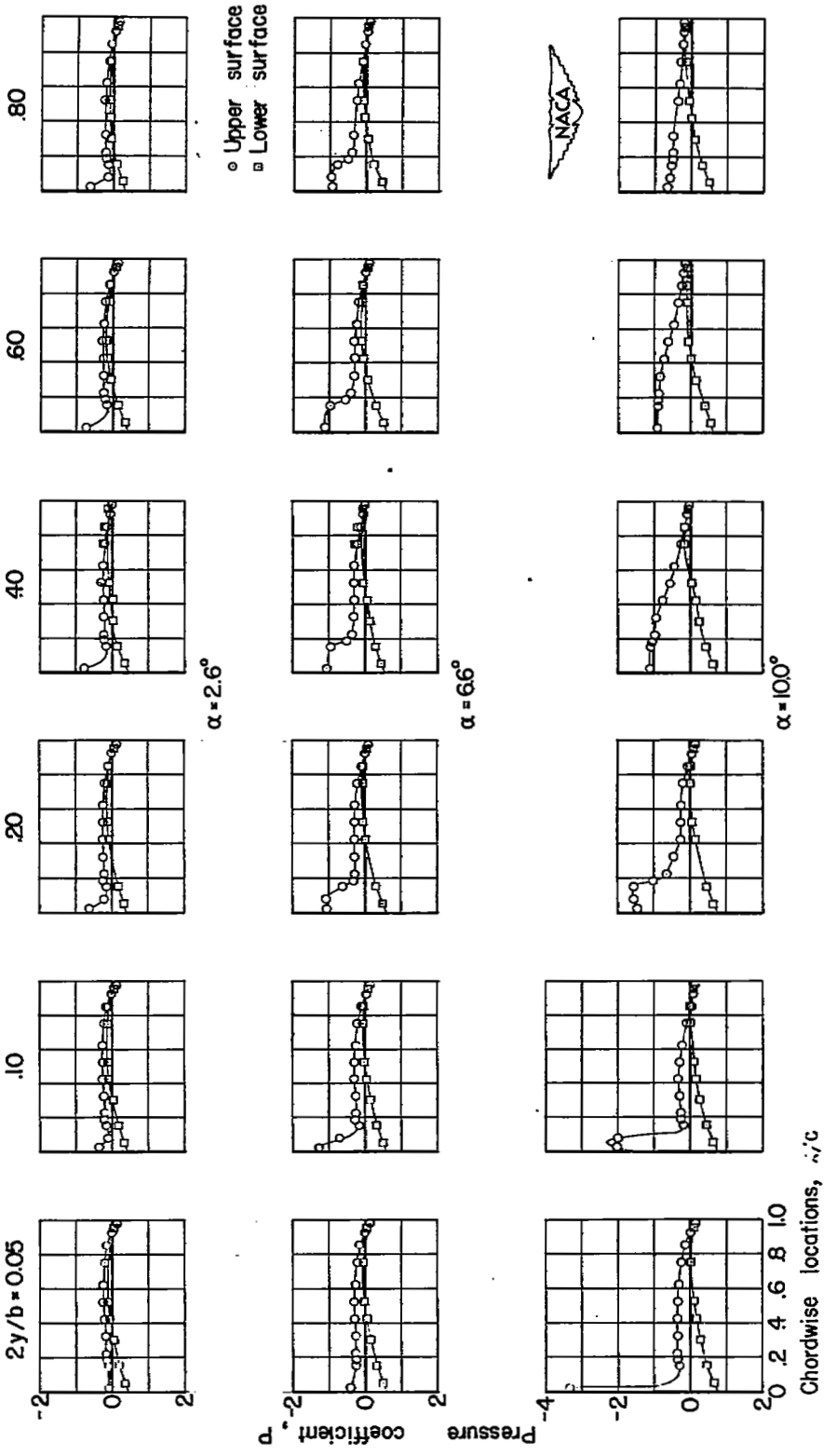

Figure 11.- Chordwise pressure distribution for six spanwise stations of the basic wing. $\psi = -9.8°$.

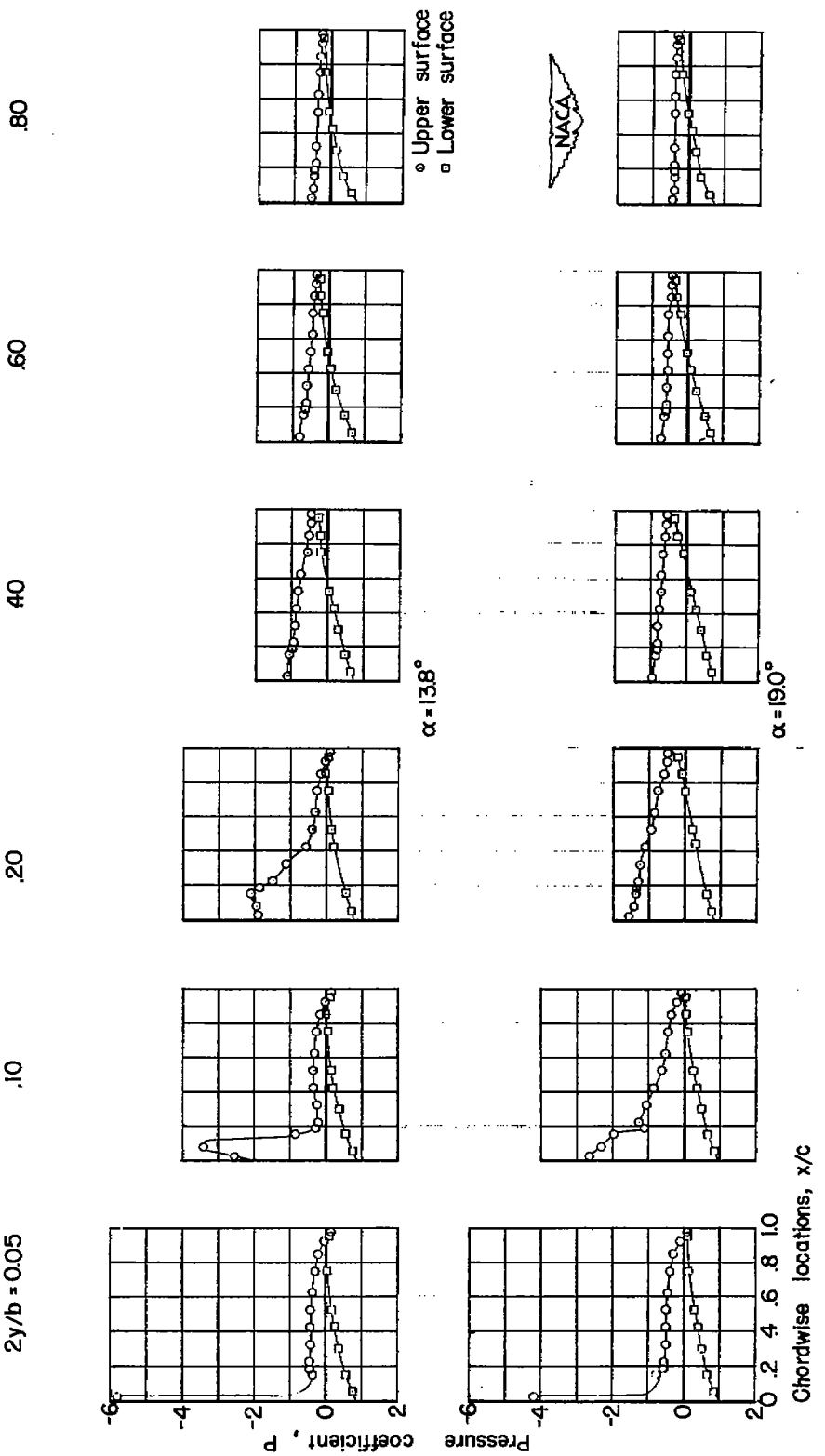

Figure 11.- Concluded.

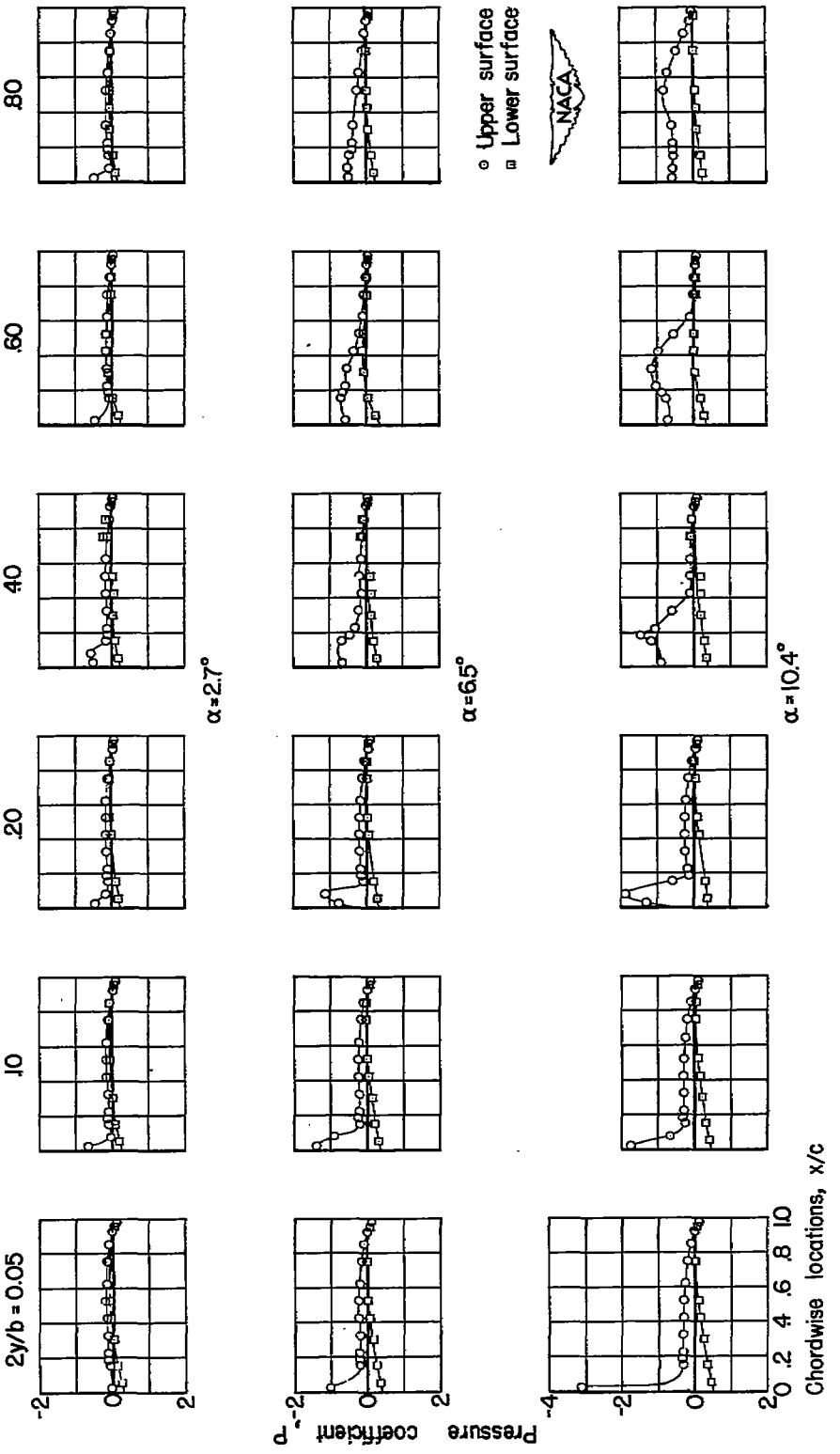

Figure 12.— Chordwise pressure distribution for six spanwise stations of the basic wing. $\psi = 9.8^{\circ}$.

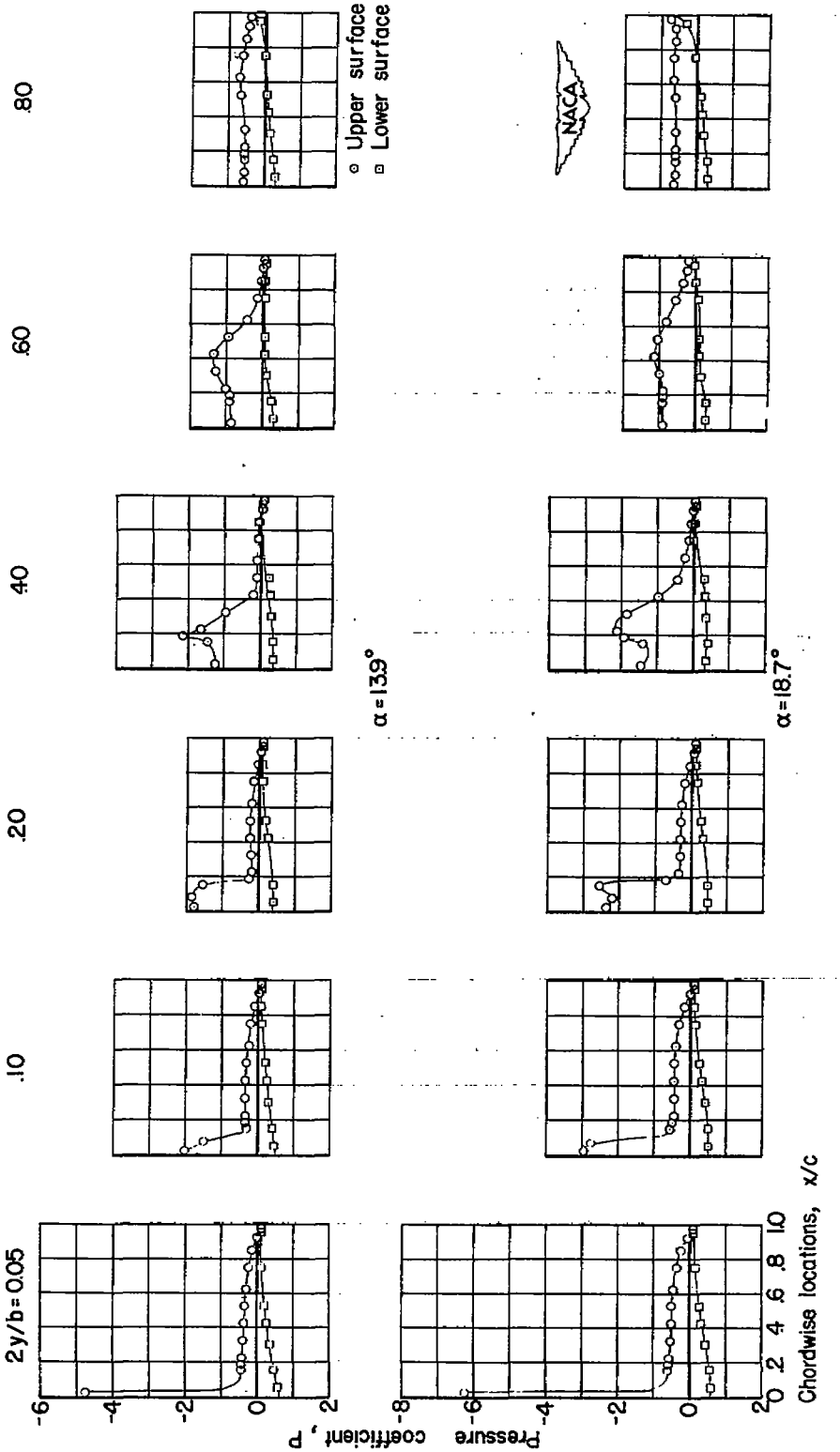

Figure 12.— Concluded.

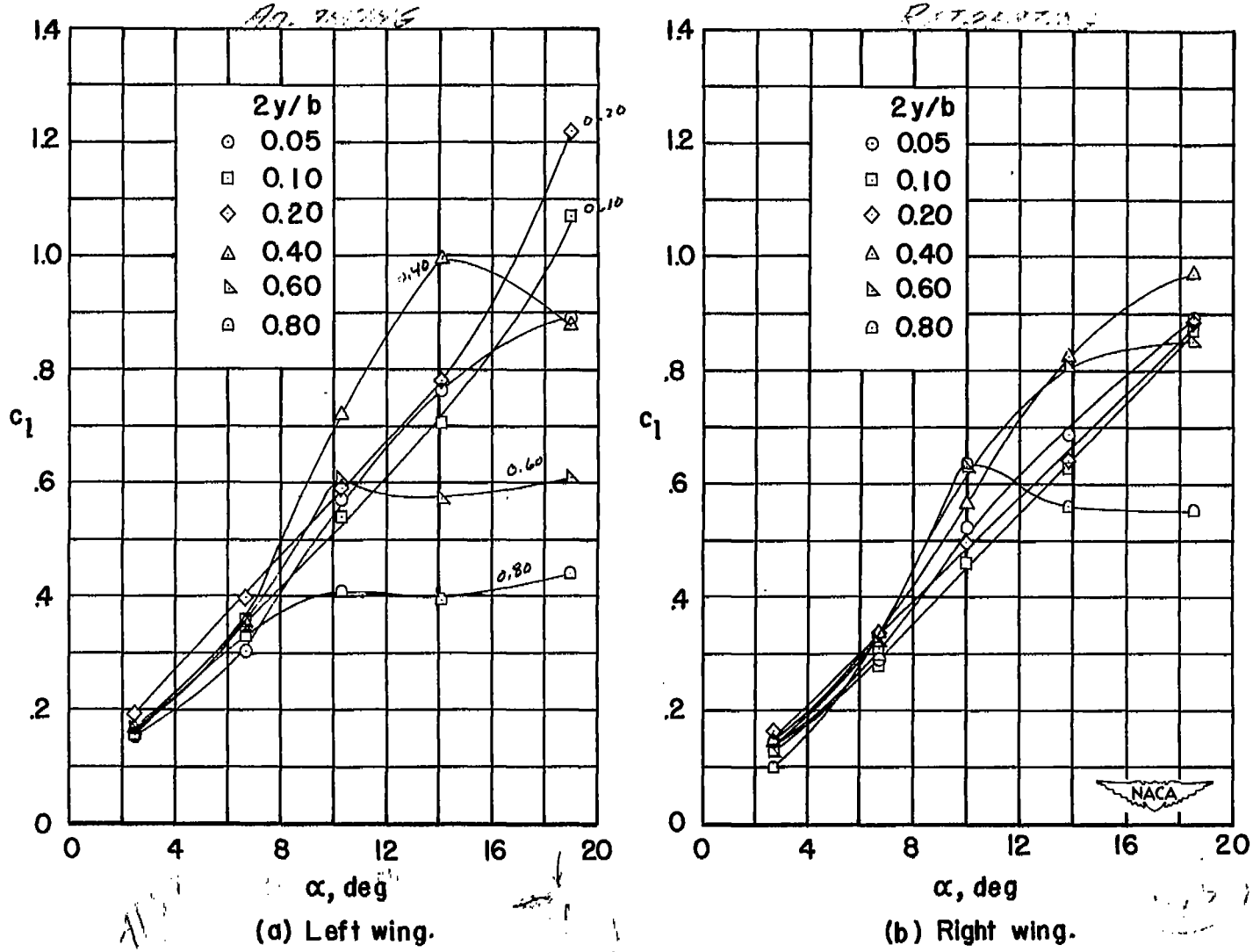

Figure 13.– Variation of section lift coefficient with angle of attack for six spanwise stations. Basic wing. $\psi = 6^\circ$.

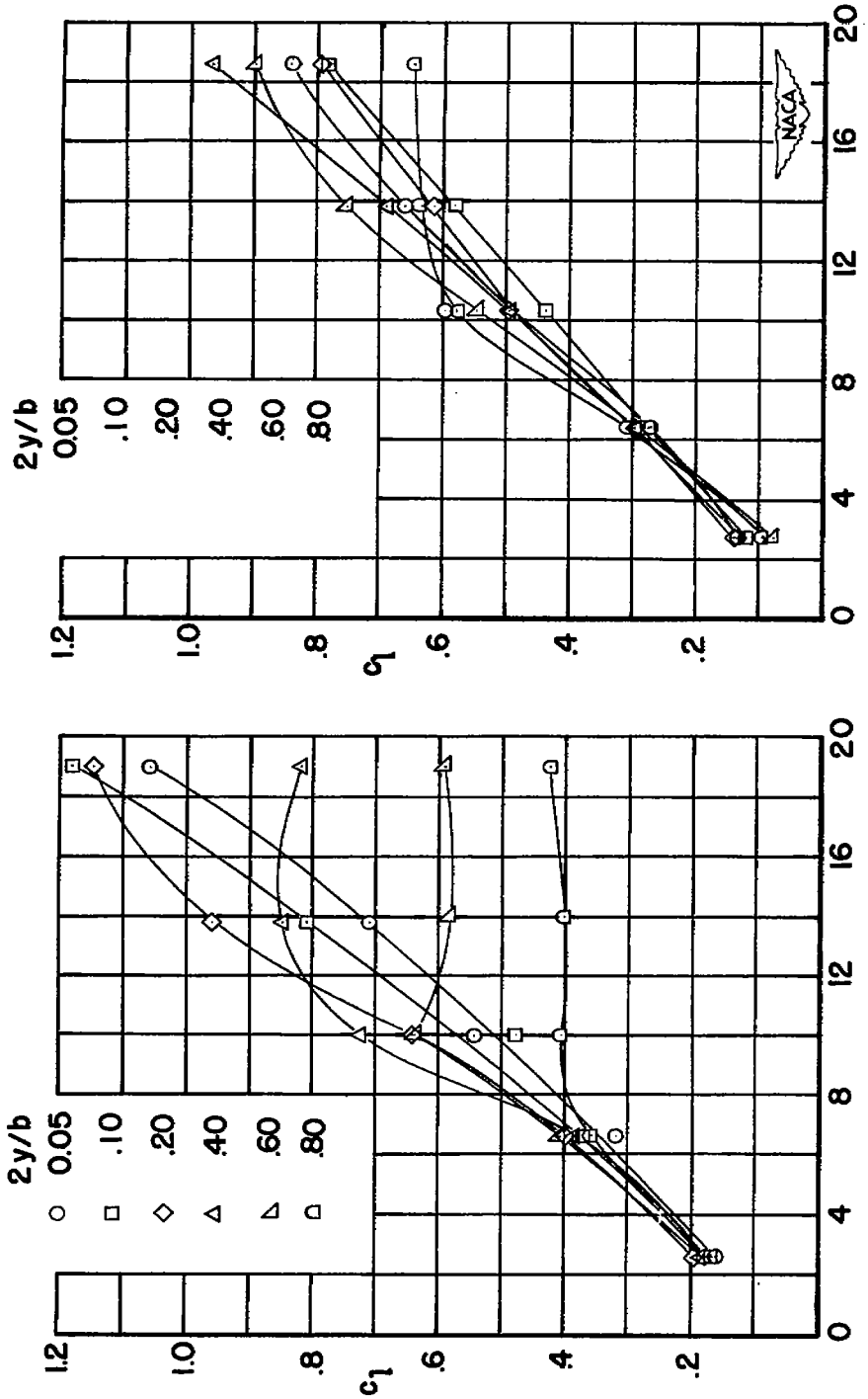

Figure 14.- Variation of section lift coefficient with angle of attack for six spanwise stations. Basic wing. $\psi = 9.8°$.

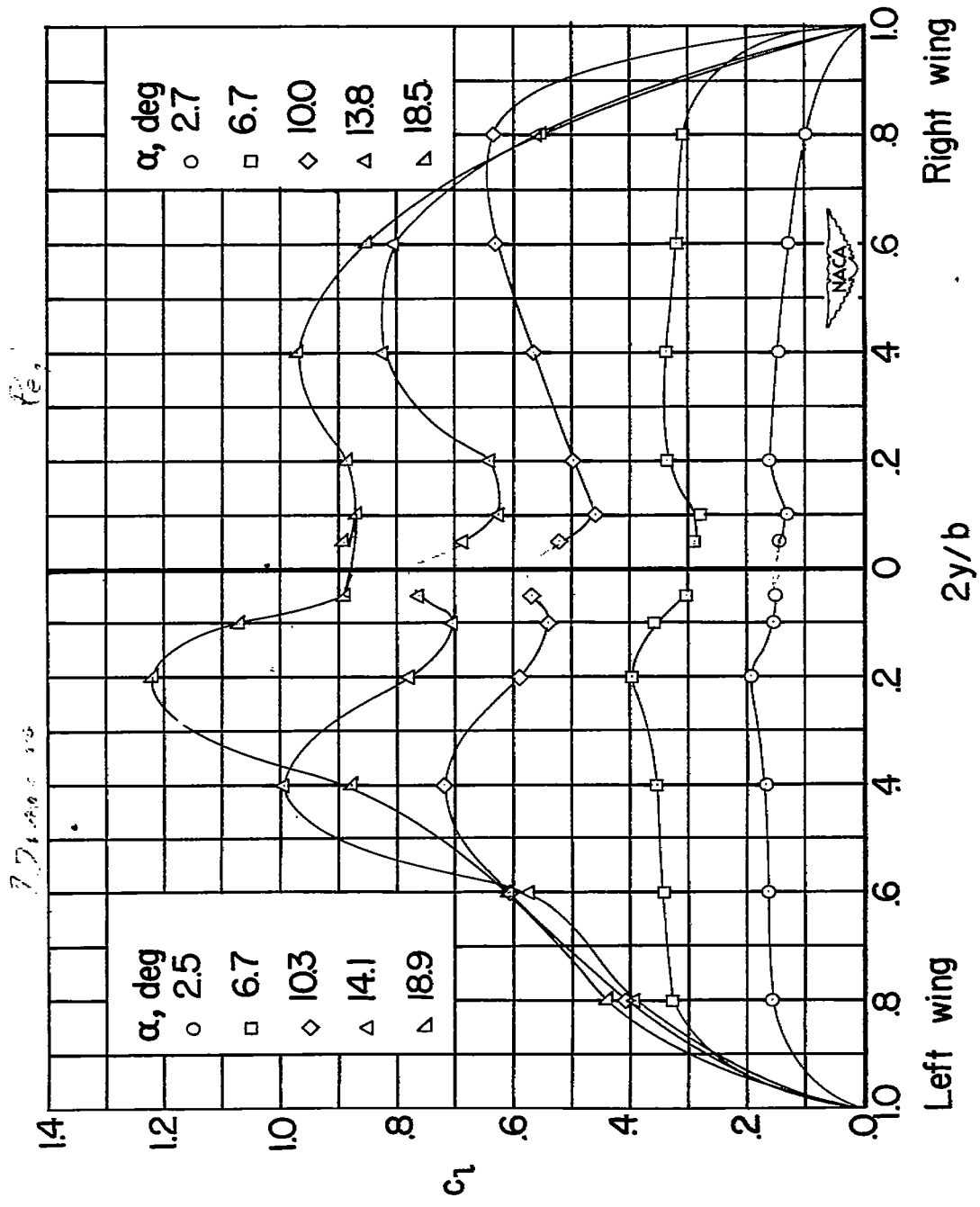

Figure 15.- Spanwise variation of section lift coefficient for several angles of attack. Basic wing. $\psi = 6^{\circ}$.

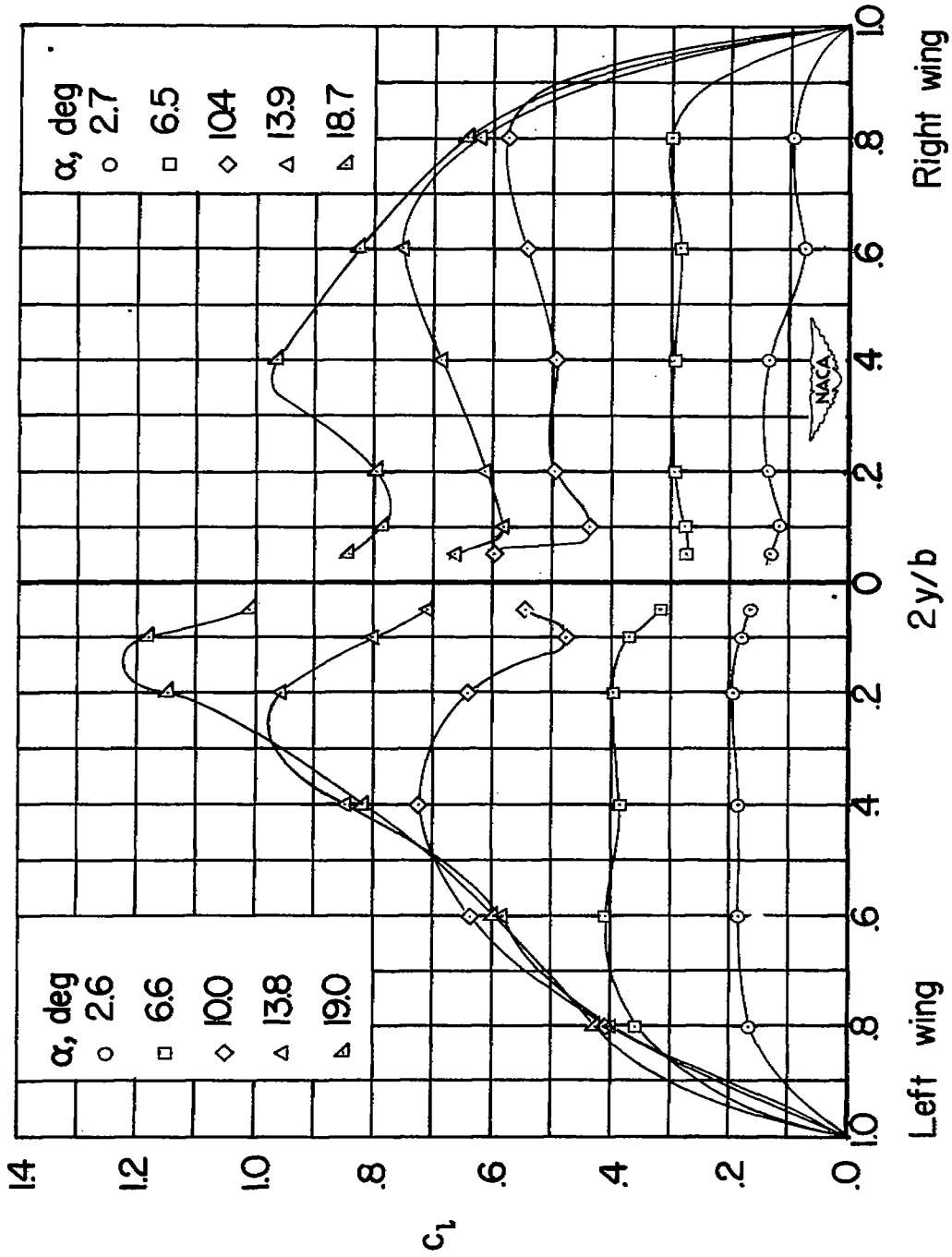

Figure 16.- Spanwise variation of section lift coefficient for several angles of attack. Basic wing. $\psi = 9.8°$.

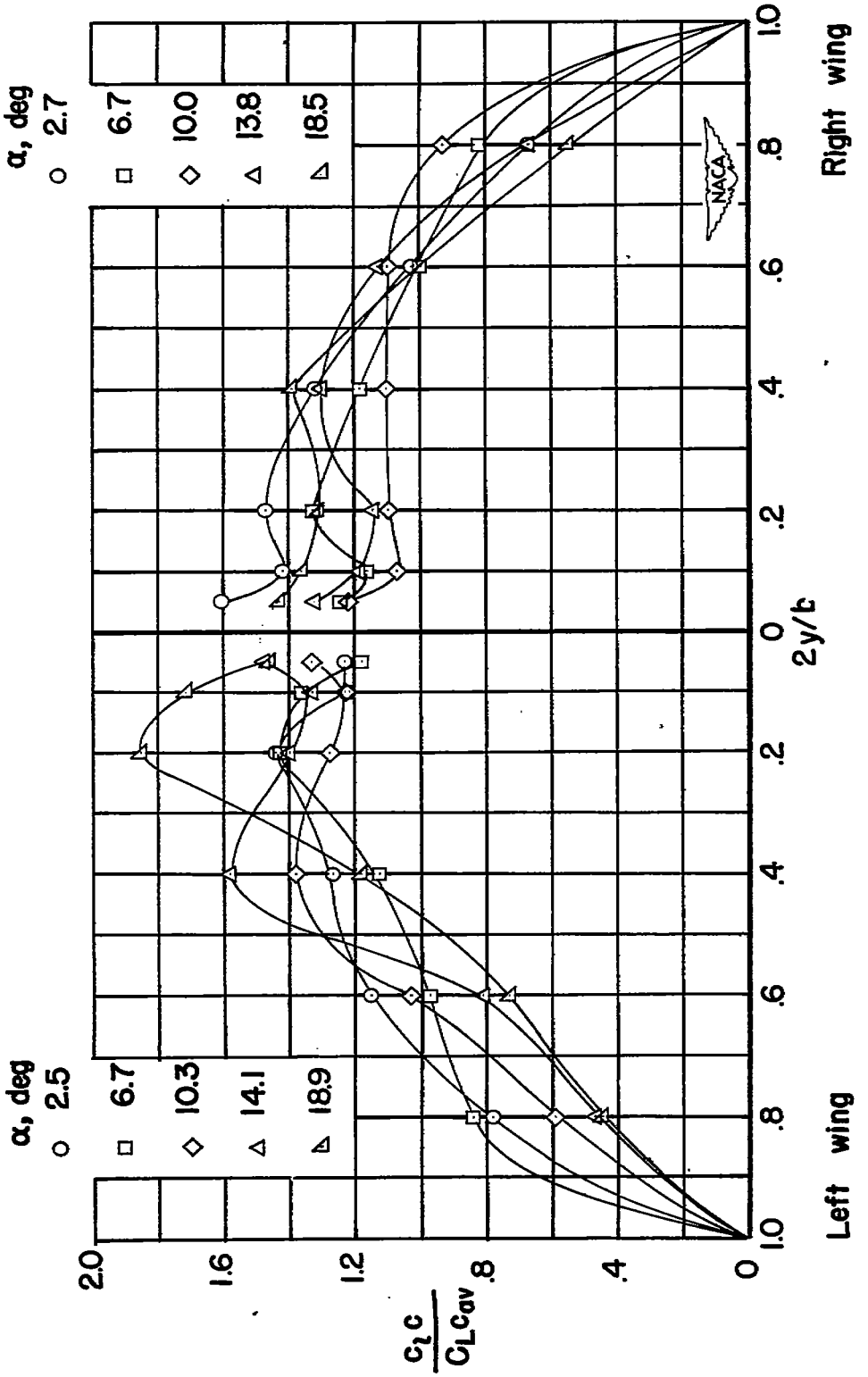

Figure 17.- Span load distribution for several angles of attack. Basic wing. $\psi = 6^{\circ}$.

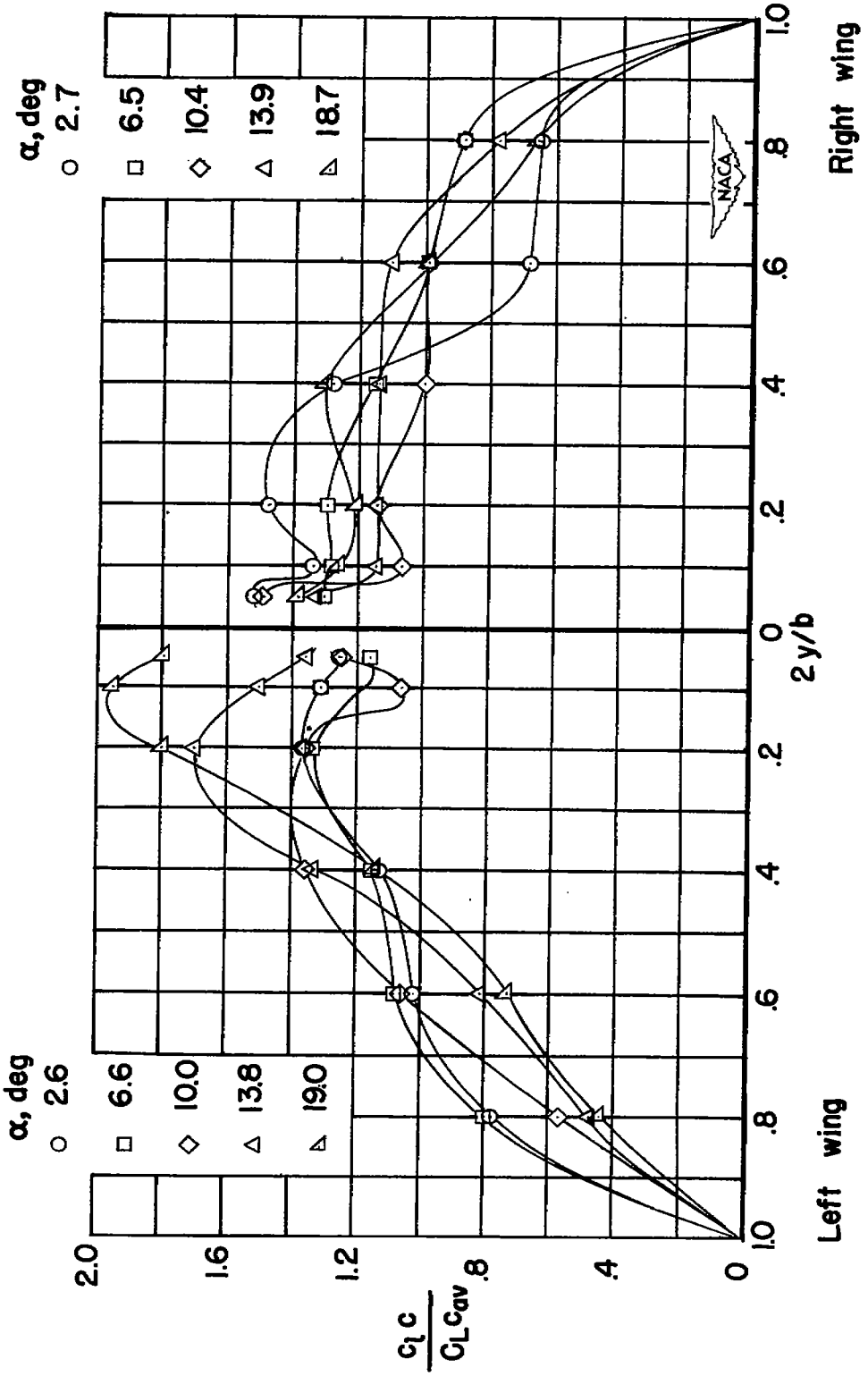

Figure 18.- Span load distribution for several angles of attack. Basic wing. $\psi = 9.8°$.

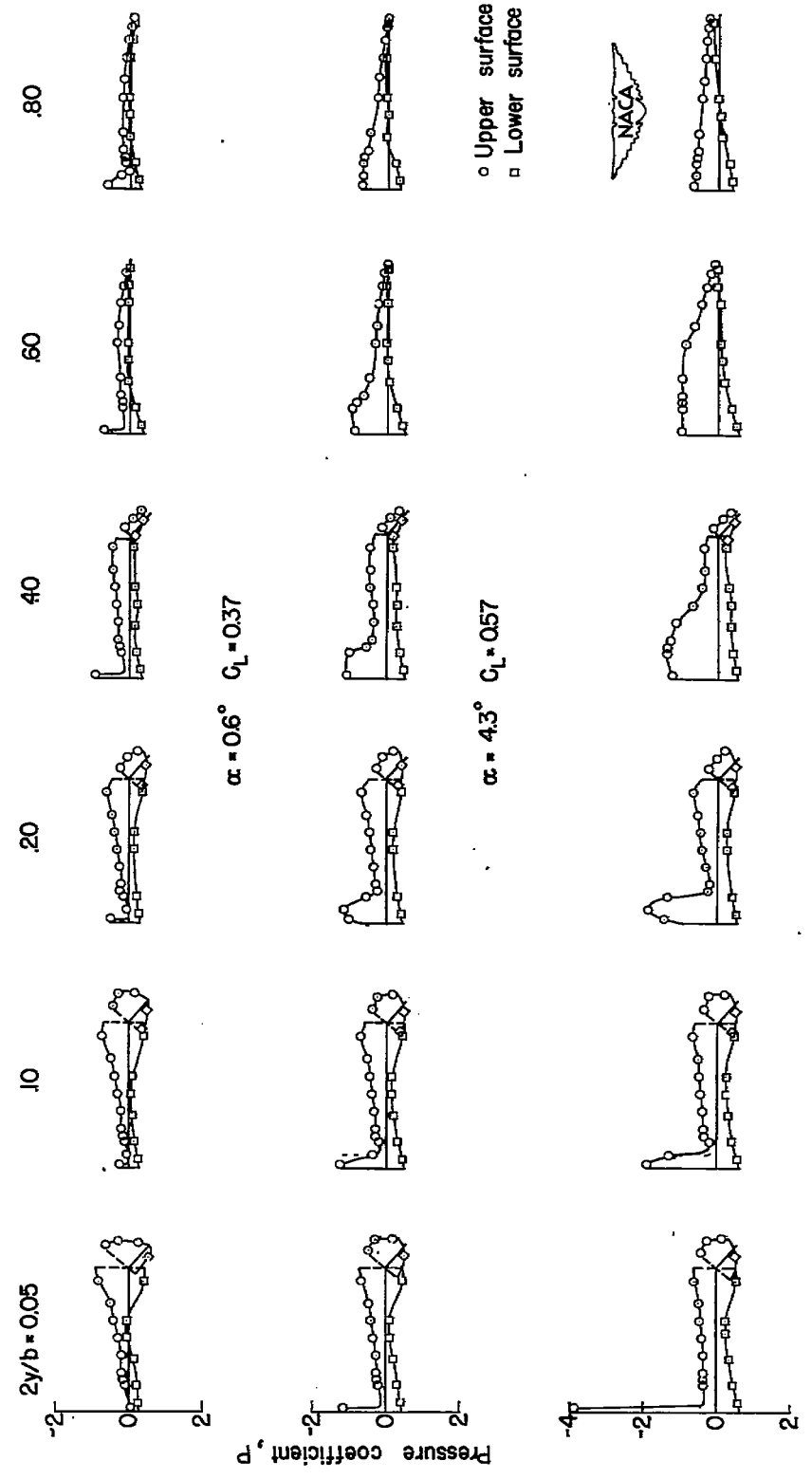

Figure 19.- Chordwise pressure distribution for six spanwise stations. Semispan plain flap deflected 40°. $\psi = 0°$.

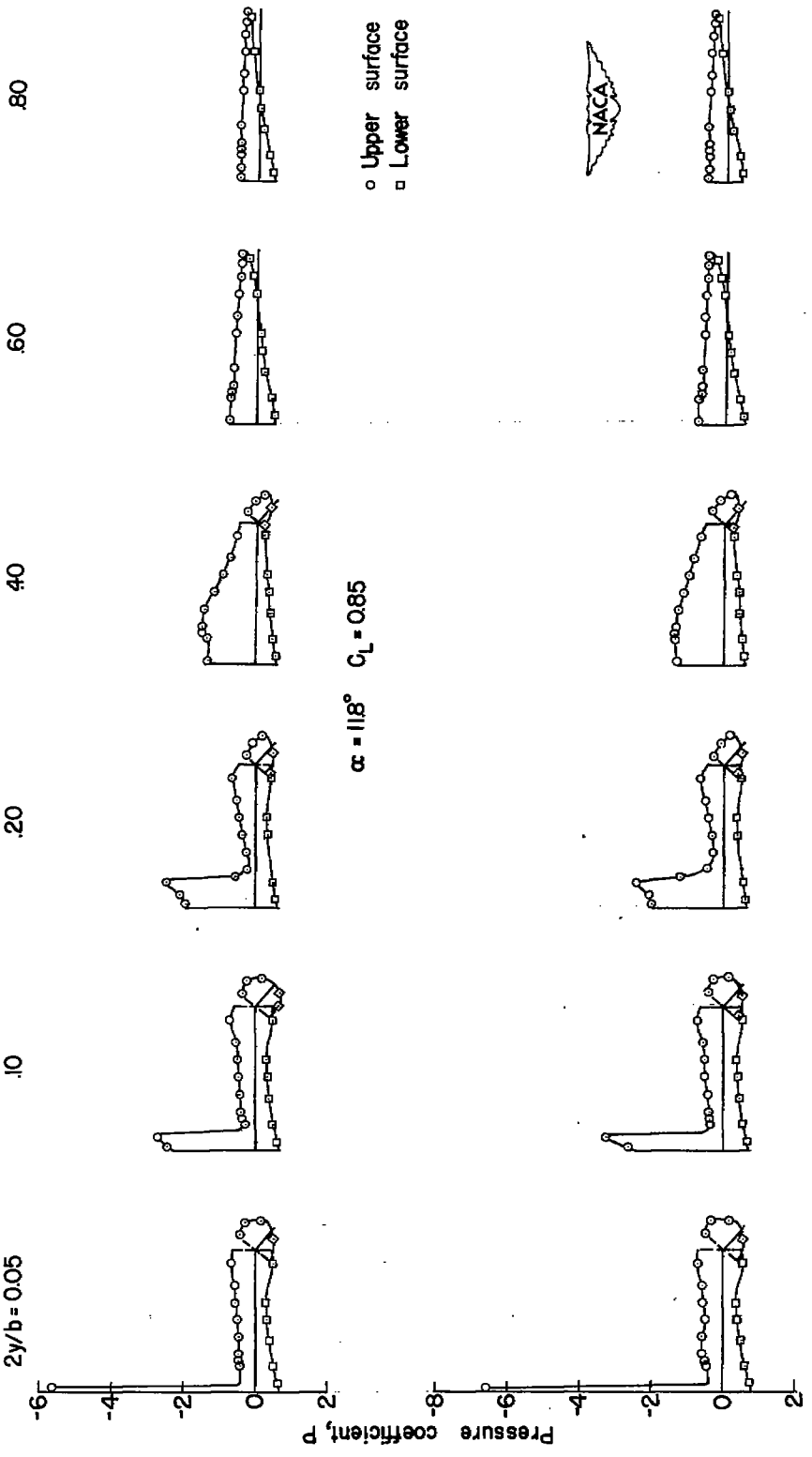

Figure 19.— Continued.

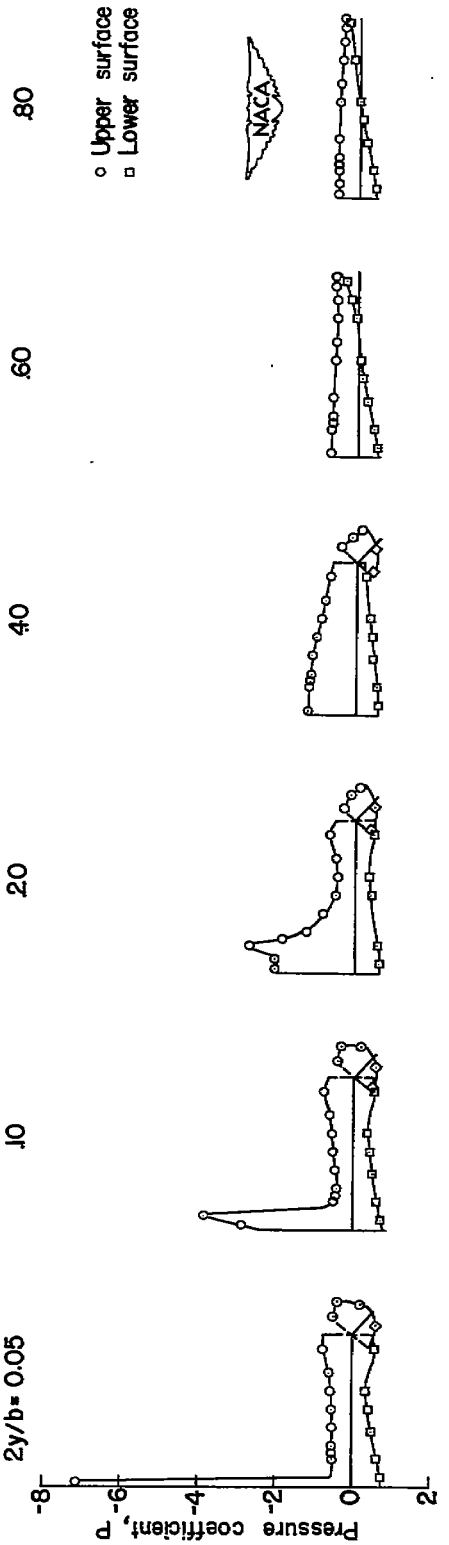

Figure 19.— Concluded. $\psi = 0$

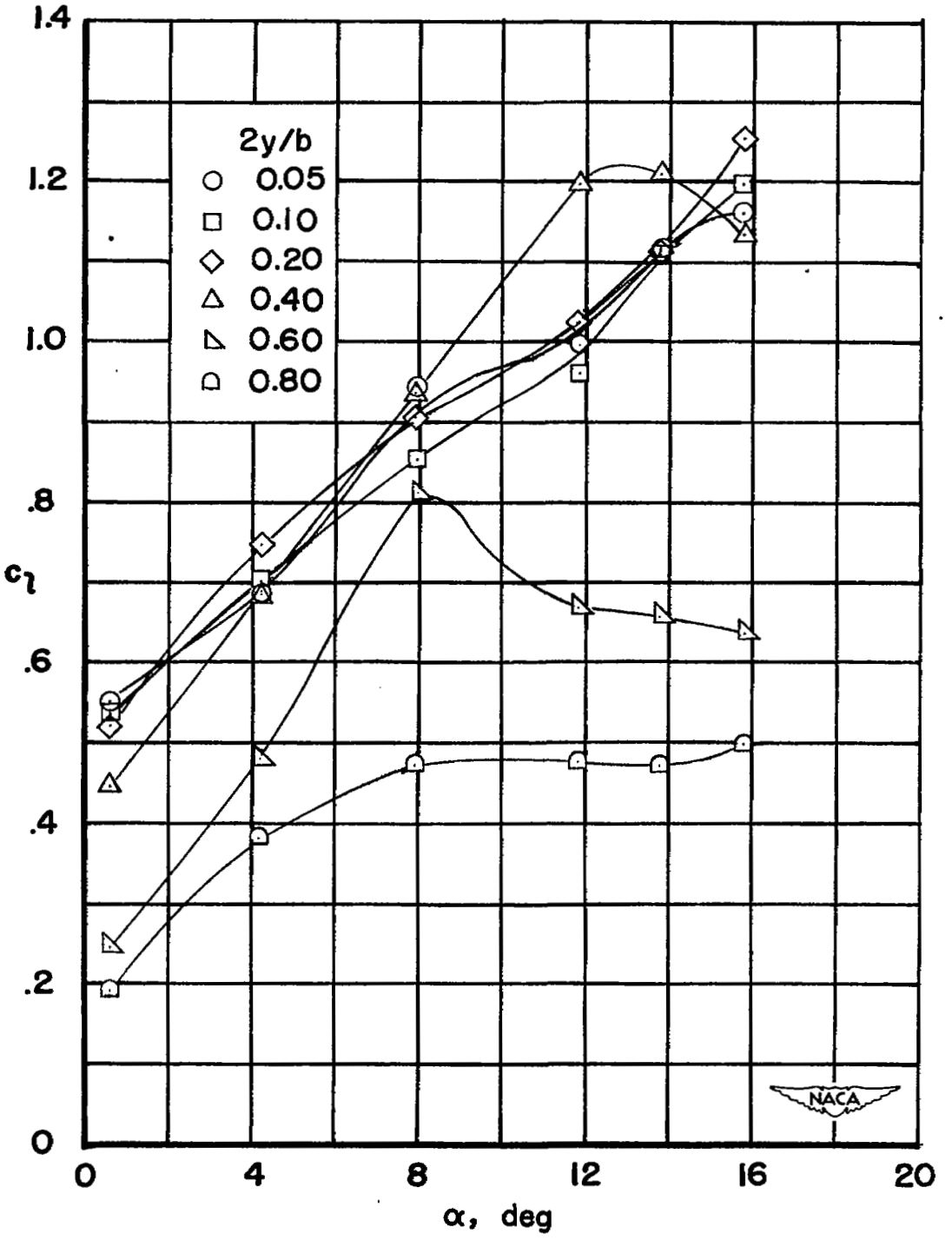

Figure 20.— Variation of section lift coefficient with angle of attack for six spanwise stations. Semispan plain flap deflected 40°. $\psi = 0°$.

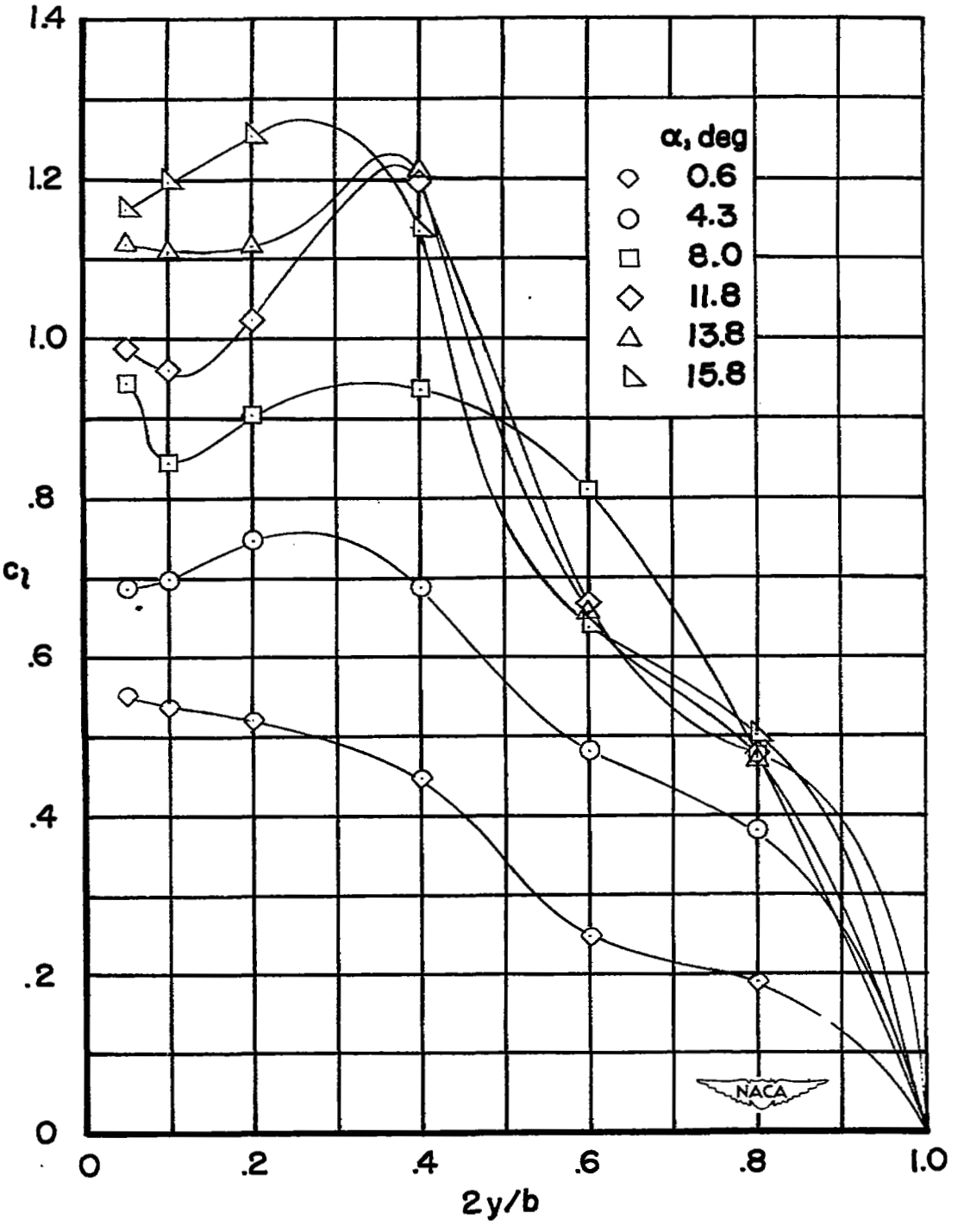

Figure 21.— Spanwise variation of section lift coefficient for several angles of attack. Semispan plain flap deflected 40°. $\Psi = 0°$.

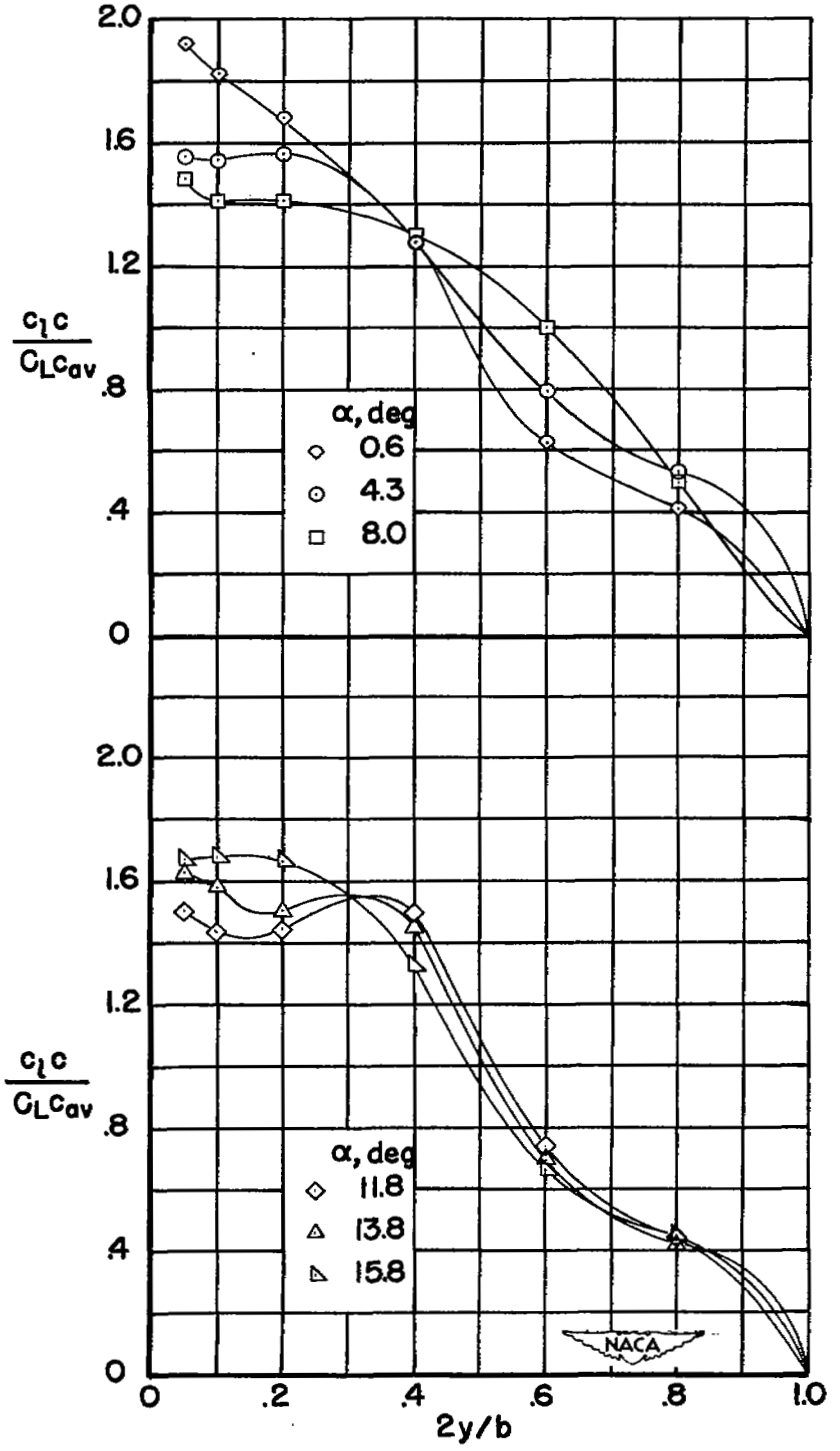

Figure 22.– Span load distribution for several angles of attack. Semispan plain flap deflected 40°. $\Psi = 0°$.

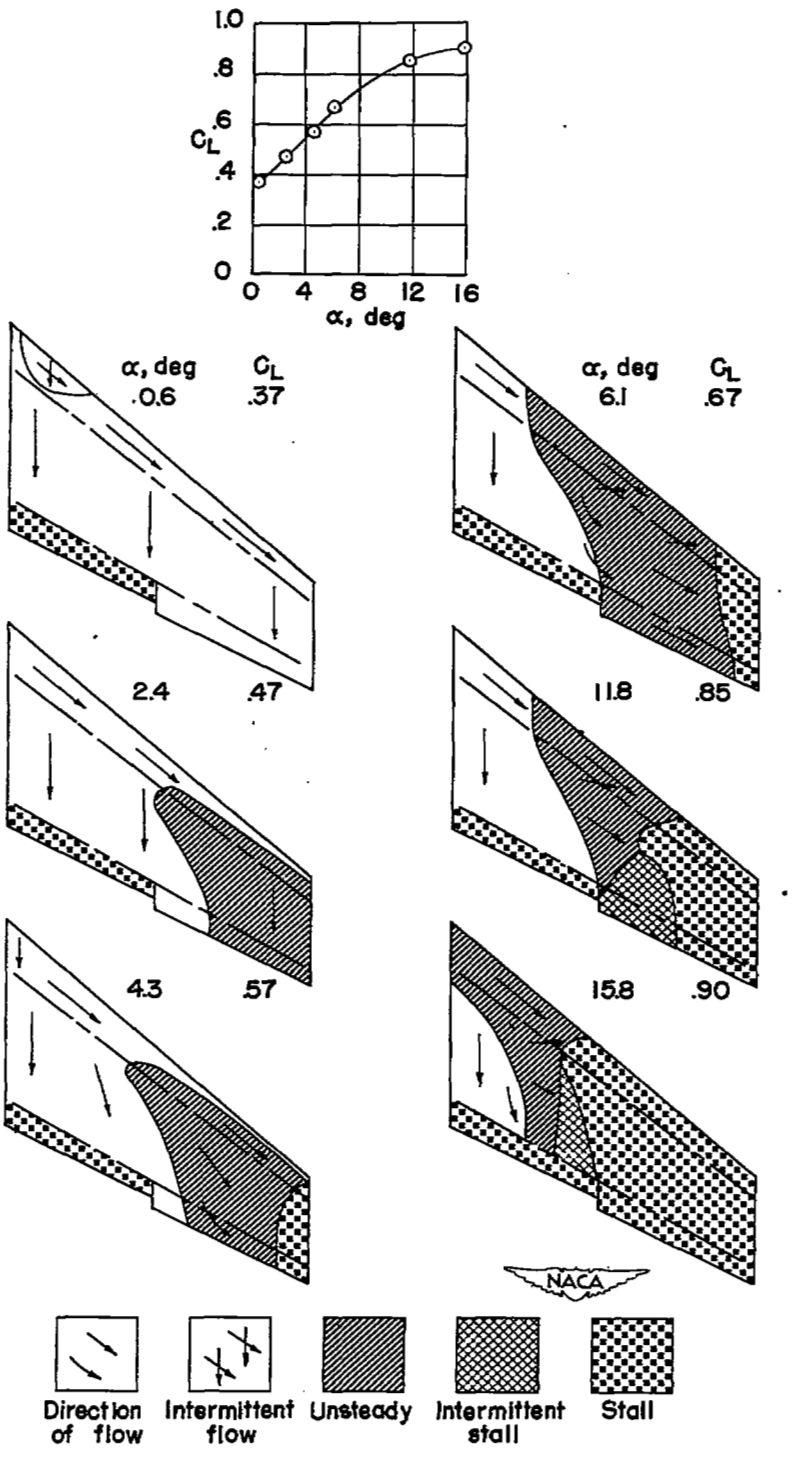

Figure 23.– Stalling characteristics of the wing with semispan plain flaps deflected 40°. $\Psi = 0°$.

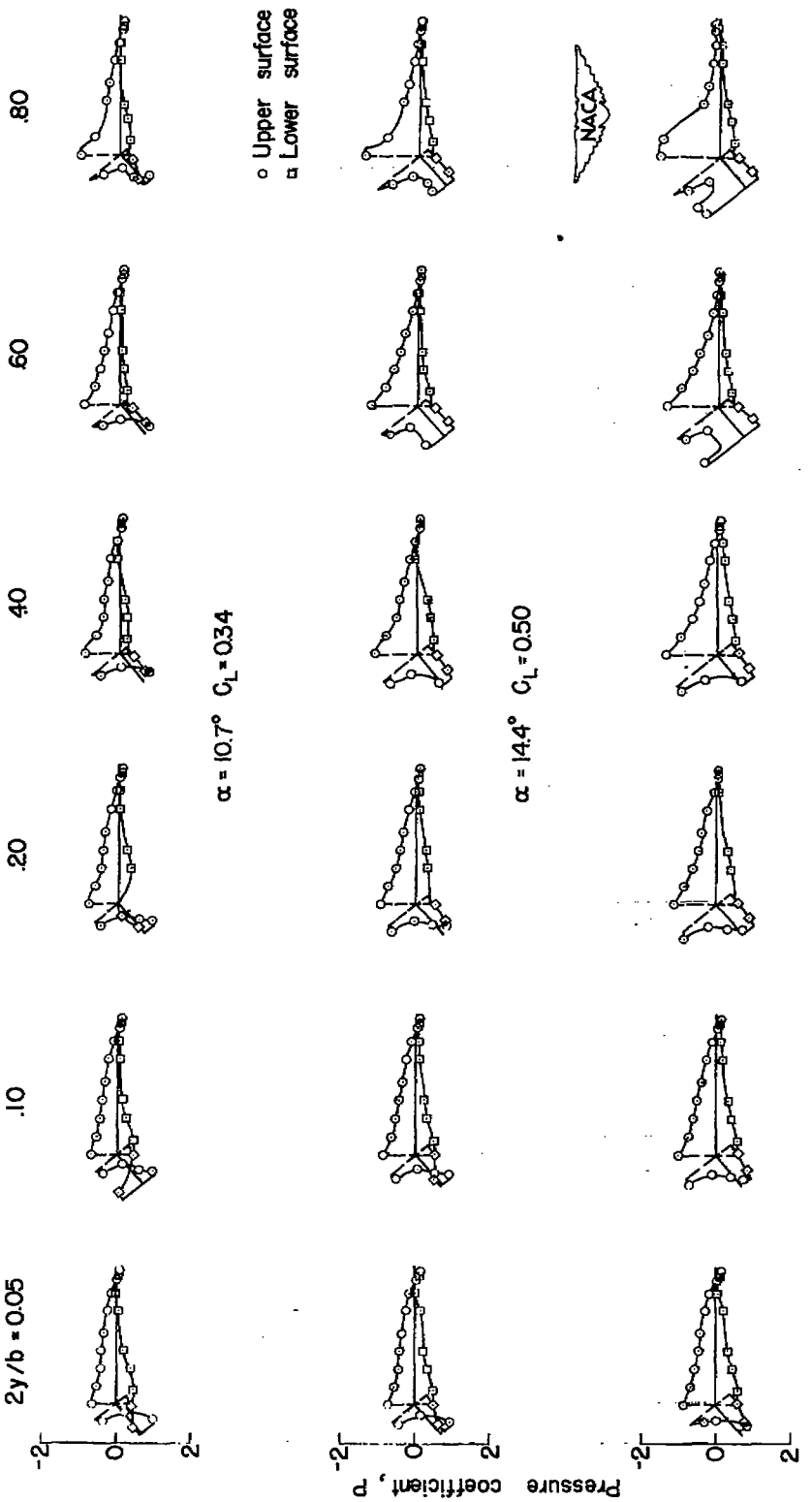

Figure 24.— Chordwise pressure distribution for six spanwise stations. Full-span drooped-nose flaps deflected 40°. $\psi = 0°$.

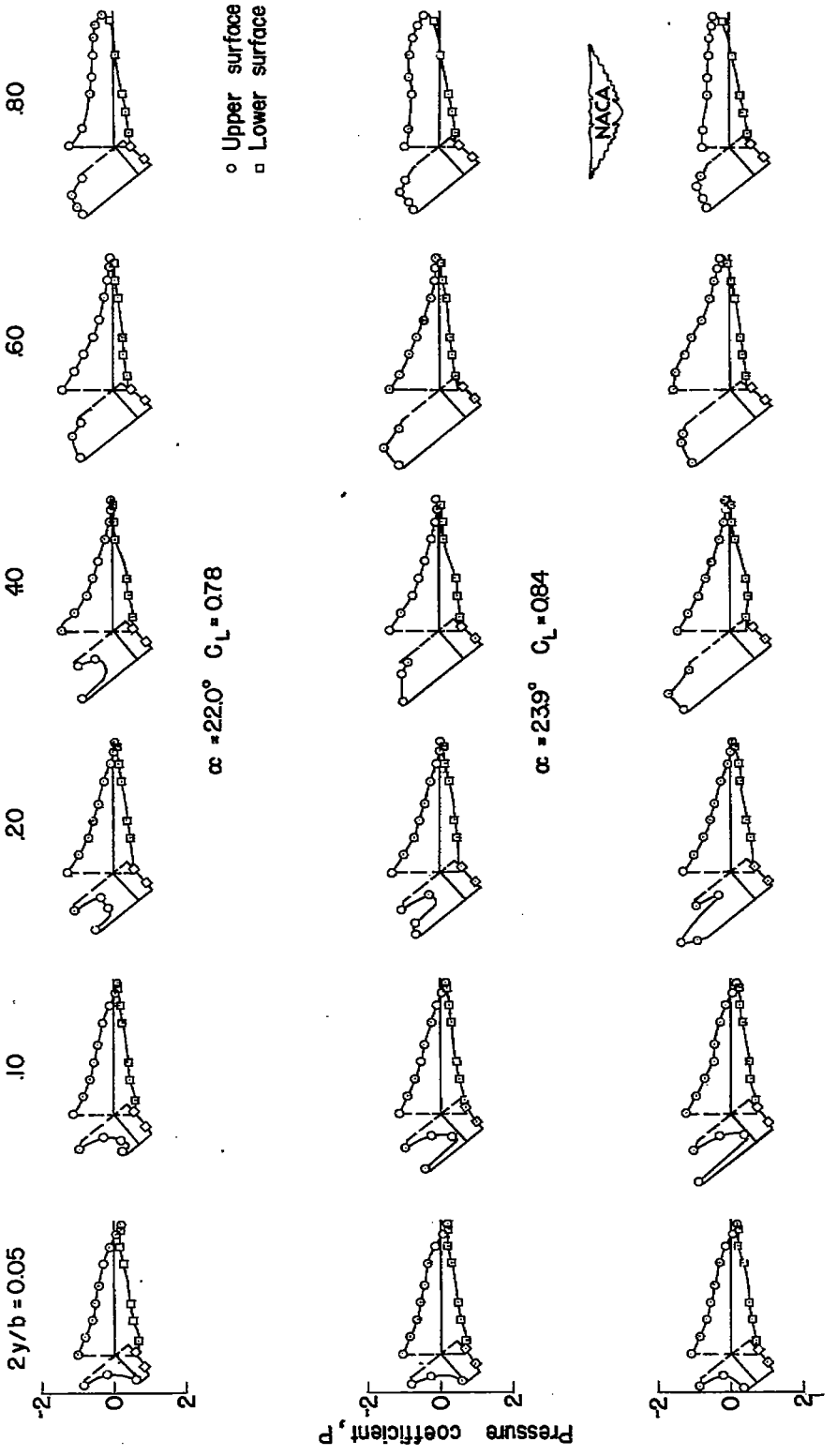

Figure 24.- Concluded. $\psi = 0$

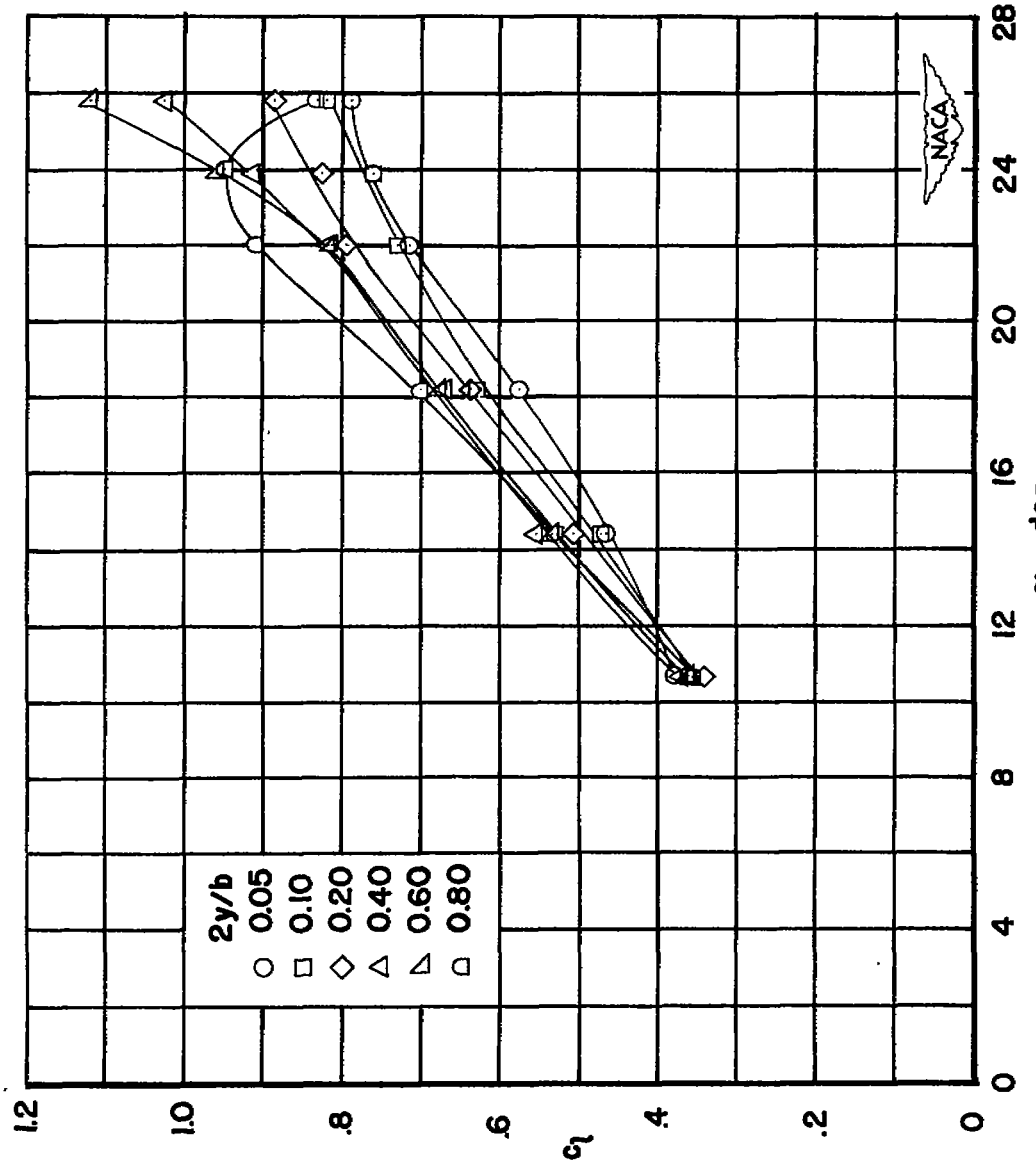

Figure 25.- Variation of section lift coefficient with angle of attack for six spanwise stations. Full-span drooped-nose flap deflected 40°. $\psi = 0°$.

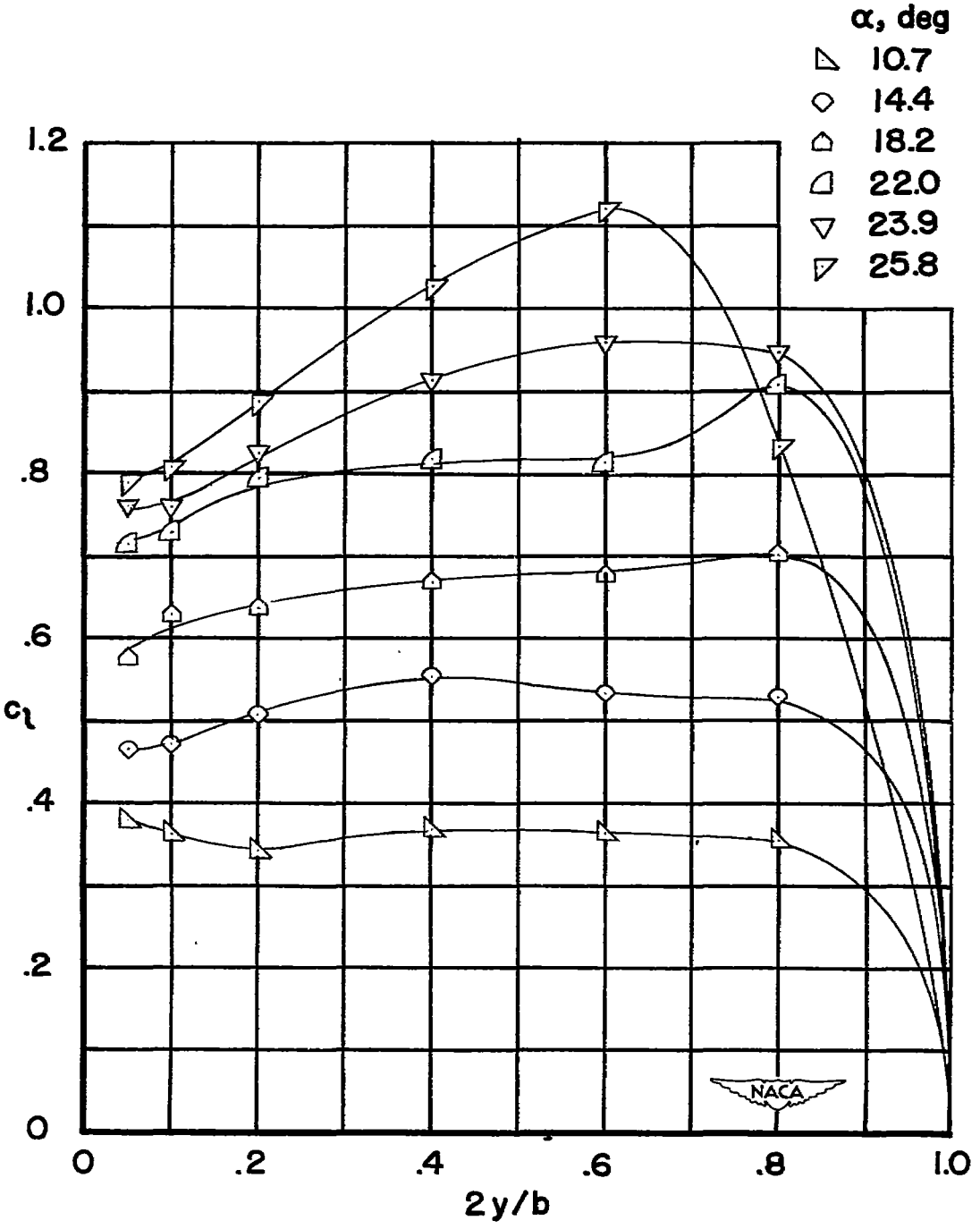

Figure 26.— Spanwise variation of section lift coefficient for several angles of attack. Full-span drooped-nose flap deflected 40°. $\psi = 0°$.

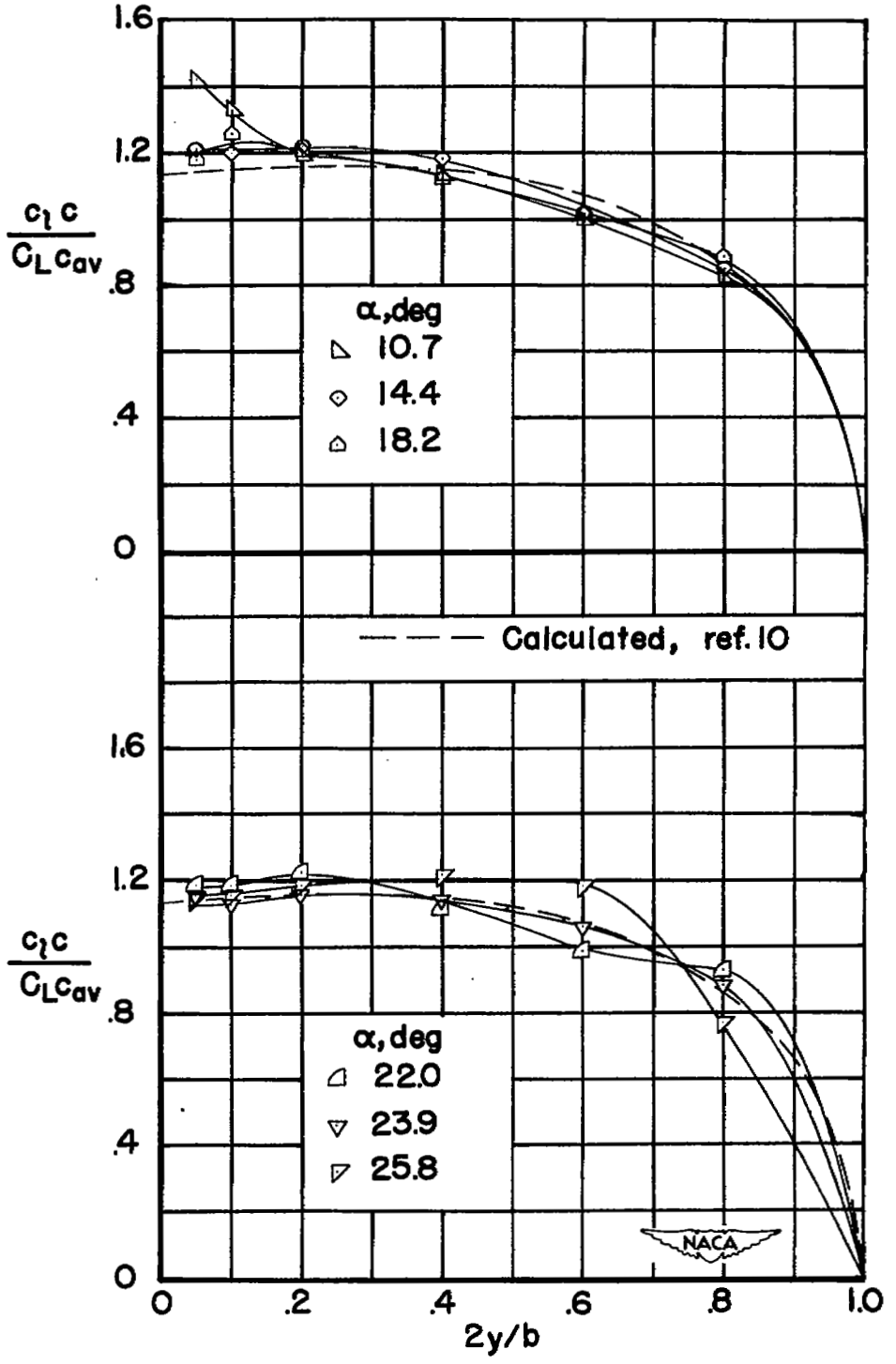

Figure 27.– Span load distribution for several angles of attack. Full-span drooped-nose flap deflected 40°. $\psi = 0°$.

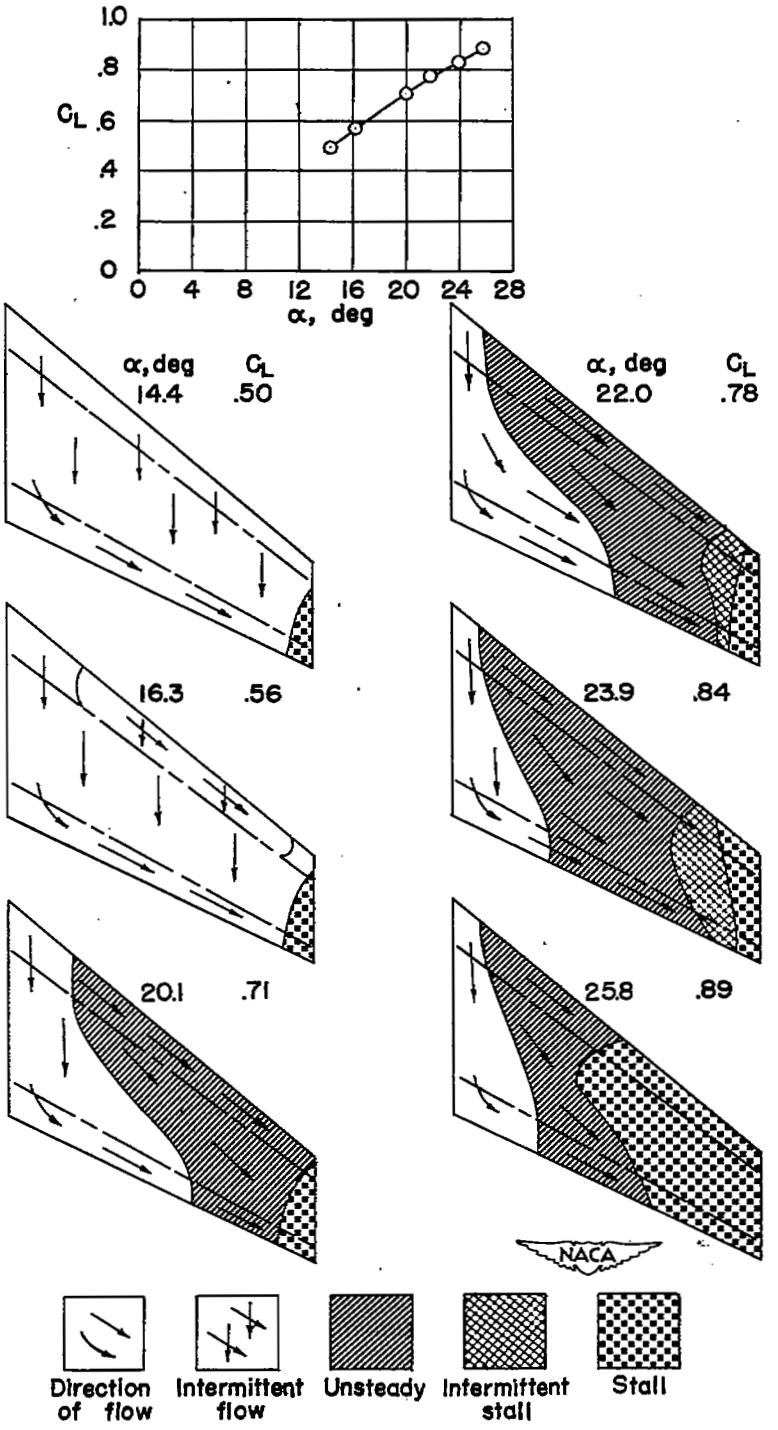

Figure 28.– Stalling characteristics of the wing with full–span drooped–nose flaps deflected 40°. $\psi = 0°$.

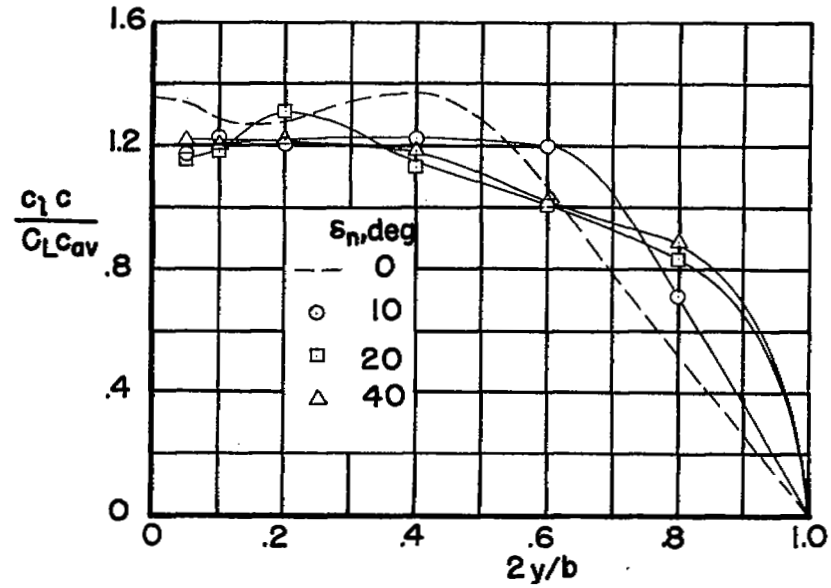

(a) $\alpha \approx 14.2°$.

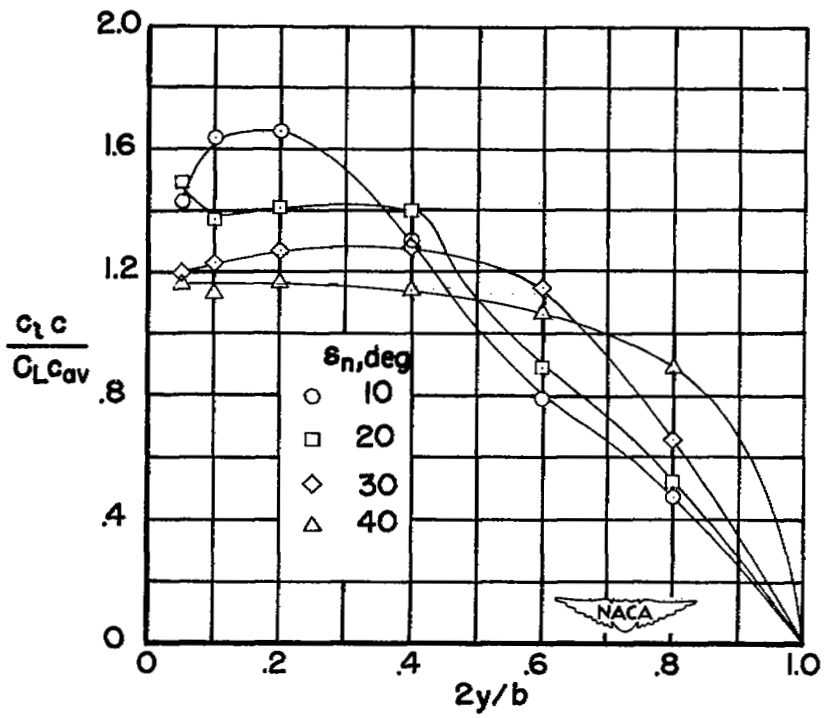

(b) $\alpha \approx 23.8°$.

Figure 29.— A summary of the effects of drooped-nose-flap deflection on span load distribution. $\psi = 0°$.

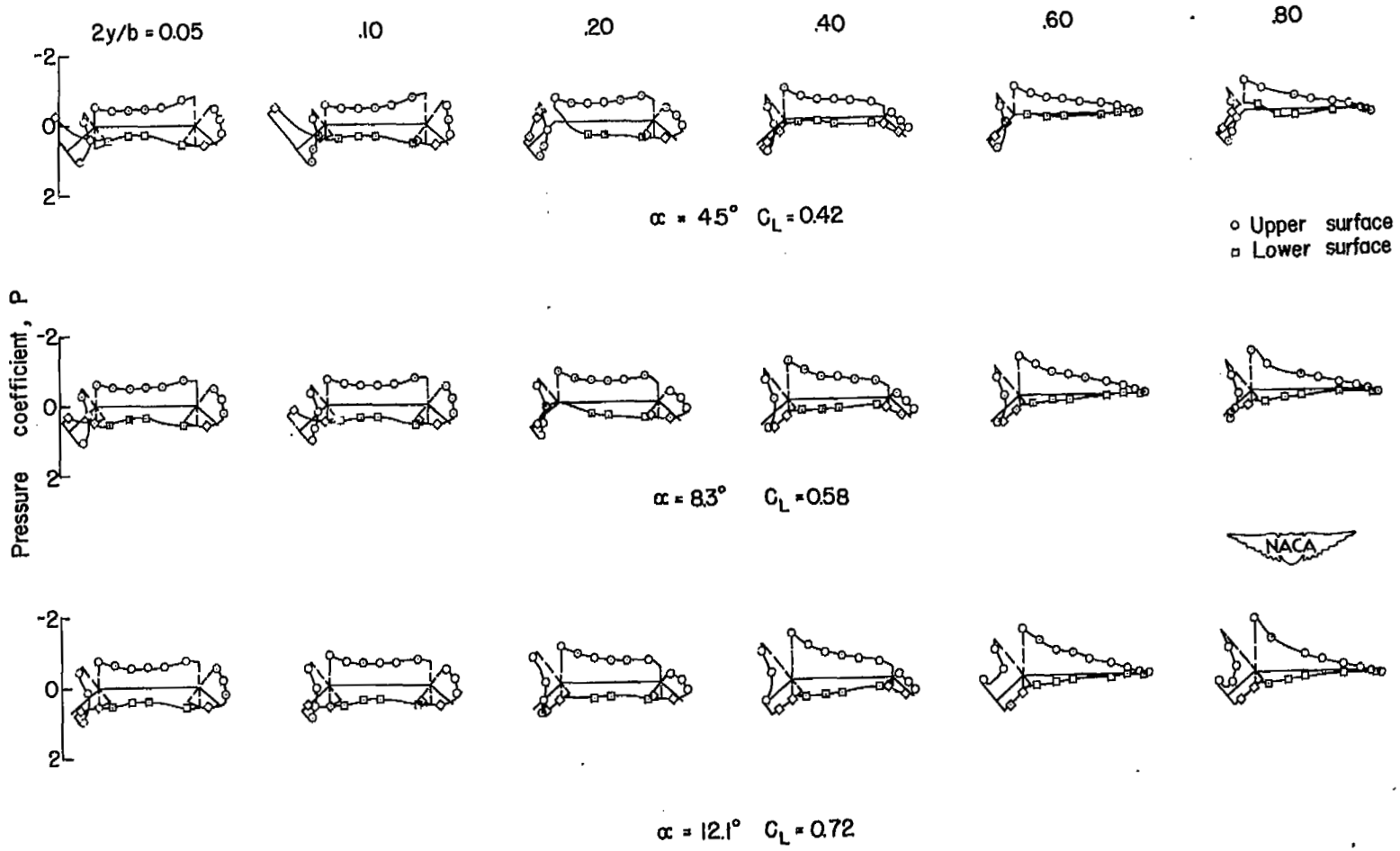

Figure 30.— Chordwise pressure distribution for six spanwise stations. Full-span drooped-nose flap and semispan plain flap deflected 40°. Ψ = 0°.

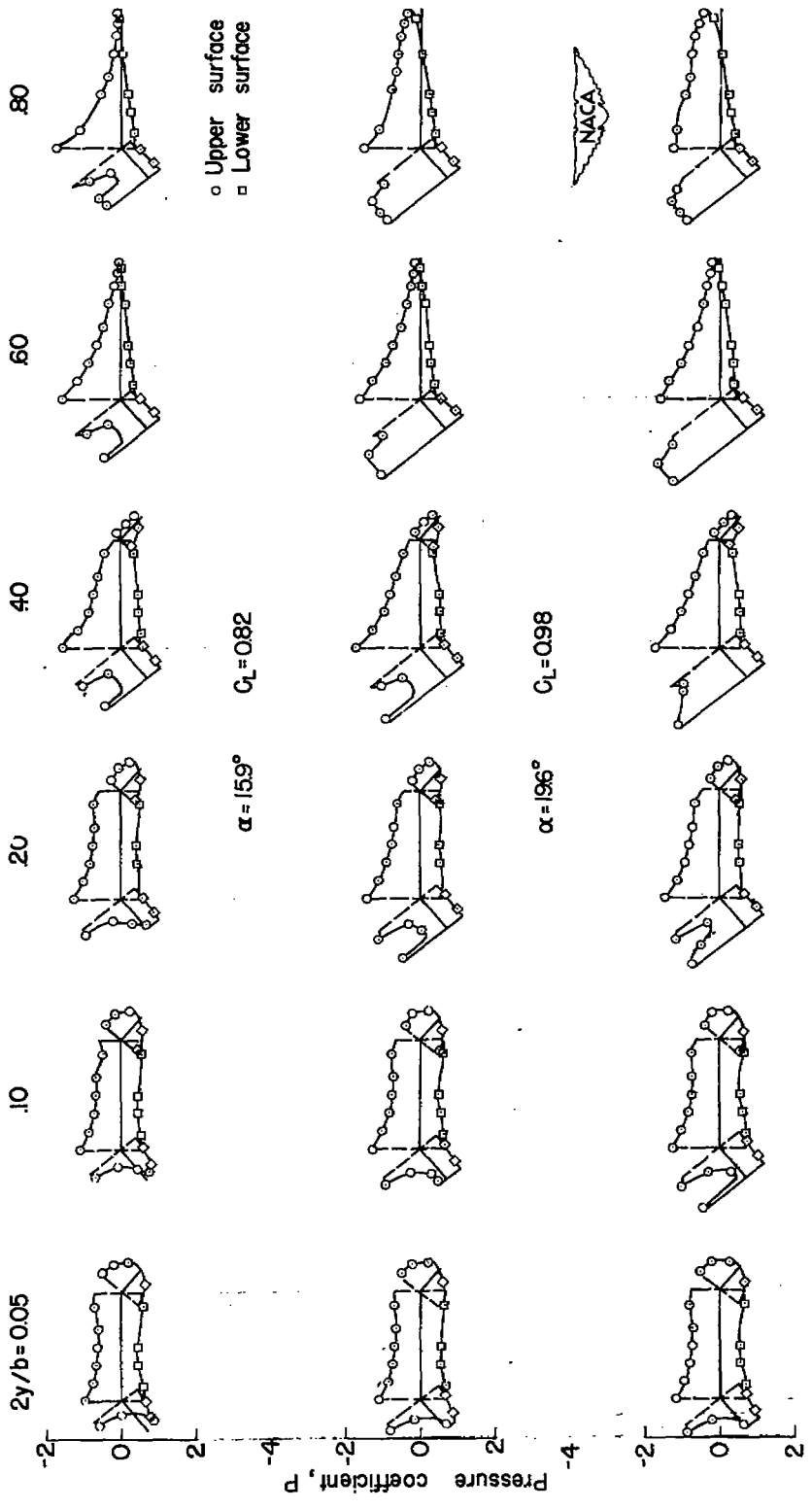

Figure 30.— Concluded.

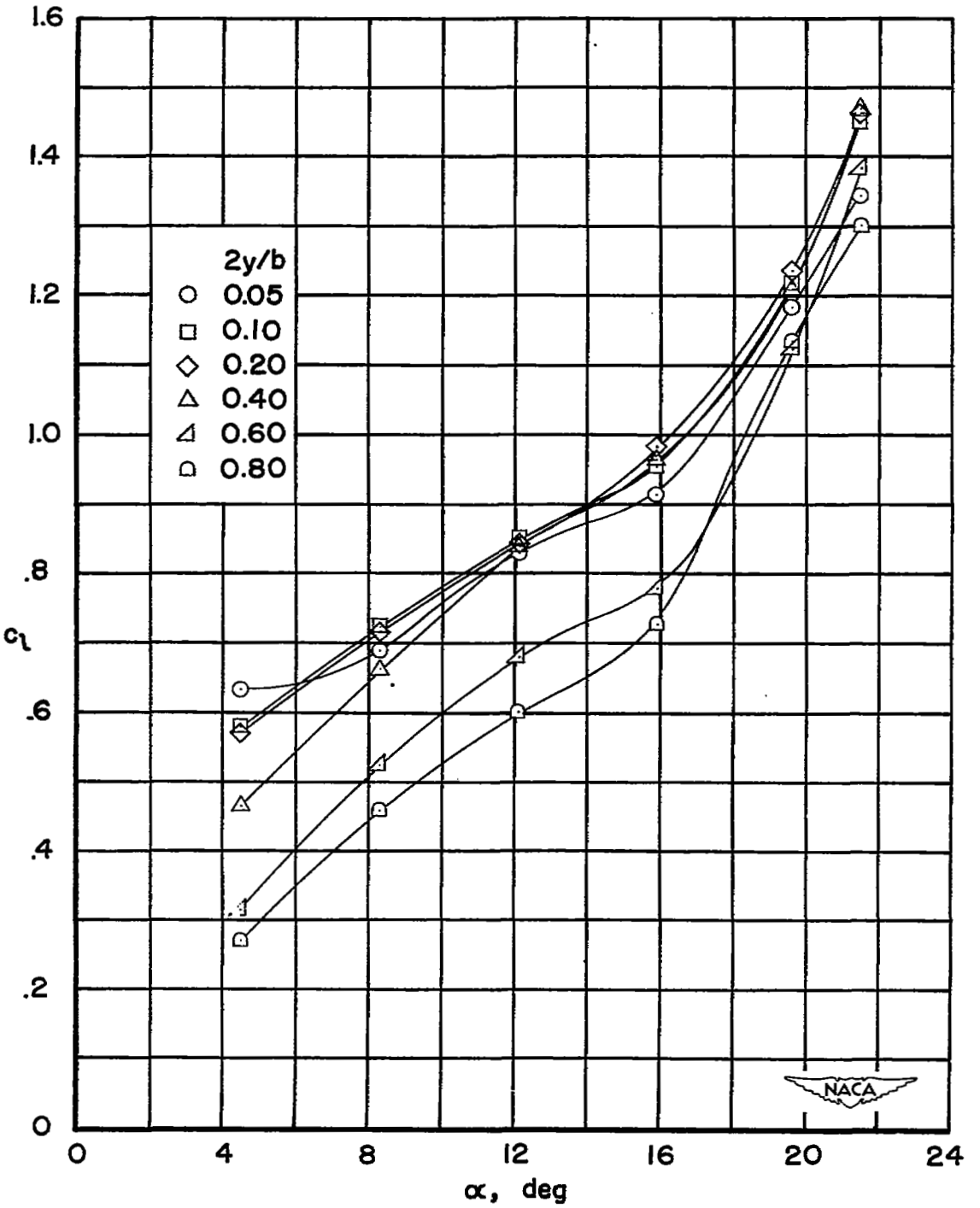

Figure 31.— Variation of section lift coefficient with angle of attack for six spanwise stations. Full-span drooped-nose flap and semispan plain flap deflected 40°. $\psi = 0°$.

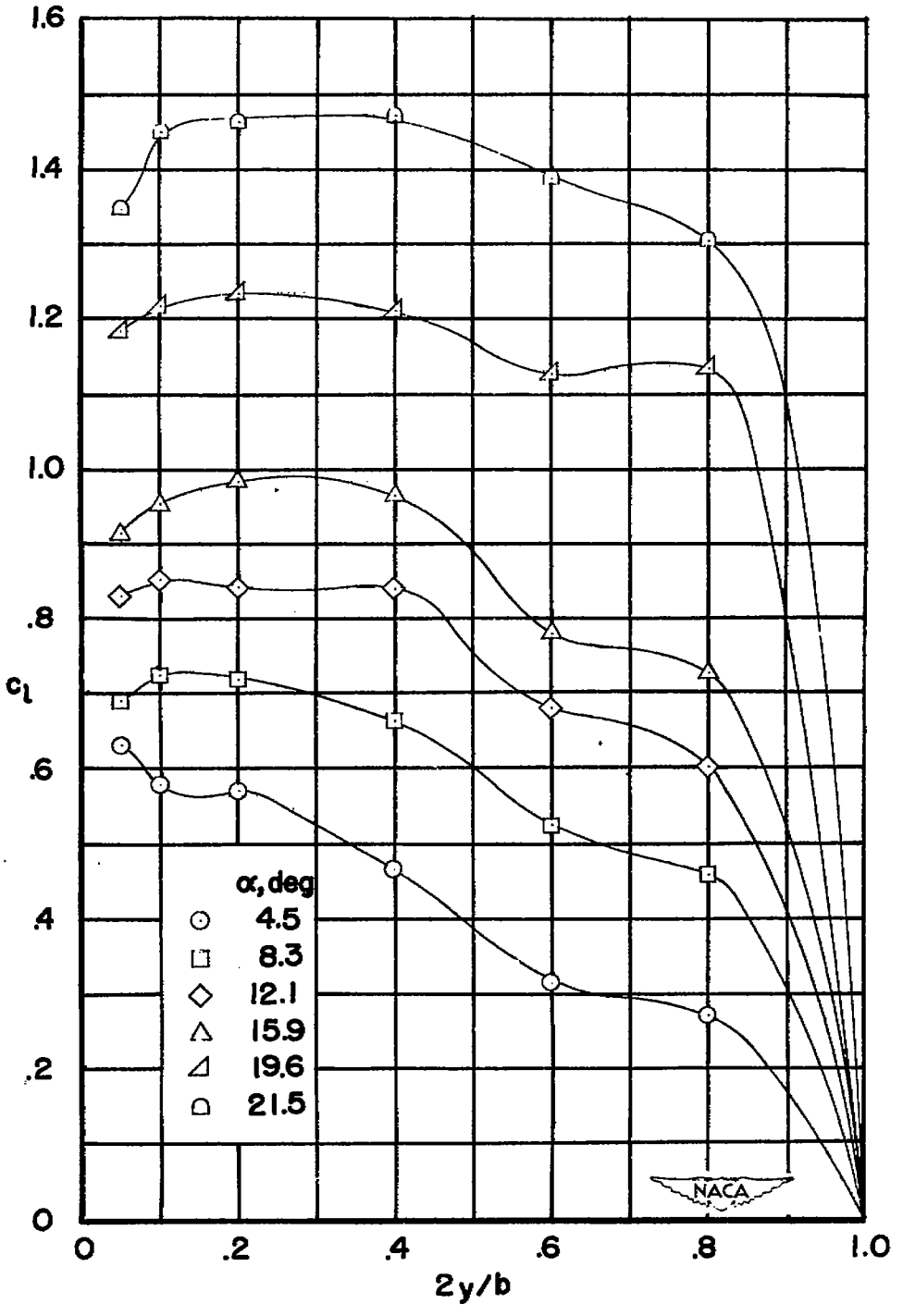

Figure 32.— Spanwise variation of section lift coefficient for several angles of attack. Full-span drooped-nose flap and semispan plain flap deflected 40°. $\psi = 0°$.

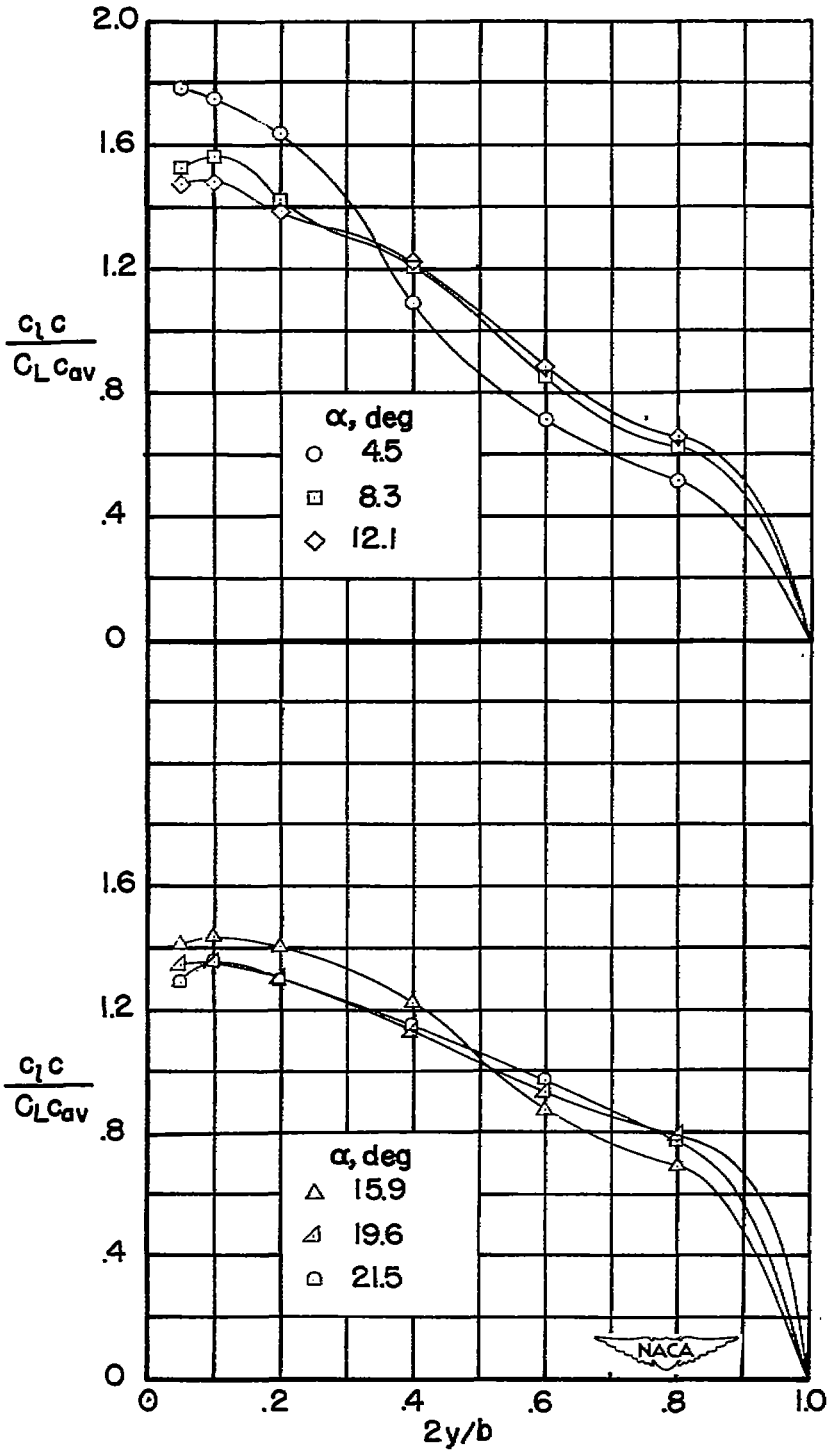

Figure 33.– Span load distribution for several angles of attack. Full-span drooped-nose flap and semispan plain flap deflected 40°. $\psi = 0°$.

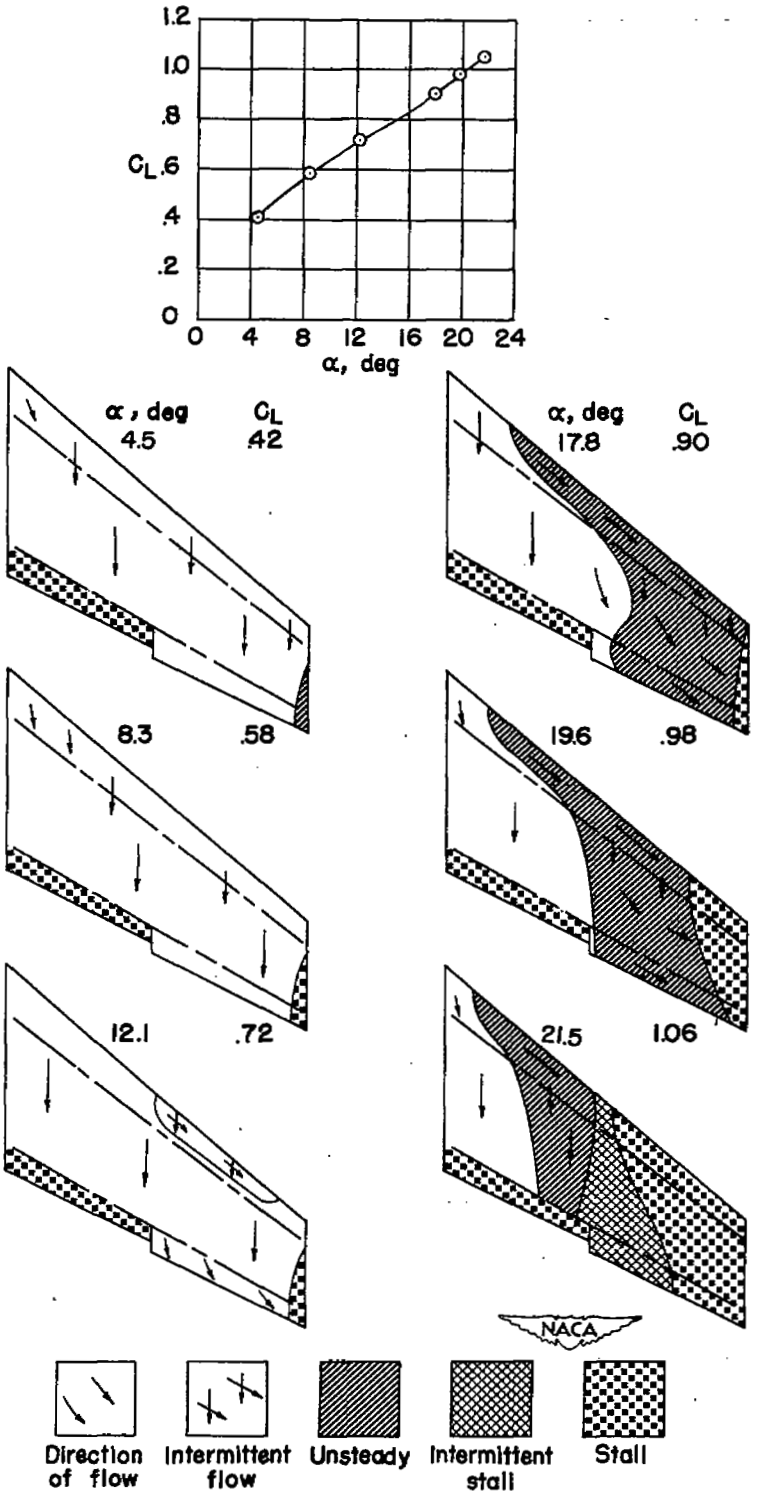

Figure 34.— Stalling characteristics of the wing with semispan plain flaps and full-span drooped-nose flaps deflected 40°. $\psi = 0°$.